NASA Contractor Report 3014

Viking Dynamics Experience With Application to Future Payload Design

Stanley Barrett, W. Paul Rader,
and Kenneth R. Payne

CONTRACT NAS1-14370
JULY 1978

NASA

NASA Contractor Report 3014

Viking Dynamics Experience With Application to Future Payload Design

Stanley Barrett, W. Paul Rader,
and Kenneth R. Payne
Martin Marietta Corporation
Denver, Colorado

Prepared for
Langley Research Center
under Contract NAS1-14370

National Aeronautics
and Space Administration

**Scientific and Technical
Information Office**

1978

CONTENTS

Figures

Tables

SUMMARY

The study described in this report had two primary objectives: first, to summarize the structural dynamics approach used on the Viking Project, indicating where detailed information and test data can be found; second, to present recommendations for improvements in the dynamics philosophy applicable to future payloads.

The information is presented in two main sections. In the first section, the Viking spacecraft, launch vehicle, and mission profile are described and methods for predicting dynamic environments and rationale for establishing test criteria are presented. Mathematical modeling techniques and loads analyses used to design the primary structure are discussed next. The total test program is outlined, followed by a description of the data acquisition system on the Viking flights.

In the second section, predicted environments are compared with measured data. Some shortcomings of current techniques for establishing dynamic environments and test margins revealed by this comparison are pointed out, and recommended improvements are indicated. The use of loads analysis and its correlation with system-level tests for different payloads are discussed. The influence of test levels and test margins on overall test program costs for various payload classes is discussed next. Finally, flight measurement, data reduction, and analysis techniques are recommended.

The report concludes with a summary of recommended approaches to dynamic problems of future payloads, including the following:

1) Establish payload classifications based on size, type of mission, weight criticality, and reliability requirements;

2) Establish a test and flight data bank for use in deriving environmental criteria related to payload classifications;

3) Develop an industrywide approach for defining design and test margins;

4) Except in special cases, eliminate sine-sweep testing as a general requirement;

5) Take advantage of recent advances in modal survey techniques, using digital control systems, and associated analysis methods;

6) Where possible, use actual ordnance devices for testing components to pyrotechnic shock environments;

7) Improve communication between industry- and government-employed dynamics groups for better interchange of test and flight data.

Page Intentionally Left Blank

INTRODUCTION

Most new spacecraft programs rely heavily on information and data from similar earlier programs. The applicability of the data varies for different technical areas. In spacecraft structural dynamics, prediction and analysis methods are generally semiempirical, depending for their accuracy on having appropriate measured data with which to refine the estimated environments and loads. Thus, dynamics data are usually applicable to new programs, if background information showing how the data were obtained is also available.

The Viking Project included an unusually extensive series of dynamics test programs at the component, subassembly, and system levels. These covered the full spectrum of dynamic environments, including launch acoustics, random vibration, booster-induced transients, pyrotechnic shock, staging events, high-speed entry into the Martian atmosphere, and landing shock. All future payloads will experience at least some of these environments, so the approach used on Viking and test data acquired should be of interest to those responsible for such payloads.

Some of the prediction methods initially used on Viking were found to be inaccurate after test data became available for comparison. In this report, improvements in these methods are proposed in several cases, or the need for additional test data pointed out.

It is suggested that a report of this type be written after each major spacecraft program, to make the data acquired available to the aerospace community for future applications.

Page Intentionally Left Blank

SYMBOLS

A(f)	acceleration spectral density at frequency f, acceleration in 1/3-octave band
a_o	speed of sound
BLDT	balloon-launched decelerator test
CDR	cumulative damage ratio
cg	center of gravity
CO/QUAD	coincident/quadrature
D	averaged weight of loaded structure where responses were measured
dB	decibel(s)
DOF	degrees of freedom
FA	flight acceptance
FM	flight modulation
f_n	fundamental frequency
f_p	frequency
FPL	fluctuating pressure level
g	force of gravity
GCMS	gas chromatograph mass spectrometer
GD/CA	General Dynamics/Convair Astronautics
g_{rms}	root mean square force of gravity
GVS	ground vibration survey
Hz	hertz
[I]	"unity" matrix
in.	inch(es)
IRU	inertial reference unit
I_{sp}	specific impulse

JPL	Jet Propulsion Laboratory
kHz	kilohertz
lb	pound(s)
lbf	pound force
lb-in.	pound-inch(es)
LDTM	Lander dynamic test model
LeRC	Lewis Research Center
LMSC	Lockheed Missiles & Space Company, Inc.
LRC	Langley Research Center
LV	launch vehicle
M	acoustic mobility function, mass
m	meter(s)
M_1	free-stream Mach number
max	maximum
max q	maximum dynamic pressure
MDS	motor-driven switch
MECO	main-engine cutoff
MES	main-engine start
MOI	Mars orbit insertion
MSFC	Marshall Space Flight Center
MSS	multispectral scanner
M_X	moment about X axis
M_Y	moment about Y axis
N	force level, newton(s), number of engines
N-m	newton-meter(s)
NASA	National Aeronautics and Space Administration

OASPL	overall sound pressure level
ODTM	Orbiter dynamic test model
P	axial load
P_{ℓ}	ambient pressure
P_a	pressure
PC	printed circuit
PEVT	pyrotechnic-environment verification test
P(f)	acoustic pressure in 1/3-octave band
PFLA	proof flight Lander adapter
P_{ref}	dB scale reference pressure
PSD	power spectral density
PSTB	pyrotechnic-shock test bed
PTC	proof test capsule
PTO	proof test Orbiter
PWL	sound power level
Q	amplification factor at resonance (inverse of 2 x damping coefficient ratio)
q	dynamic pressure
Qual	qualification
RCS	reaction control system
rms	root mean square
RTG	radioisotope thermoelectric generator
SN	Strouhal number
S/N	signal-to-noise ratio
SPL	sound pressure level
SRM	solid rocket motor
s	second(s)

T	maximum engine thrust, thrust per engine
t	skin thickness
TA	type approval, type assurance
TC	Titan/Centaur
TESS	terminal-engine shutdown switch
TD	terminal descent
TDLR	terminal descent and landing radar
TF	test factor
U_∞	free-stream velocity
UAMS	upper-atmosphere mass spectrometer
V	Viking
VBI	Viking biology instrument
VODS	Viking Orbiter dynamic simulator
VDS	Viking dynamic simulator
VL	Viking Lander
VLC	Viking Lander Capsule
VLCA	Viking Lander Capsule adapter
VLS	Viking Lander System
VO	Viking Orbiter
VPO	Viking Project Office
V-S/C	Viking Spacecraft
VSCA	Viking Spacecraft adapter
VTA	Viking transition adapter, Viking truss adapter
W	weight of unloaded support structure
w	average surface density of loaded panel
W_c	weight of supported components

β	contour angle of blunt body
γ	ratio of specific heats
ΔC_p	boundary-layer fluctuating pressure coefficient
δ^*	boundary-layer displacement thickness
ρ	density of atmosphere, material density
ρa_o	characteristic impedance of atmosphere to sound

Subscripts:

E	Earth
M	Mars
n	"new" vehicle
r	"reference" vehicle

Program Description

The objective of the Viking Project was to significantly advance the knowledge of Mars by direct measurement in the atmosphere and on the surface and by observation of the planet during approach and from orbit. Particular emphasis was placed on obtaining information concerning biological, chemical, and environmental factors relevant to the existence of life on Mars. Figure 1 summarizes the mission and shows the various maneuvers and separations between Earth launch and Mars landing. While the spacecraft was in Mars orbit, photographs were taken and measurements made to obtain image, thermal, and water-vapor information for landing-site selection for the Viking Landers (VLs) and for the study of dynamic and physical characteristics of the planet and its atmosphere. During entry through the Martian atmosphere, data were obtained on atmospheric structure and composition at high altitudes. After landing, experiments were conducted on the surface to search for evidence of living organisms and organic compounds, study the properties and elemental composition of the surface material and the atmosphere, and to visually characterize the landing site using steroscopic cameras.

The launch vehicle (LV) for the Viking '75 mission was the Titan IIIE/Centaur D-1T configuration--a four-stage vehicle (fig. 2). At lift-off, the vehicle weighed 635 000 kg (1.4 M lb) and developed 10.23 MN (2.3 M lb) of thrust from the Stage 0 solid rocket motors.

The Viking Spacecraft (V-S/C) consisted of two main portions--the Orbiter (VO) and Lander. The Orbiter (fig. 3) used an octagonal bus structure that contained 12 equipment bays and four smaller compartments for mechanical equipment. Four identical hinged solar panels and a boom-outrigger to support the high-gain antenna were connected to the bus structure. The propellant tank, pressurant tank, and engine support structure were attached beneath the bus structure.

The Lander comprised five major substructures (fig. 4). The bioshield was designed to exclude biological contamination from the Lander from sterilization until biocap separation during the Earth-Mars cruise. To protect the Lander from aerodynamic heating during entry, the base cover and aeroshell encapsulated it in the bioshield. Figure 5 shows the Lander body supported by its three landing legs. It housed many scientific experiments and electronic components, either mounted on the outside of the structure or supported by the equipment plate. The three landing legs provided energy absorption to minimize landing shock loads and provide stable support to the Lander during its operational life on Mars.

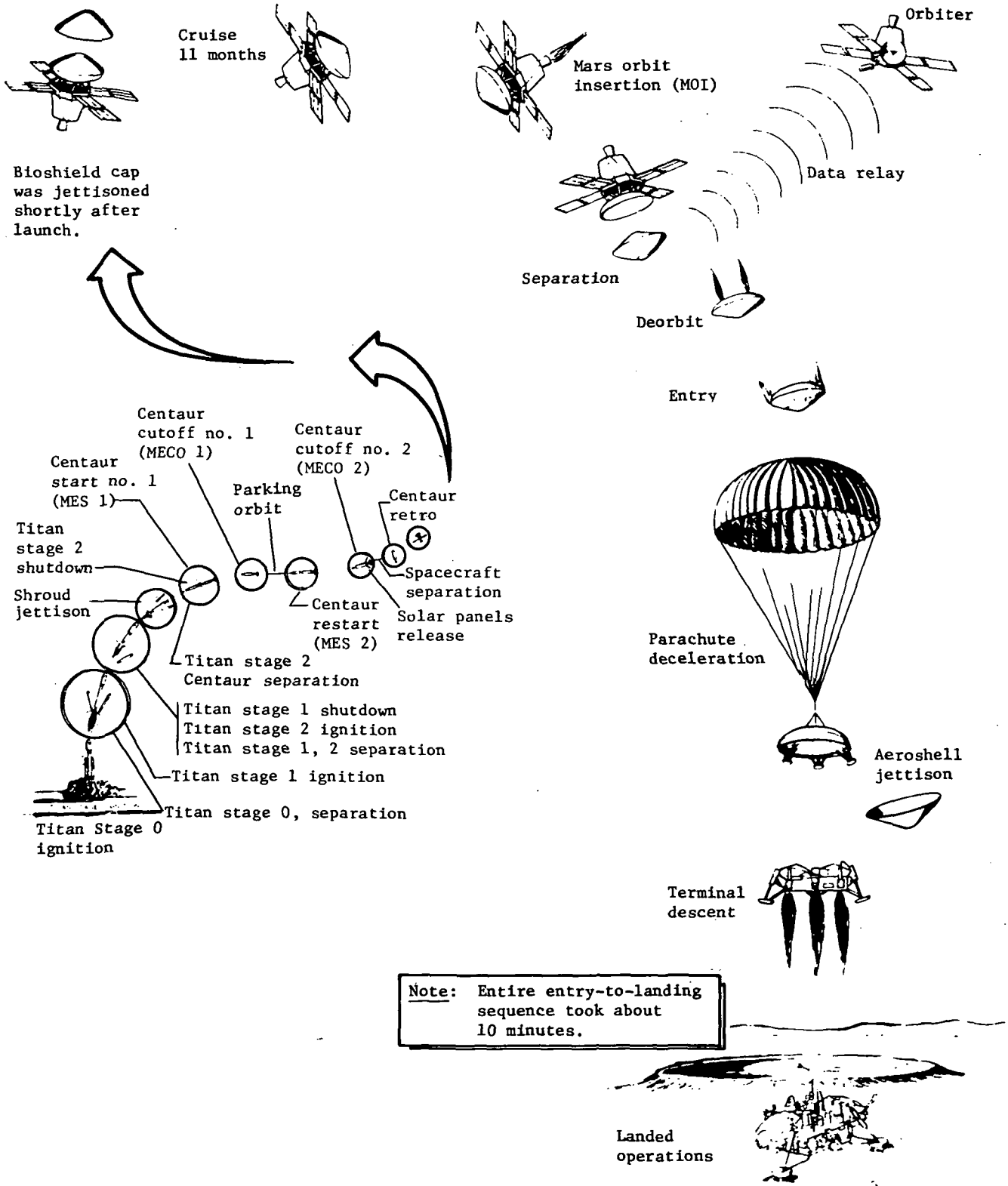

Figure 1.-. Viking mission sequence.

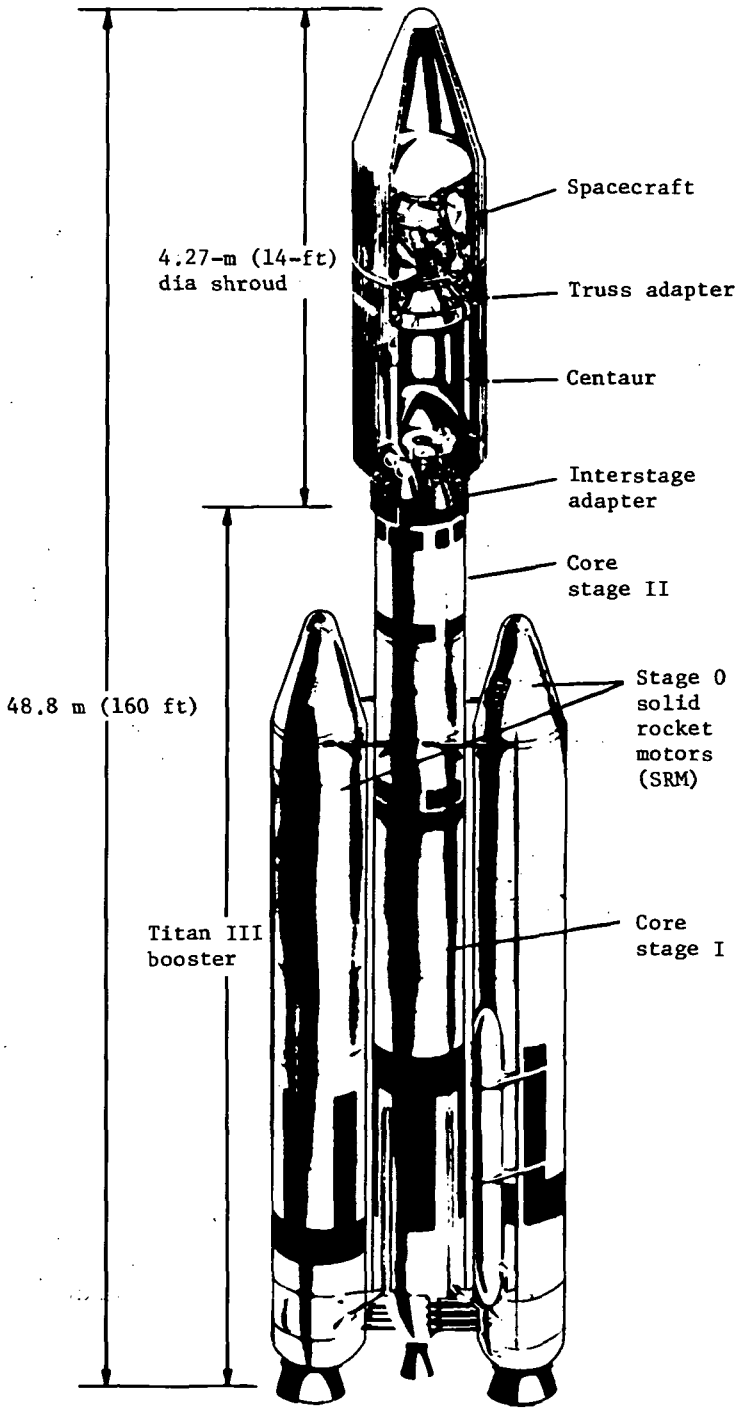

Figure 2.- Viking space vehicle.

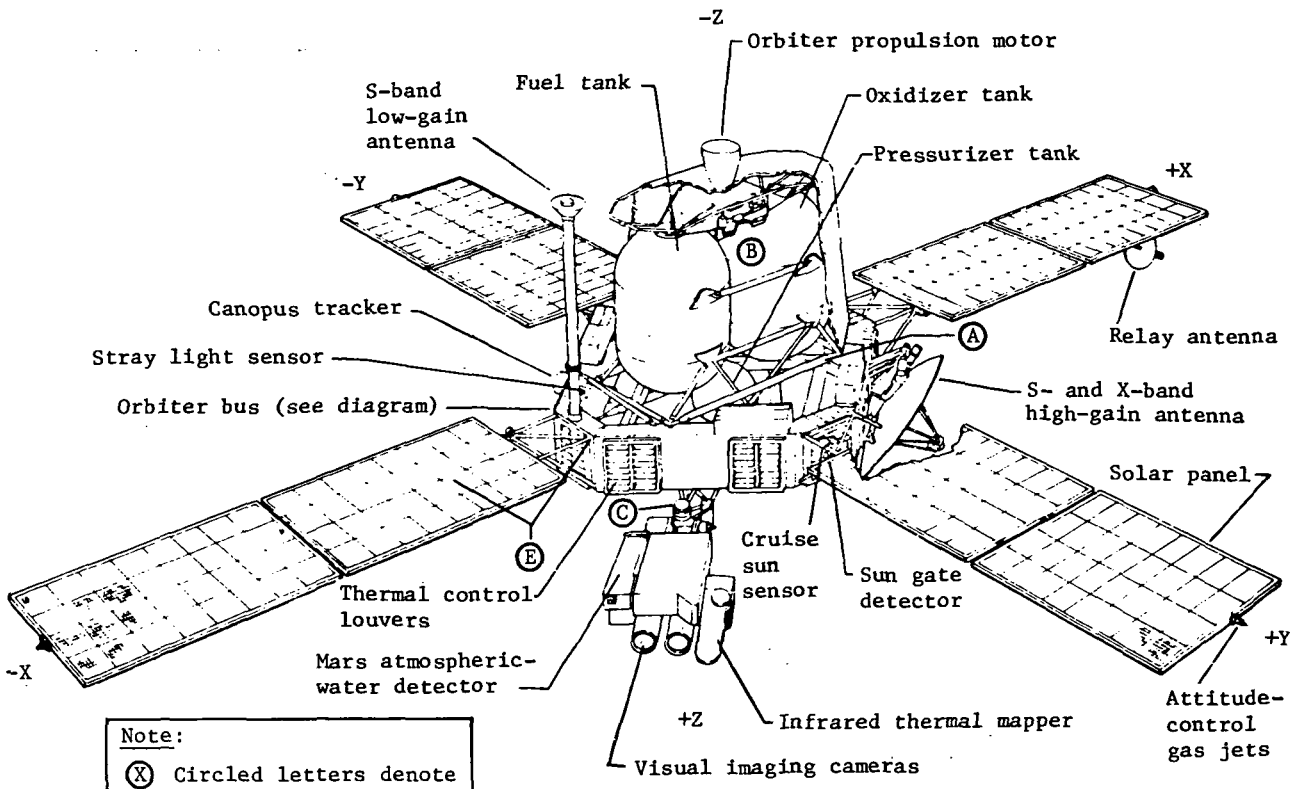

Note:

Ⓧ Circled letters denote primary structure used in loads analyses.

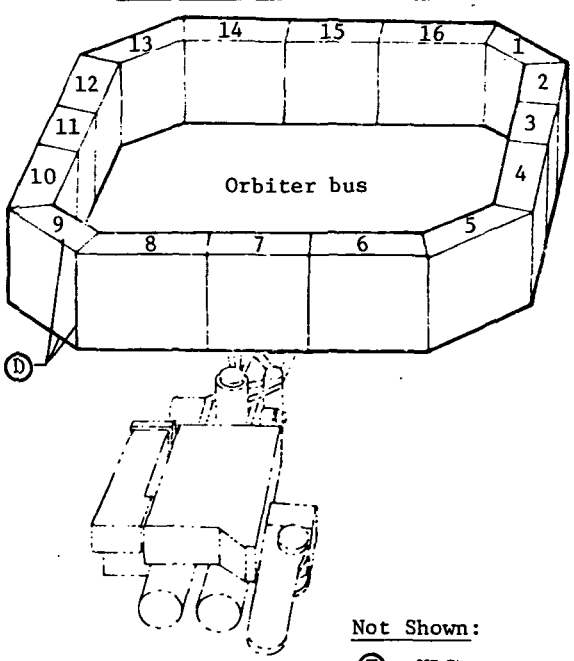

Not Shown:

Ⓕ VLC truss

Ⓖ VSC adapter truss

Bay	Subsystem/components
1	Radio frequency subsystem, modulator demodulator subsystem, X-band transmitter
2	Computer command subsystem
3	Reaction-control assembly high-pressure module
4	Data storage subsystem
5	Attitude-control subsystem and articulation-control subsystem
6	Flight data subsystem
7	Scan platform subsystem
8	Visual imaging subsystem, Mars atmospheric-water detection subsystem
9	Battery assembly
10	Power-source electronics assembly
11	Reaction-control assembly high-pressure module
12	Power processing and distribution assembly
13	Battery assembly
14	Digital tape-recorder assembly
15	Relay radio subsystem, relay telemetry subsystem pyrotechnic control subassembly
16	Radio frequency subsystem

Figure 3.- Viking Orbiter.

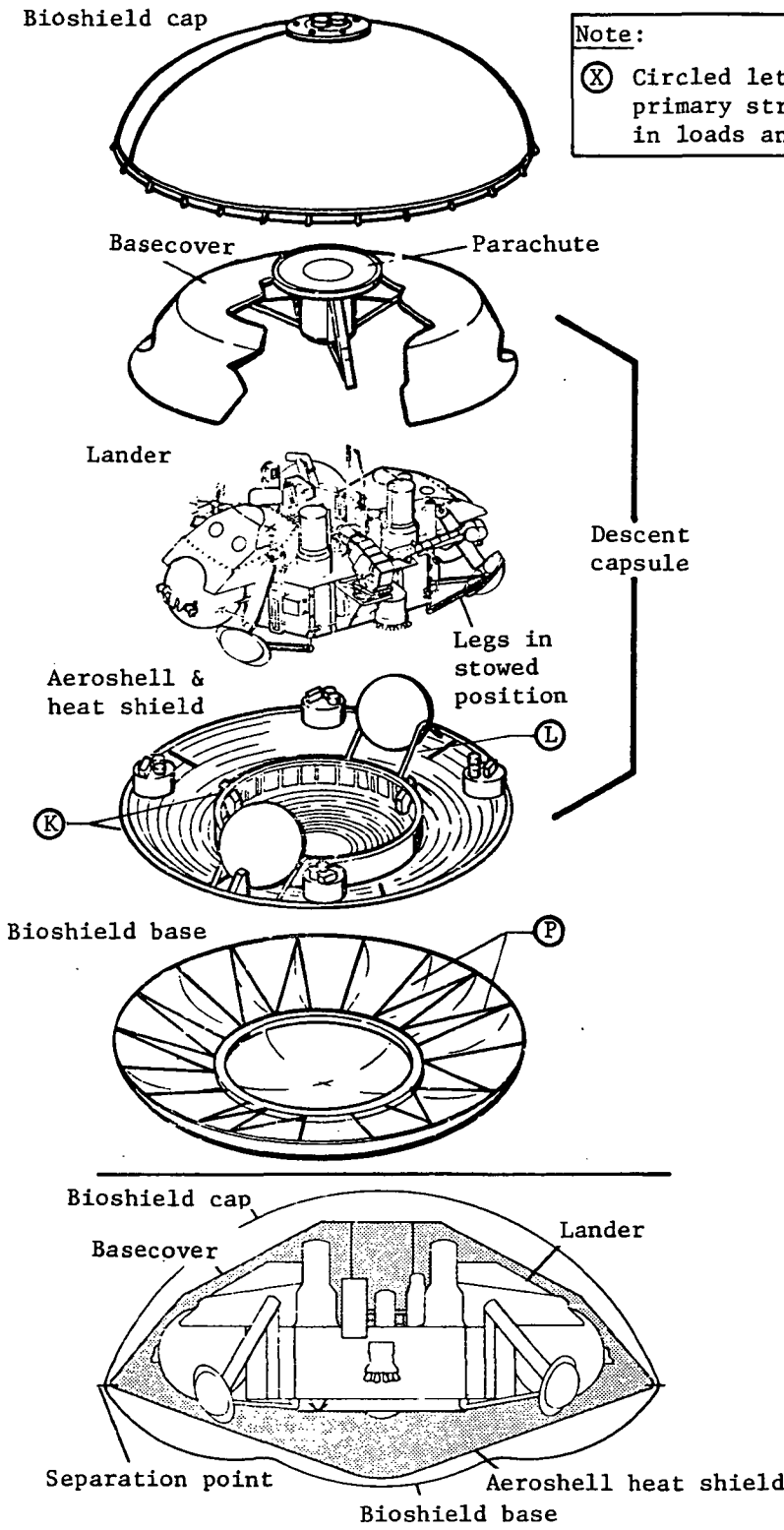

Figure 4.- Viking Lander Capsule.

Note:
Ⓧ Circled letters denote primary structure used in loads analyses.

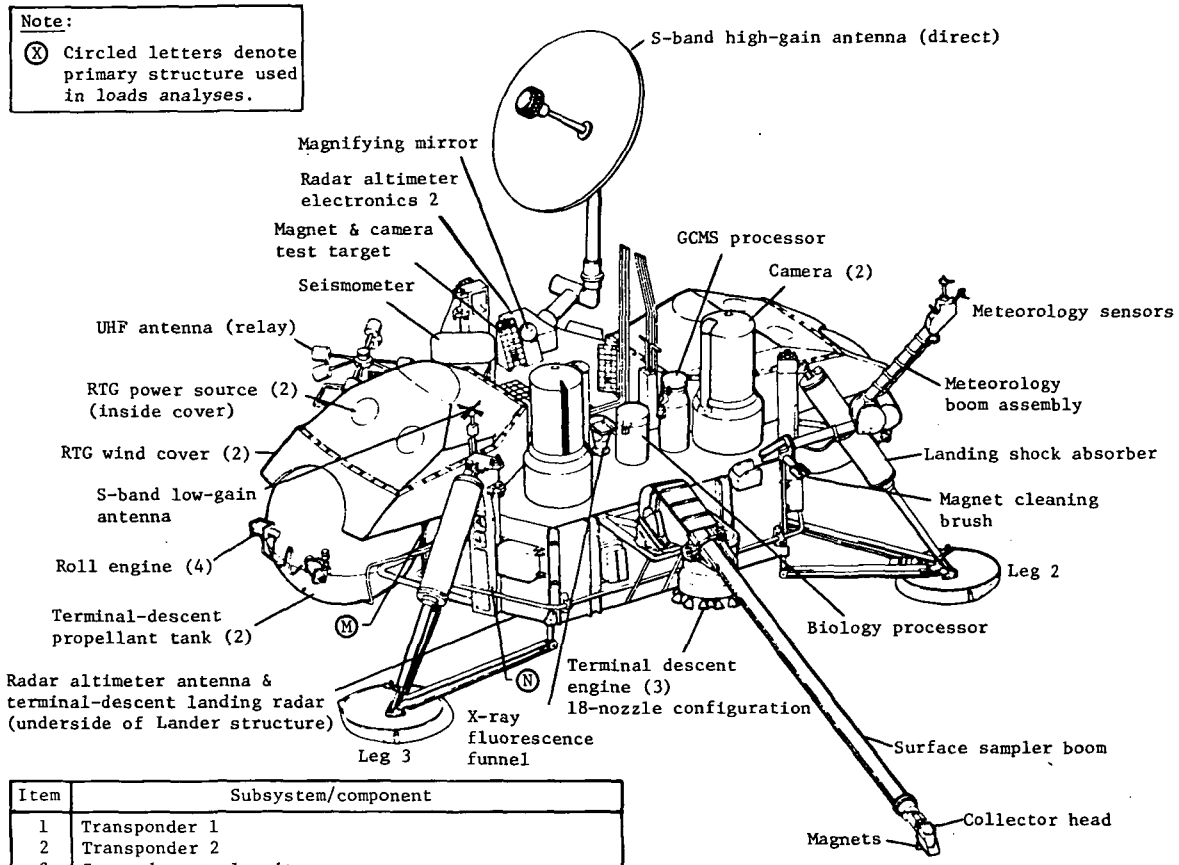

Item	Subsystem/component
1	Transponder 1
2	Transponder 2
3	Command control unit
4	Microwave components
5	Traveling wave tube amplifier 1
6	Traveling wave tube amplifier 2
7	Data storage memory
8	Tape recorder
9	Ambient pressure transducer
10	Meteorology electronics assembly
11	Gas chromatograph mass spectrometer
12	Gas chromatograph mass spectrometer processor
13	Biology instrument
14	Biology processor
15	Surface sampler control assembly
16	Camera duster assembly
17	Battery assembly 1
18	Battery assembly 2
19	Ultrahigh-frequency radio assembly
20	Guidance control and sequencing computer
21	Data acquisition and processor unit
22	Power conditioning and distribution assembly
23	X-ray fluorescence spectrometer
24	Radioisotope thermoelectric generator coolant loop
25	Thermal switch 2
26	Thermal switch 1
27	Terminal descent landing radar
28	Inertial reference unit
29	Radar altimeter antenna
30	Valve drive amplifier
31	Radar altimeter electronics
32	Lander pyrotechnic control assembly 1
33	Lander pyrotechnic control assembly 2

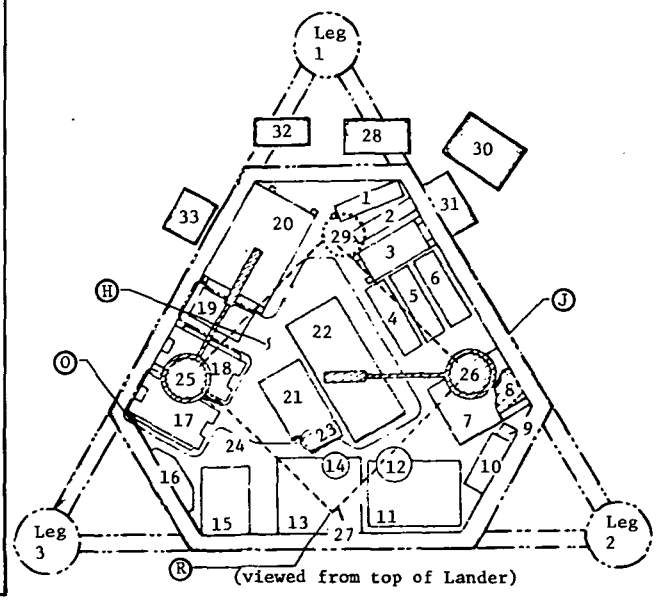

Figure 5.- Lander details and equipment locations.

Successful delivery of the Viking Lander required the launching of 635 000 kg (1.4 M lb) of hardware, performance of 11 precise staging operations, and soft landing a 635-kg (1400-lb) vehicle containing delicate instruments on an unknown surface. The mission thus subjected the spacecraft to an unprecedented range of dynamic environments.

Environments and Criteria

During the Viking mission, the spacecraft was subjected to a wide range of dynamic conditions, encompassing nearly all environments encountered in any previous NASA mission. Table 1 lists these environments, and the analytical or empirical techniques used to evaluate their levels are discussed in this section.

TABLE 1.- SOURCES OF DYNAMIC ENVIRONMENTS

	Acoustics	Random vibration	Sine vibration	Pyro shock	Landing shock	Steady state	Transients
Ground test	X	X	X	X	X		
Launch (powered flight)	X	X		X		X	X
Cruise		0		X		0	0
Deorbit		0		X		0	0
Entry and parachute	X	X		X		X	X
Terminal descent	X	X		X		X	
Landing					X		X
Postlanded				X			

0 = negligible load environment.

Low-frequency (0 to 50 Hz) structural loads resulted from quasi-static conditions superimposed on various transient events occurring during launch, entry, and landing. The analytical process employed to define low-frequency design loads is described in the Loads Analysis section.

Acoustic environments.- From the viewpoint of the acoustician, the three most significant phases of the Viking mission were:

1) Lift-off and boost through the Earth's atmosphere;

2) Mars entry;

3) Terminal descent to the Martian surface.

Primary emphasis is placed on the lift-off and boost environments; however, for potential future applications to planetary exploration payloads, entry and terminal-descent prediction techniques are briefly described.

During the lift-off and boost phases, acoustic environments were derived from measured data on previous Titan IIIC vehicles adjusted to account for the Titan-Centaur configuration. For lift-off, the adjustment consisted of application of the inverse-square law, resulting in a maximum overall external level of 148 dB on the fairing at the aft section of the spacecraft (fig. 6). Figure 7 shows the associated spectrum.

The transonic external environment was derived from aerodynamic noise data acquired from three different sources: Titan flight measurements and wind-tunnel test data for Saturn and X-15 models. To define the external environment in the region spanned by the Viking Spacecraft, noise data were adjusted to account for differences in free-stream dynamic pressures and nose fairing configurations (Strouhal effect). The region included the aft part of the 15° conic section, the cone-cylinder joint, and the forward one-third of the cylindrical section of the nose fairing. As shown in figure 6, overall levels predicted for three regions were 152.5 dB in the area of the 15° conical section, 162 dB in the region of the cone-cylinder joint, and 157.5 dB in the area aft of the cone-cylinder joint. Because the highest noise levels produced by oscillating shock waves in the area of the cone-cylinder joint were developed on only a localized area of the fairing, this source contributed little to the noise level inside the fairing. Therefore, the maximum predicted level (157.5 dB) in the area aft of the cone-cylinder joint was used as the reference external level in deriving the levels inside the fairing.

Noise reduction provided by the payload fairing was derived from external and internal flight measurements from previous Titan flights and included adjustments for fairing-surface density. These noise reduction spectra, (fig. 8) were applied to applicable external levels to define the acoustic environments to which the Viking spacecraft would be subjected during lift-off and boost. Figure 9 shows the resulting spectra. The noise reduction provided by the aeroshell was calculated to be a uniform 3 dB across the full frequency band. This was used to derive the acoustic levels on the Lander body. Aerodynamic noise during Mars entry was generated by pressure fluctuations at the aeroshell surface and by separated flow turbulence at the base-cover surface. Two analytical techniques were used for the aeroshell. The first employed a procedure from reference 1 in which the overall sound pressure level (OASPL) was given by:

$$\text{OASPL (dB)} = 81.5 + 20 \log P_1 \cdot f(M_1, \beta) \qquad (1)$$

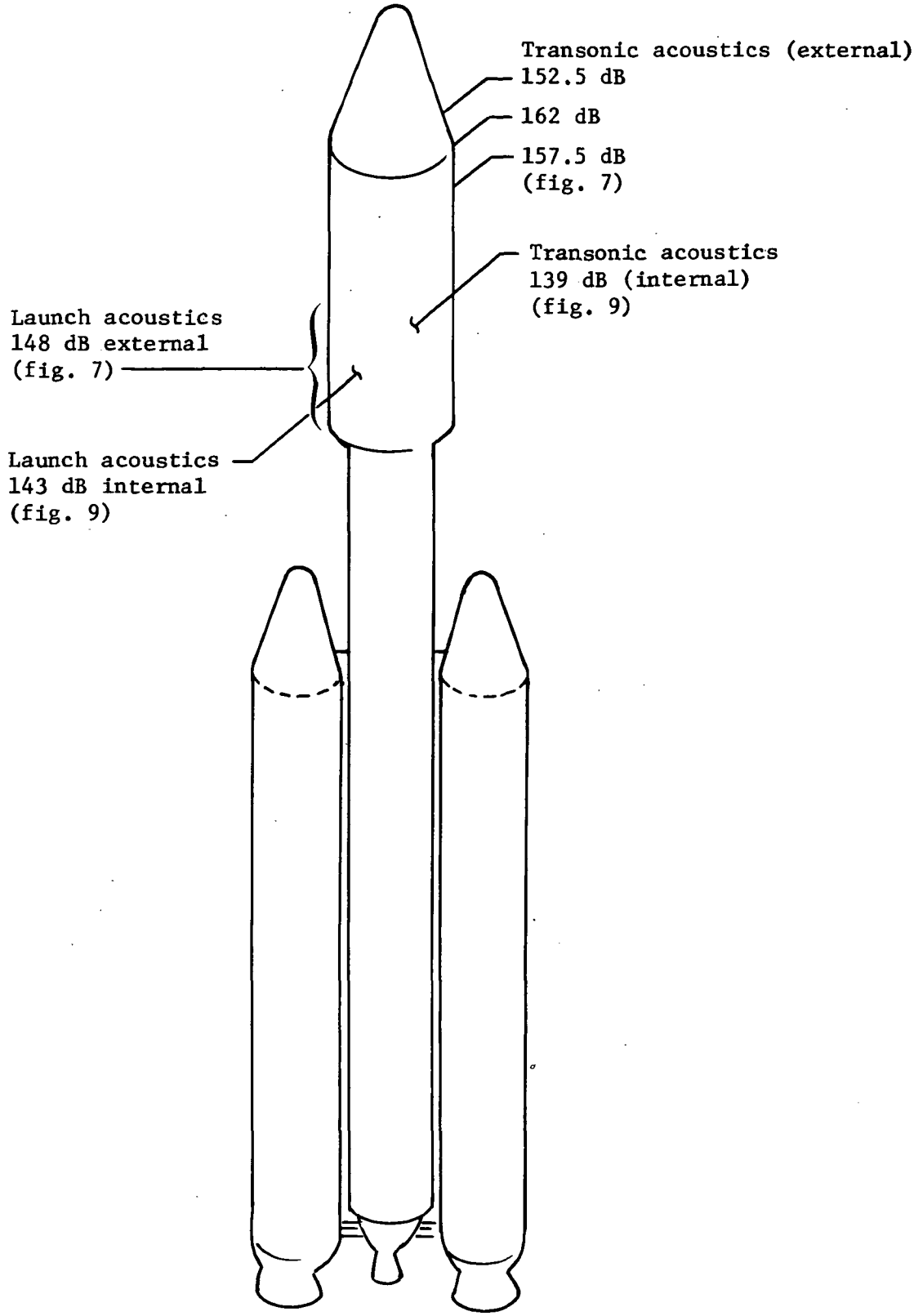

Figure 6.- Viking acoustic levels.

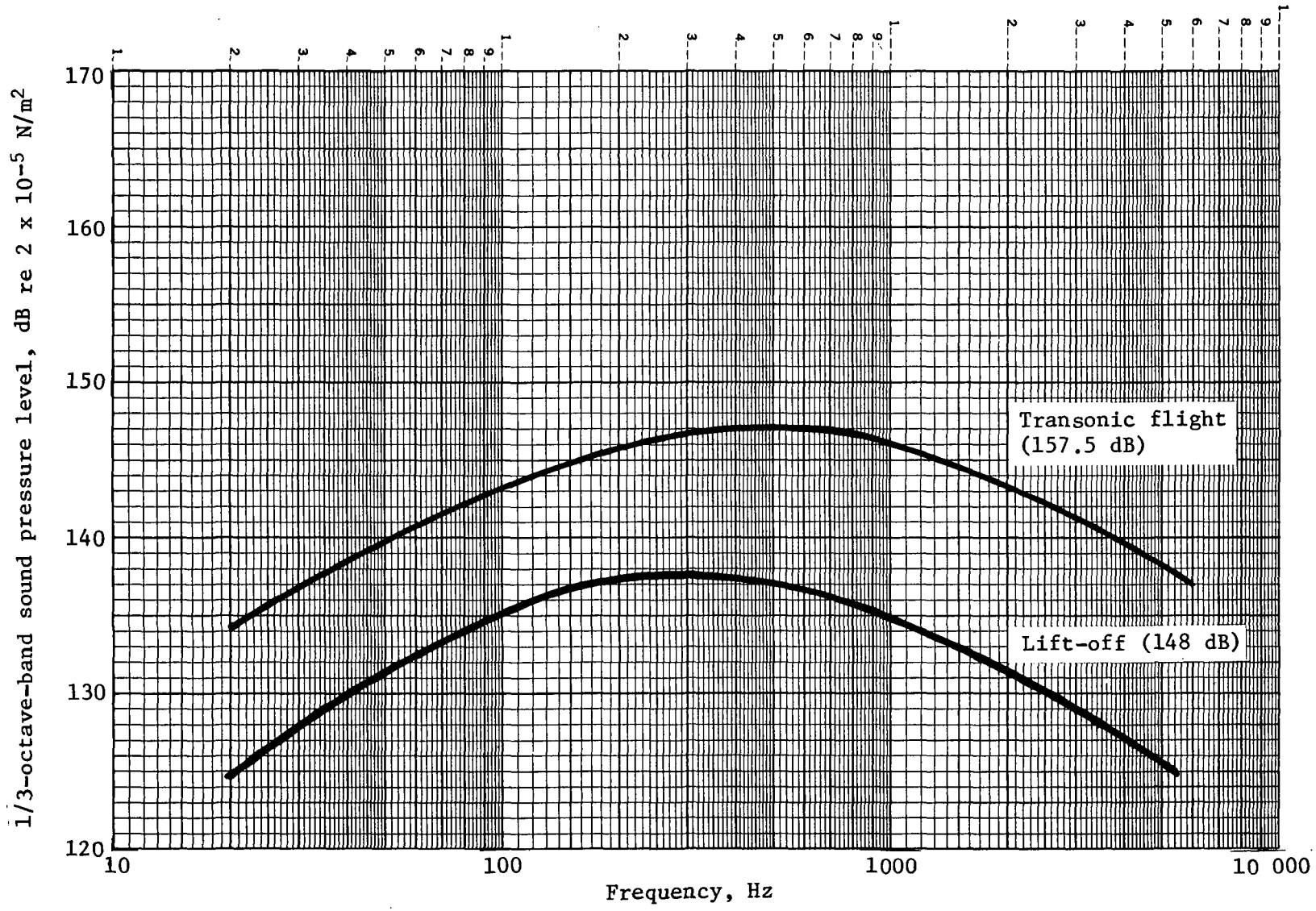

Figure 7.- Acoustic spectra outside space vehicle fairing.

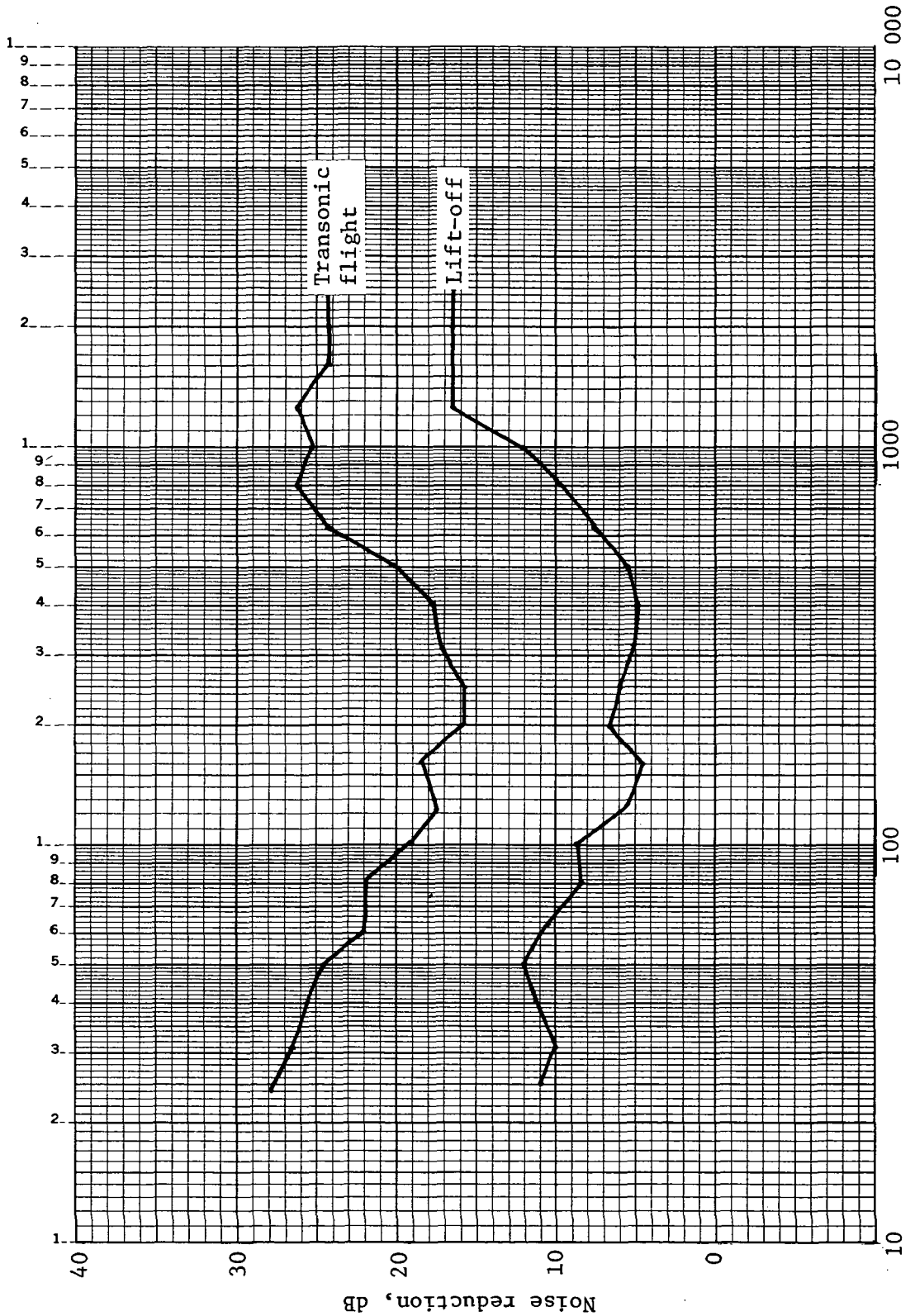

Figure 8.- Noise reduction spectra for space-vehicle fairing.

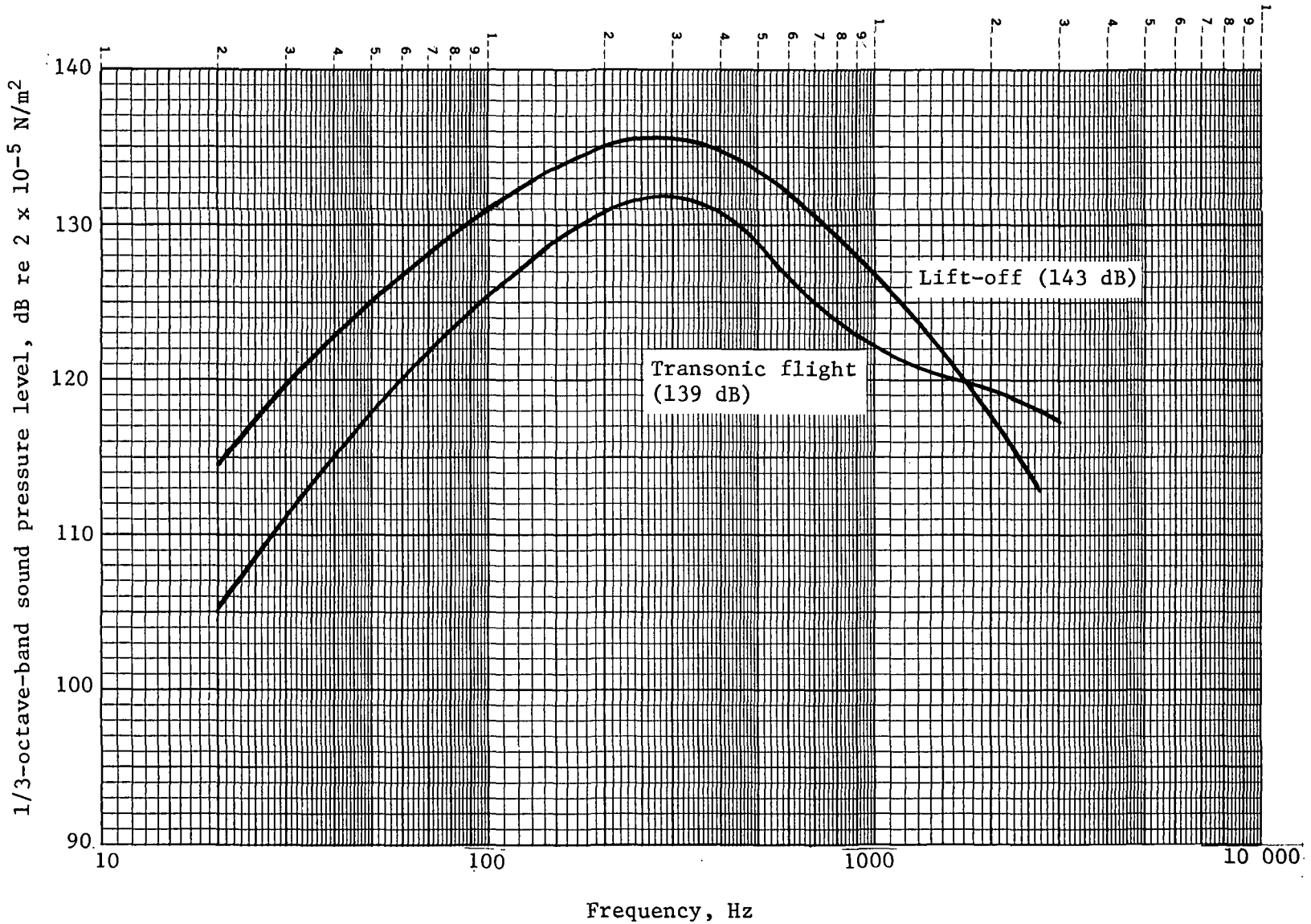

Figure 9.- Predicted acoustic spectra inside of fairing.

where:

P_1 = ambient pressure;

M_1 = free-stream mach number;

β = contour angle of blunt body;

and

$$f(M_1, \beta) = 1.35 \left(\frac{\gamma}{\gamma - 1}\right) (\sin^2\beta) \times \left\{(\sin^2\beta) \frac{1 - \gamma}{\gamma} - 1\right\} M_1^2 \qquad (2)$$

where:

γ = ratio of specific heats.

At the time of maximum dynamic pressure (max q) during Mars entry, the values of the parameters in equation (2) were predicted to be:

$P_1 = 42.6$ N/m^2 (0.89 psf) | $\beta = 1.22$ rad (70°)

$M_1 = 17$ | $\gamma = 1.1$

Values shown are for the specified worst-case atmosphere. Using these values, a maximum overall noise level of 114 dB was computed.

The second technique for predicting aeroshell boundary-layer noise is given in reference 2, which outlines a number of procedures for predicting entry acoustical environments for space vehicles. The boundary-layer fluctuating pressure coefficient (ΔC_p) versus Mach number for the recommended noise prediction procedure in reference 2 covers the Mach number range from 0 to 5. Characteristics of the data indicate that the data may be accurately extrapolated at least to Mach 6, so this extrapolation was performed, yielding $\Delta C_p = 0.001$. For conservatism, this value was assumed applicable to the aeroshell boundary layer at Mach 17 (max q), although the data show that ΔC_p decreases continuously at supersonic Mach numbers. The overall sound pressure level (OASPL) was computed using this ΔC_p and the worst-case atmosphere (max q) value in the relation

$$\text{OASPL (dB)} = 20 \log \frac{\Delta C_p \times q}{P_{ref}} \qquad (3)$$

where:

$\Delta C_p = 0.001$;

$q = 7928\ N/m^2$ (165.6 psf);

$P_{ref} = 2.011 \times 10^{-5}\ N/m^2$ (4.2×10^{-7} psf), dB scale reference pressure.

Maximum OASPL computed from this equation was 111 dB.

The noise spectrum shown in figure 10 was derived from plots of nondimensional power spectra of turbulent boundary-layer pressure fluctuations versus Strouhal number, referenced to boundary-layer displacement thickness (δ^*) and vehicle free-stream velocity (U_∞) in reference 1. An average spectrum plot was used to predict boundary-layer noise. This spectrum was converted from a power spectrum to a 1/3-octave-band pressure spectrum by the method of integration and computation of normalized decible levels for the 1/3-octave-band pressure values. The peak amplitude of the normalized pressure spectrum derived from reference 2 was at a Strouhal number (SN) of 0.36. This was equivalent to a frequency (f_p) of 49 kHz, as determined from the following relation

$$SN = \frac{2\pi\ f_p\ \delta^*}{U_\infty} = 0.36 \qquad (4)$$

where:

f_p = frequency

$\delta^* = 3.68$ mm (0.145 in.);

U_∞ = VLC velocity at max q = 3124 m/s (1.23×10^5 ips).

This value of δ^* was an average of the values predicted for the major part of the aeroshell surface at max q. It was obtained from the Viking Lander Capsule (VLC) Mars-entry aerodynamic analyses. Because noise criteria for the VLC (except base cover) were defined only from 20 to 10 kHz, that part of the noise spectrum defined in figure 9 does not include the peak of the predicted spectrum. The 1/3-octave-band amplitudes of the normalized fluctuating pressure spectrum were given values that provided an OASPL of 114 dB in the range of concern. This was the higher OASPL derived by using the two independent prediction techniques previously described.

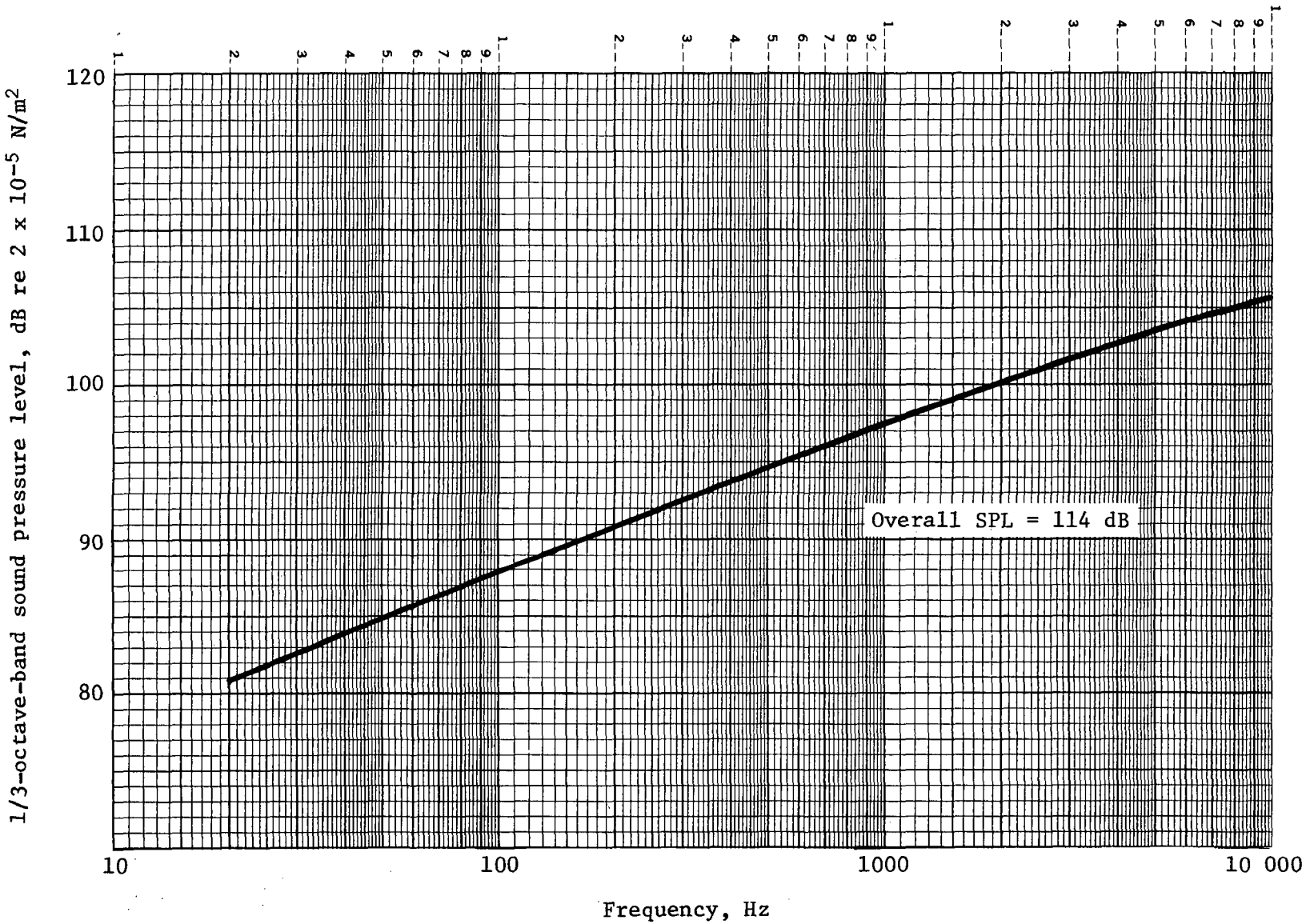

Figure 10.- Predicted aerodynamic noise spectrum for aeroshell during Mars entry.

The maximum aerodynamic noise environment of the base cover during entry transonic flight was predicted using the results of a wind-tunnel test of an 8% scale model of the VLC entry vehicles. Noise spectra were derived from the fluctuating pressure measurements recorded at five places on the model base cover during nine test runs conducted with selected aerodynamic parameters and 34 angles of attack. The spectra were adjusted by amplitude and frequency scaling factors to correlate with the full-scale VLC and Mars-entry aerodynamic parameters. The highest OASPL of the adjusted test data spectra was 121 dB.

Due to the tolerances on VLC model design, wind-tunnel test conditions, instrumentation, and the degree of accuracy of the data scaling technique, there is an estimated margin of uncertainty of 5 dB in the adjusted noise spectra. A flat spectrum was therefore defined (fig. 11) to describe the environment to which the base cover would be exposed during transonic flight, covering the range from 1 to 50 Hz, with 1/3-octave-band levels of 114 dB and an overall level of 126 dB.

The Viking Lander would be subjected to acoustic noise generated by the terminal propulsion engines for a maximum of 42 seconds during terminal descent, with significant noise levels occurring for about 17 seconds.

The sound power level (PWL) generated by a terminal propulsion engine firing in an Earth atmosphere was predicted using a technique involving empirical relationships developed from acoustic and engine parameter data acquired during rocket engine firings described in reference 3. The following relation was employed to calculate the predicted overall PWL of a terminal propulsion engine in an Earth atmosphere.

$$\text{PWL (dB)} = 96.1 + 13.5 \log \left(T \times I_{sp}\right) \tag{5}$$

where:

T = maximum engine thrust = 2224 N (500 lb);

I_{sp} = 227.5 seconds.

The overall PWL computed with this relation was 164 dB. Effects of Martian atmospheric properties on the generation and propagation of acoustic noise had to be determined. For a given engine, overall PWL generated is a function of the atmospheric pressure and speed of sound in the atmosphere:

$$\text{PWL} \propto \frac{P_a}{a_o^5} \tag{6}$$

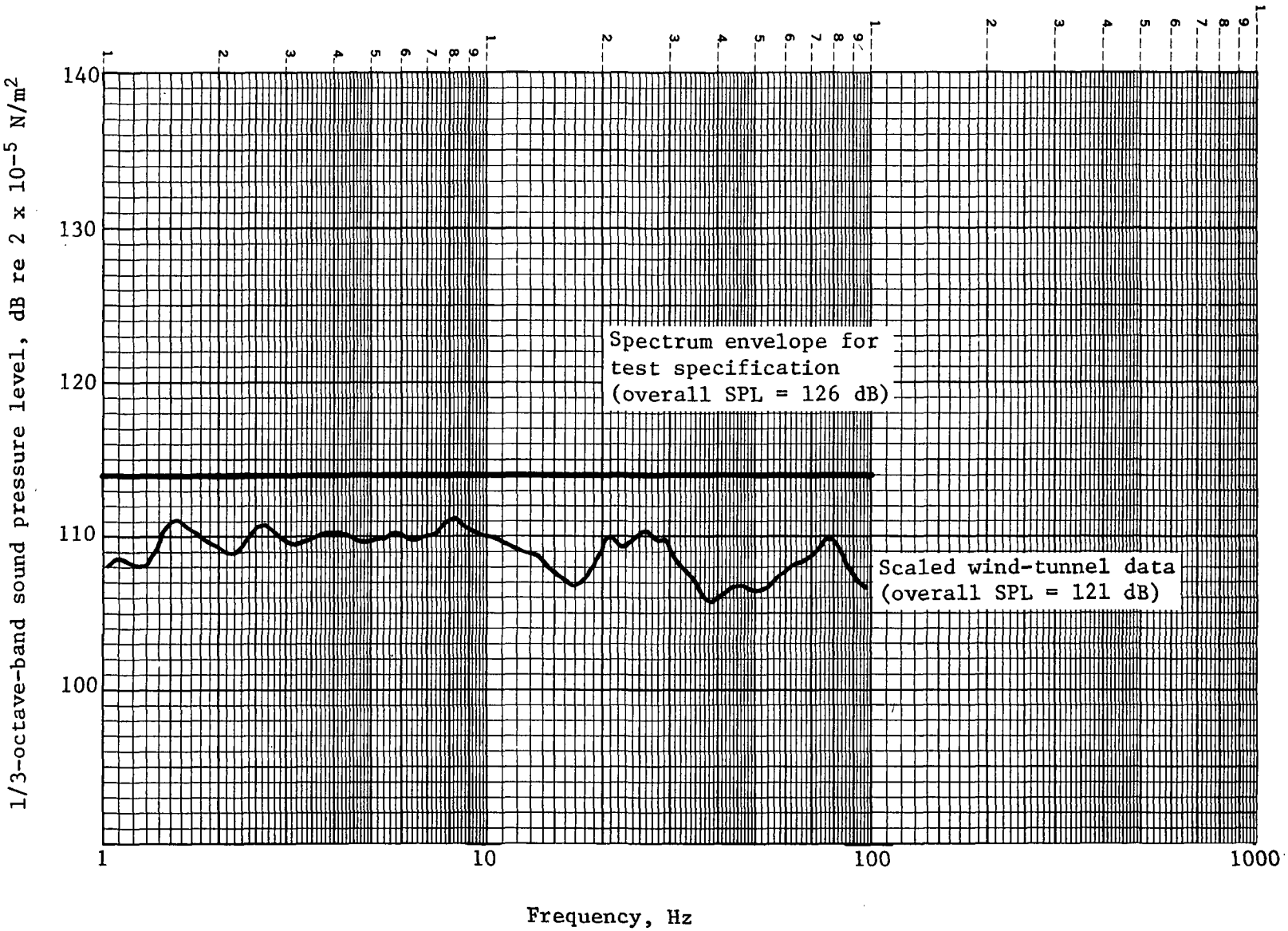

Figure 11.- Predicted aerodynamic noise spectra for base cover during Mars entry.

where:

P_a = pressure;

a_o = speed of sound.

For an example, see reference 4. The difference between the PWL generated in the Martian atmosphere and that on Earth was obtained using the ratio

$$\frac{PWL_M}{PWL_E} = \frac{\left(P_a / a_o^5\right)_M}{\left(P_a / a_o^5\right)_E} \tag{7}$$

where:

P_a = 100 N/m^2 (20.886 lb/ft^2) for Mars and 1.013 x 10^5 N/m^2 (2115.076 lb/ft^2) for Earth atmosphere;

a_o = 222 m/s (72.178 fps) for Mars and 344 m/s (128.609 fps) for Earth atmosphere;

subscripts M and E = Mars and Earth.

The ratio obtained with these atmospheric factors was 8.8 x 10^{-2}, equal to a PWL difference of -10.5 dB for the Martian atmosphere relative to the PWL on Earth. The propagation of sound energy in a given atmosphere is a function of the characteristic impedance of the atmosphere, ρa_o, where ρ is the density of the atmosphere and a_o is the speed of sound (ref 5.) The sound pressure level at a given point away from a noise source is related to the characteristic impedance by

$$P_{rms} \propto \left(\rho a_o\right)^{\frac{1}{2}} \tag{8}$$

The difference between the sound pressure level at a given distance from the source in the Martian atmosphere and from one on Earth was obtained from the ratio

$$\frac{\left(P_{rms}\right)_M}{\left(P_{rms}\right)_E} = \frac{\left(\rho a_o\right)_M^{\frac{1}{2}}}{\left(\rho a_o\right)_E^{\frac{1}{2}}} \tag{9}$$

where:

ρ = 2.86 x 10^{-5} g/cm^3 (1.785 x 10^{-3} lb/ft^3) for Mars and 1.225 x 10^{-3} g/cm^3 (7.647 x 10^{-2}) for Earth.

The ratio obtained with these characteristic impedances was 0.123 (-18.2 dB). Thus, the noise level at a given distance from a terminal propulsion engine was predicted to be 28.7 dB lower in the Martian atmosphere than in the Earth atmosphere. From Viking drawings, it was determined that all components were more than 0.5 m (1.64 ft) from the nozzle exit of the nearest terminal propulsion engine. In Earth's atmosphere, the sound pressure level at a point 0.5 m from the noise source was calculated to be 149 dB. The OASPL in the Martian atmosphere was then 149 - 28.7 = 120.3 dB. The effect of noise from the other two engines combined with that of the nearest resulted in the prediction of a maximum noise level of 122 dB for locations 0.5 m from a given engine. The spectrum shape shown in figure 12 was derived from acoustic measurements obtained during the firing of Titan IIIA liquid rocket engines. The frequency content of the measured data envelope was shifted upward by a Strouhal number of 5.8, calculated from

$$SN = \frac{\text{nozzle diameter x frequency}}{\text{exit velocity}}$$

Summary of acoustic levels.- Table 2 summarizes the overall SPLs predicted for the VLC.

TABLE 2.- SUMMARY OF ACOUSTIC LEVELS

Region	Overall SPL, dB re 2 x 10^{-4} dynes/cm^2				Spectrum shape shown in figure
	Lift-off	Transonic	Mars entry	Terminal descent	
Outside payload fairing	148	158			7
Inside fairing, outside bioshield	143	139			9
Inside bioshield, outside aeroshell	143	139	114		9 10
Inside bioshield, outside base cover	143	139	126		9 11
Inside aeroshell, outside Lander	140	136	111	122	9 12

Random vibration environment.- Random vibration levels resulting from the acoustic environments described in the previous section were estimated using established empirical prediction methods (references 6, 7, 8) summarized in reference 9.

Random vibration environments for Lander body-mounted components were developed using the Barrett method (ref 6). In the original method, vibration and acoustic data measured on Saturn

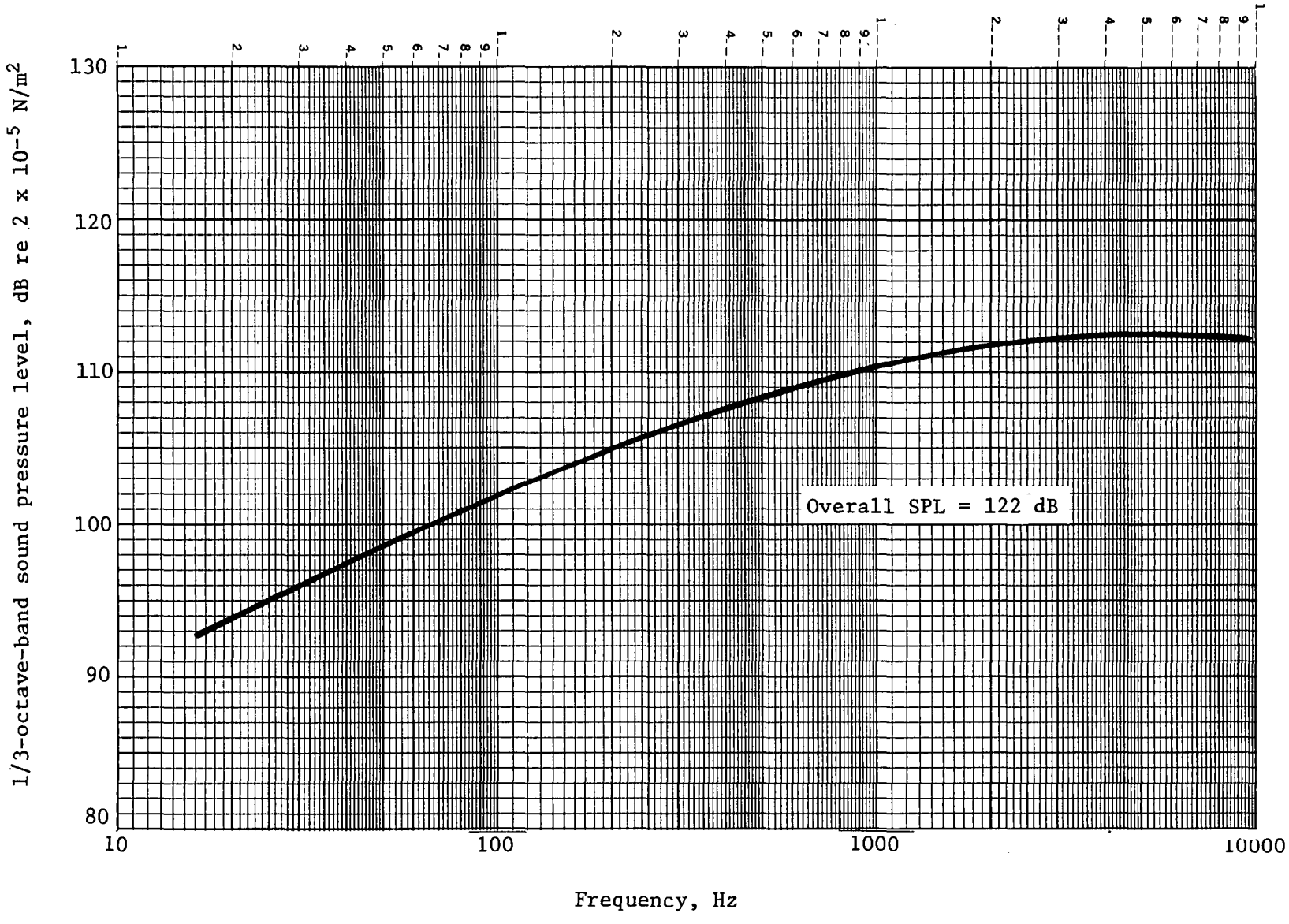

Figure 12.- Acoustic spectrum at upper surface of Viking Lander during operation of terminal descent engines.

vehicles were used as a reference base. For the Viking, acoustic data from previous Titan flights were used to modify the shape of the reference response spectrum. The method involved scaling acoustic pressure, surface density of the structure, and mass-loading effects to adjust the magnitude of the reference spectrum, in the following manner

$$A(f)_n = A(f)_r \left(\frac{P_n}{P_r}\right)^2 \left(\frac{\rho_r\, t_r}{\rho_n\, t_n}\right)^2 \left(\frac{W}{W + W_c}\right)_n \qquad (10)$$

where:

$A(f)$ = acceleration spectral density at frequency f;

P = rms acoustic pressure;

ρ = material density;

t = skin thickness;

W = weight of unloaded support structure;

W_c = weight of supported components;

subscripts n and r = "new" and "reference" vehicles.

The "Forward Bulkhead" reference spectrum (fig. 13, taken from ref 6) was used for body-mounted components.

Figure 14 compares typical Saturn V and Titan acoustic spectra at lift-off measured in the region of the payloads. It is evident from this plot that the Saturn launch environment includes considerably more low-frequency acoustical energy than the Titan launch environment. Figure 15 shows the predicted random vibration spectrum obtained by direct application of the Barrett method, and a modified spectrum that reflects the difference in the shapes of the Saturn and Titan acoustic spectra. The third curve in figure 15 envelopes the modified spectrum and is also drawn to satisfy the requirement for having an overall level of at least 6 g_{rms}. This was a Viking Project Office (VPO) citerion for the minimum flight acceptance (FA) test spectrum, based on recommendations developed by Simpkinson (ref 10) after a study of Apollo component test data.

For components mounted on the aeroshell, random vibration levels at lift-off were also derived by applying the Barrett method, modified as discussed above. In this case the "skin stiffeners" curve (fig. 16) was first used as the reference spectrum. For uniformity and testing convenience, it was decided to envelope the predicted environment using the spectrum shape derived for body-mounted components, with an overall level of 9.7 g_{rms}.

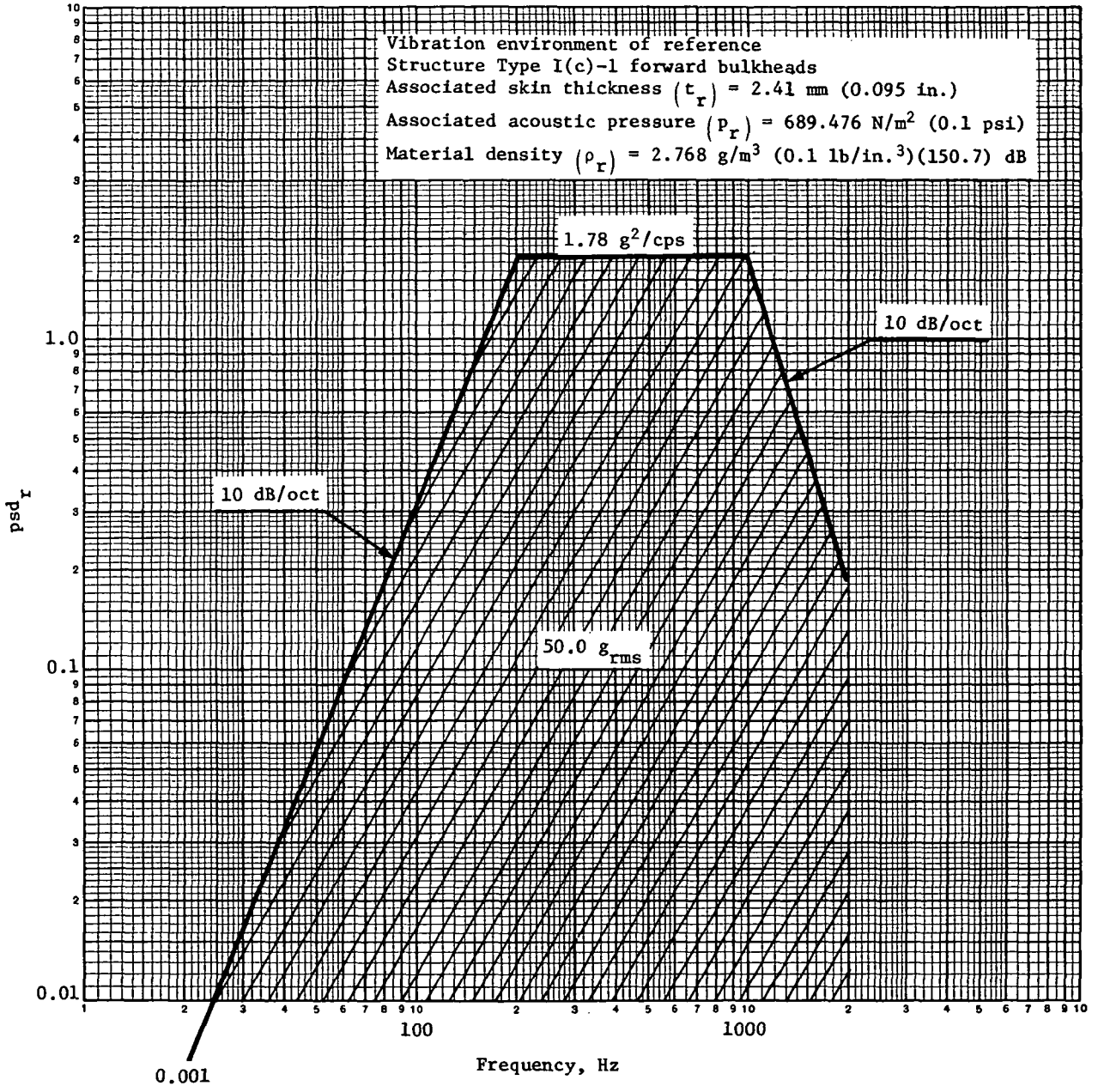

Figure 13.- Reference random environment, Type I(c)-1 - forward bulkheads.

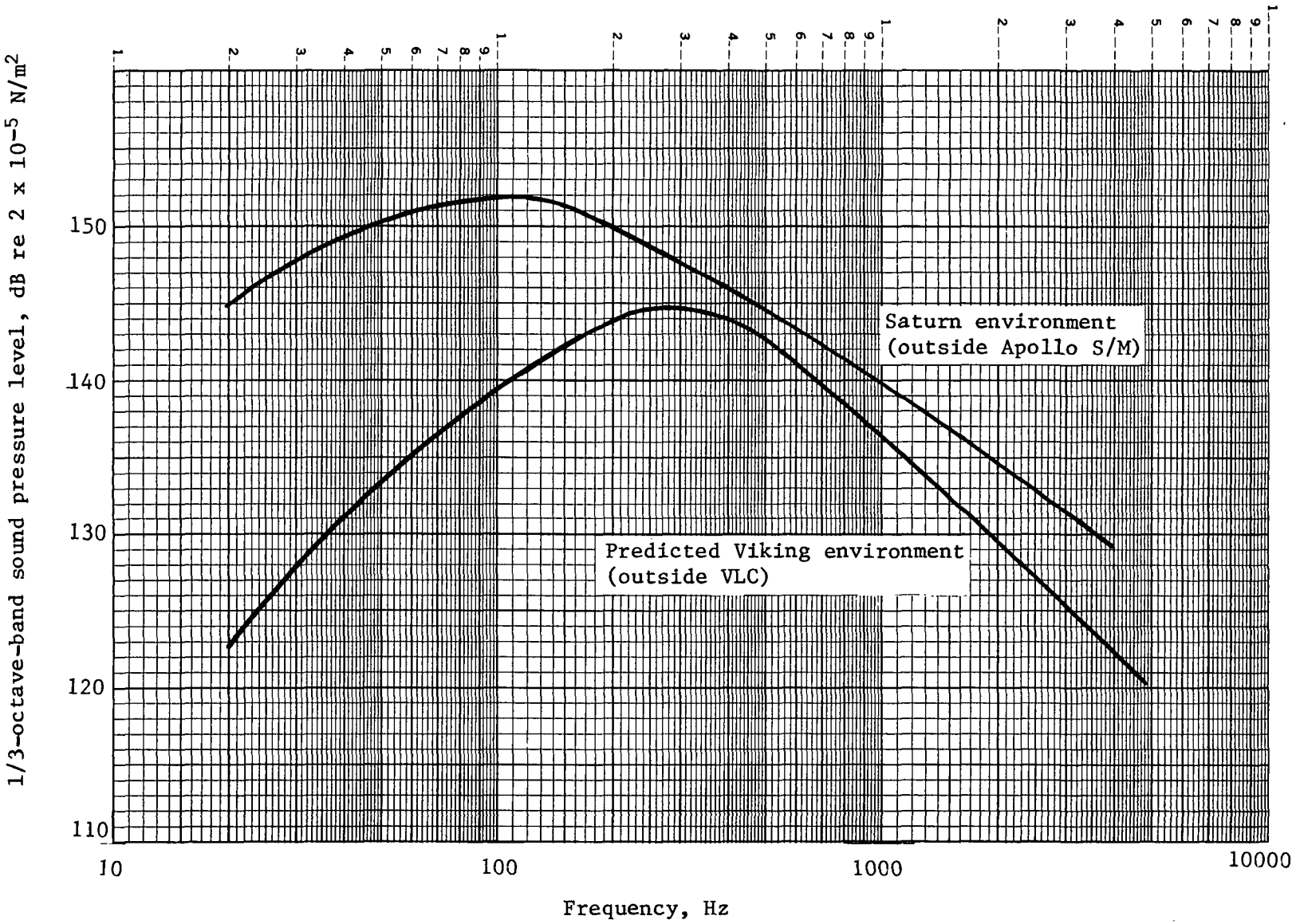

Figure 14.- Comparison of Viking and Saturn acoustic environments.

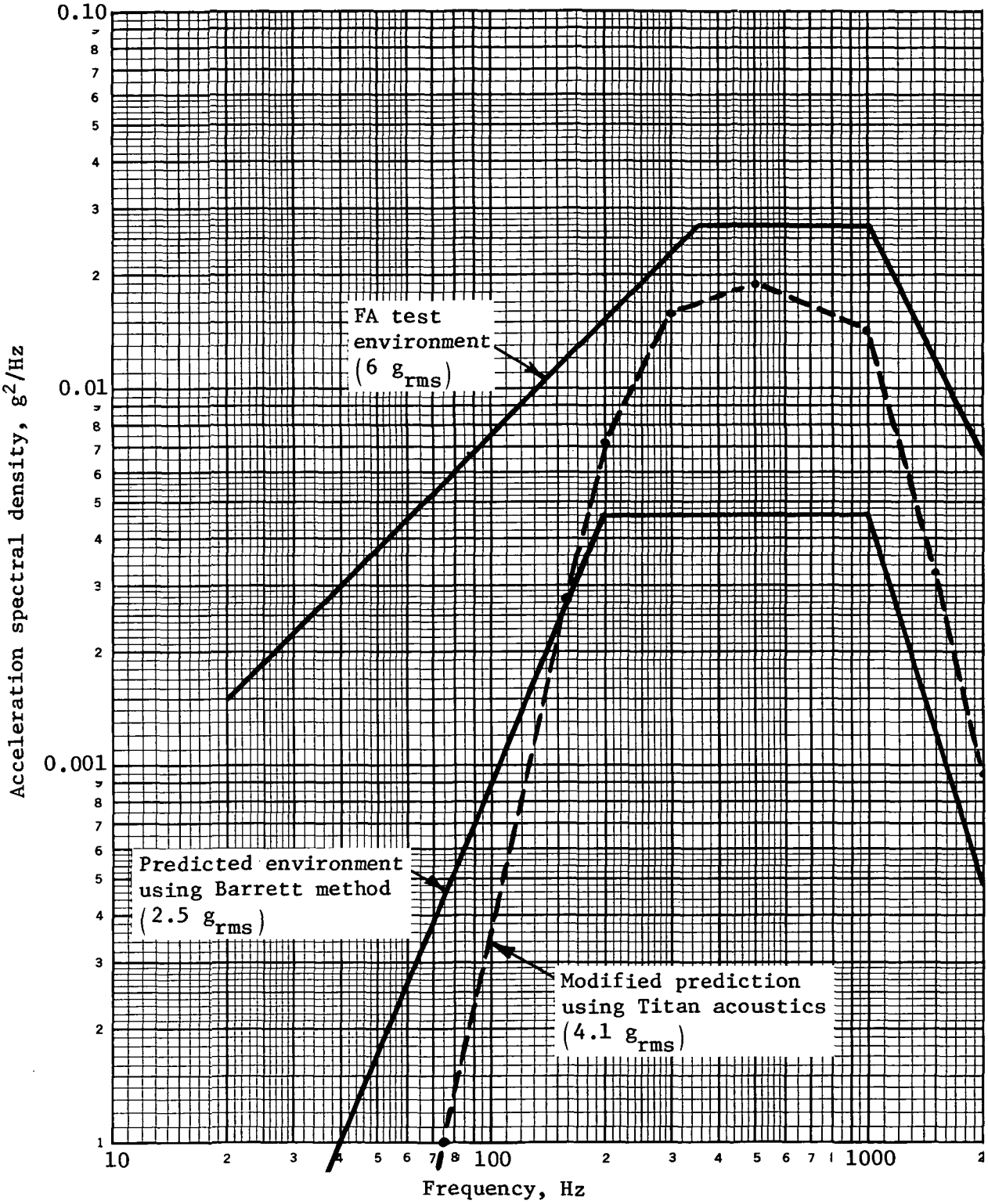

Figure 15.- Derivation of random vibration FA test spectrum for Lander body-mounted components.

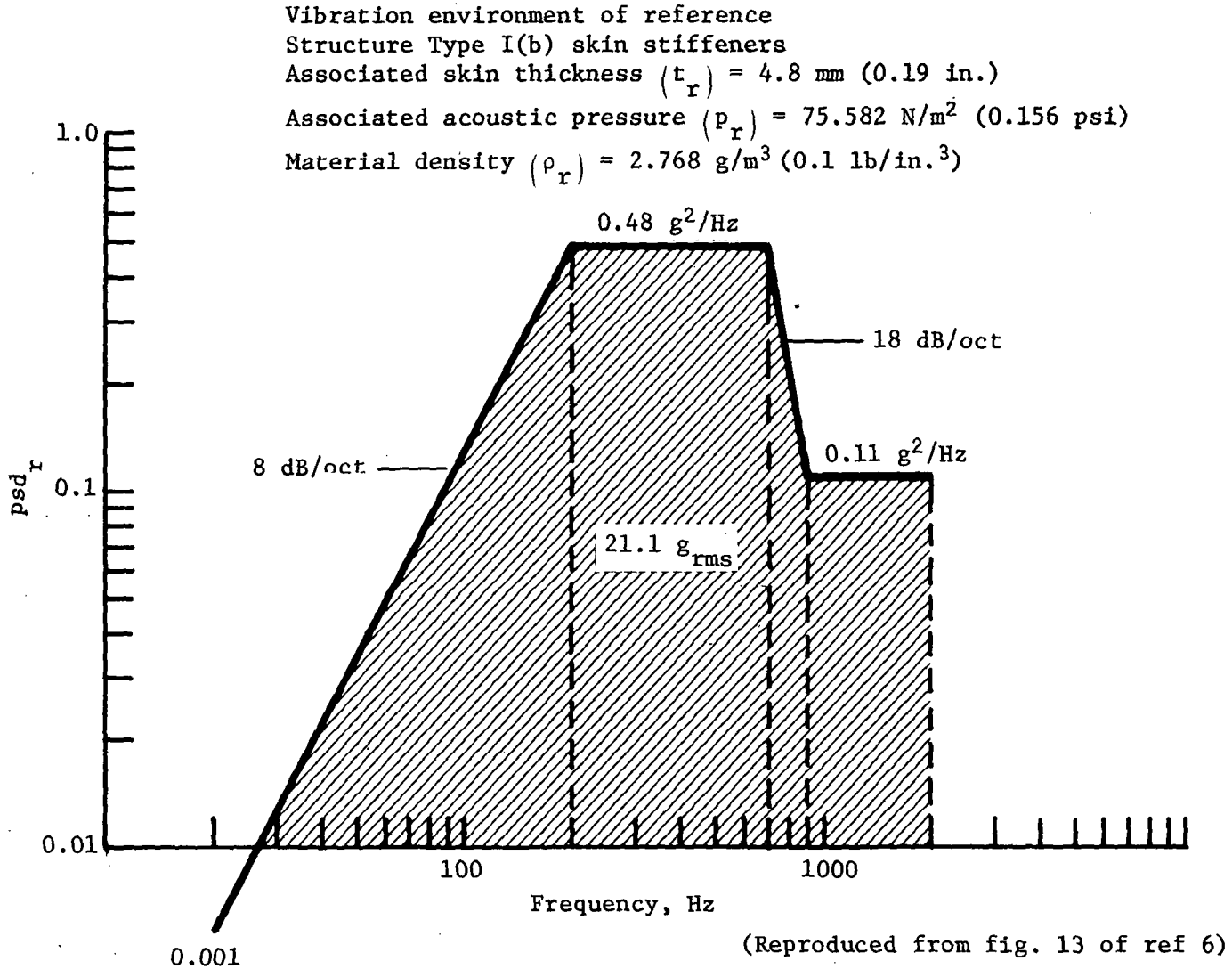

Figure 16.- Reference random environment, Type I(b) - skin stiffeners.

The random vibration environment for body-mounted components during Mars entry was estimated to be insignificant. For the aeroshell components in the entry condition, the Barrett method was again applied, leading to a spectrum with an overall level of 6.9 g_{rms}. Finally, for the body-mounted condition during terminal descent, mechanically induced vibration from terminal-engine operation was estimated by extrapolating vibration data measured on Titan vehicles during Stage I captive firings for engine components considered not responsive to the acoustic environment, so that measured responses were primarily mechanically induced.

The extrapolation relationship used for this estimate was

$$A(f)_n = A(f)_r \frac{N_n T_n D_r}{N_r T_r D_n} \tag{11}$$

where:

A(f) = acceleration spectral density at frequency f;

N = number of engines;

T = thrust per engine;

D = averaged weight of loaded structure where responses were measured;

subscripts n and r = new and reference payloads.

The parameters used for this calculation were

$A_r = 0.9\ g^2/Hz$ $N_r = 2$ $N_n = 3$

$T_r = 1\ 080\ 000$ N (242 750 lb)

$T_n = 2225$ N (500 lb)

$D_r = 1700$ kg (3750 lb)

$D_n = 500$ kg (1100 lb)

giving a value for the new spectrum peak of $A_n = 0.0095\ g^2/Hz$. Because the resulting spectrum was enveloped by the standardized 6 g_{rms} spectrum, the latter was again specified for FA tests.

Figure 17 summarizes predicted vibration environments for body-mounted and aeroshell-mounted components during launch, entry, and terminal descent.

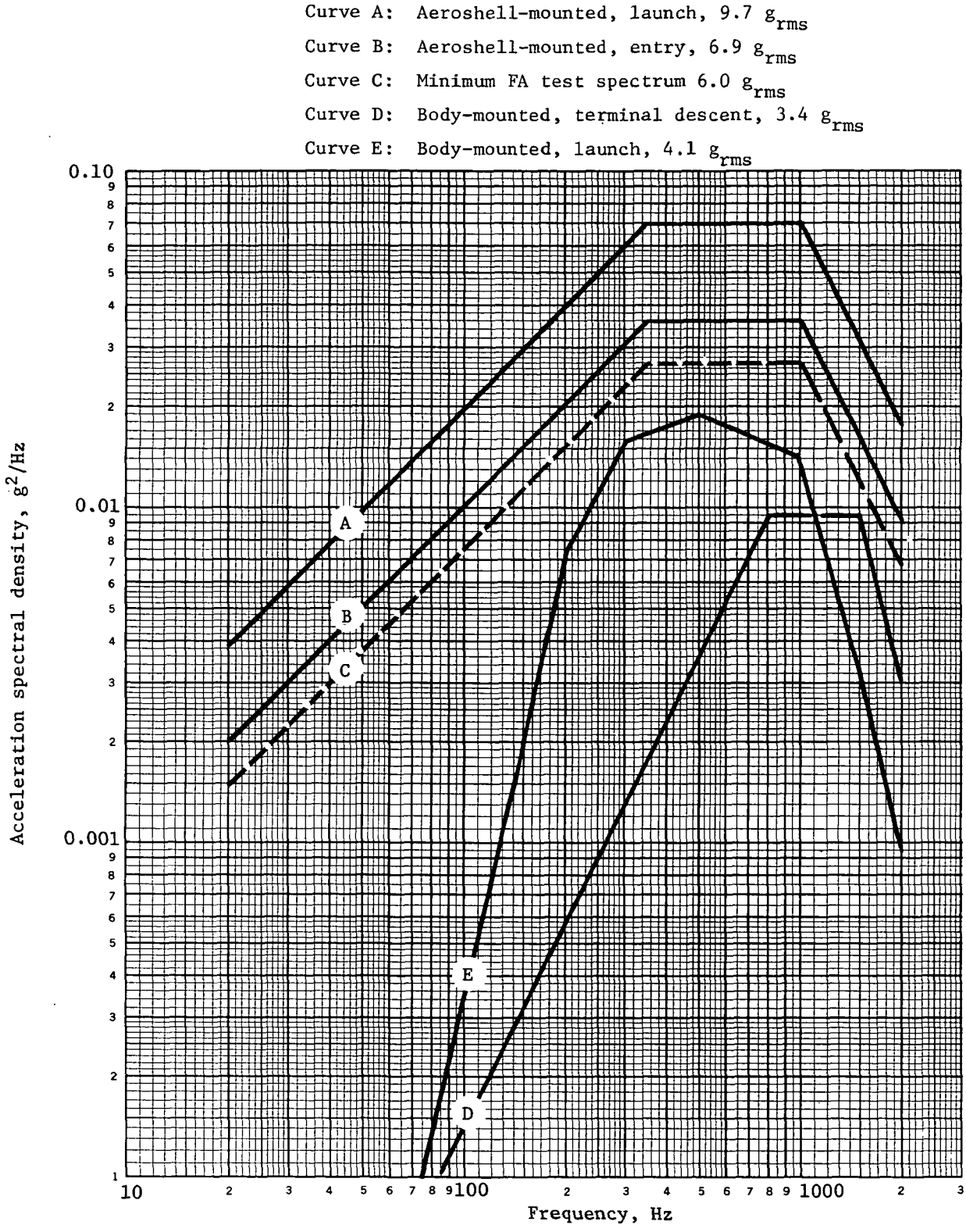

Figure 17.- Summary of predicted random vibration environments for VLC components.

Steady-state acceleration environment.- During the operation of the LV, VO, and VL propulsion systems, sustained accelerations were applied to the V-S/C in the forward direction of its longitudinal (flight) axis. This included five phases of LV powered flight: operation of the Titan III Stage 0, I, and II engines, and two burns of the Centaur engines. Also included were firings of the VO engine for midcourse maneuvers during interplanetary cruise and a firing for Mars orbit insertion and trim of the V-S/C in Mars orbit, which decelerated the vehicle. In this phase, an additional VO engine firing was performed to adjust the orbit of the VO for subsequent mission operations. Finally, the VL was subjected to sustained deceleration from operation of the terminal propulsion engines during terminal descent.

Table 3 shows maximum axial acceleration or deceleration applied to the LV, V-S/C, VO, or VL; corresponding thrust generated by the operative propulsion system; and weights of these vehicle configurations for each mission phase. Axial accelerations or decelerations shown were determined by the ratio of propulsion thrust to vehicle weight. Maximum acceleration applied to the V-S/C in any transverse axis, due to flight deviations of the thrust axis from the LV longitudinal axis, was predicted to be 1.5 g, occurring during Titan III Stage I flight.

TABLE 3.- STEADY-STATE ACCELERATION REFERENCE DATA

Mission phase	Event	Vehicle configuration	Propulsion system	Vehicle weight, kg (lb)	Thrust, N (lb)	Acceleration, g
Launch & trans-Mars injection	End of LV Stage I powered flight	Viking space vehicle	Titan III Stage I engines	63 500 (140 000)	2.33×10^6 (523 000)	3.74
Interplanetary cruise	Midcourse maneuvers	V-S/C	VO engine	3 520 (7 760)	1 335 (300)	<0.1
Mars orbit	Mars orbit insertion & trim	V-S/C	VO engine	2 340 (5 160)	1 335 (300)	<0.1
Mars orbit	Orbit adjustment	VO	VO engine	890 (1 980)	1 335 (300)	0.15
Terminal descent	End of engine operation	VL	Terminal propulsion engines	600 (1 324)	6 675 (1 500)	-1.13

Sustained deceleration was applied to the VLC in the direction of its flight axis during entry into, and descent through, the Martian atmosphere. This occurred during lifting entry, with aerodynamic forces acting only on the aeroshell, and during descent, with these forces also acting on the main parachute. Maximum-drag sustained deceleration at the time of maximum dynamic pressure (max q) during the entry phase was estimated to be 11.3 g. Maximum deceleration applied in the transverse axes due to angle of attack was not expected to exceed 2 g. Deceleration was analytically computed using current vehicle configuration and lifting entry-trajectory parameters. The principal parameters used in this computation were:

VLC weight	958 kg (2 113 lb)
Entry velocity	3 110 m/s (10 200 fps)
Entry angle	-0.34 rad (-19.5°)
Lift/drag ratio	0.135
Mars atmosphere	Minimum scale height.

These parameters define the most severe dynamic pressure environment, and hence the highest deceleration load applied to the VLC of any prospective combination of vehicle configuration, entry trajectory, and Martian atmosphere. The max q computed for this worst-case set of parameters was 7930 N/m^2 (165.6 psf).

Maximum transient deceleration applied to the VLC during parachute deployment was calculated to be 8 g, reducing to 1 g in about 12 seconds.

Transient vibration environment.- The Viking Engineering Steering Group set up a team to identify and evaluate sources of booster-induced transient vibration, and establish a sinusoidal test requirement and techniques to cover this frequency range. Other transient events like landing and pyrotechnic shock are treated in later sections. The test team comprised personnel from Langley Research Center, Martin Marietta, and the Jet Propulsion Laboratory.

The Viking spacecraft was subjected to transient vibration at several points in the Mars mission. Based on results of Titan IIIC and IIID loads analyses and actual measurements on the Titan IIIC vehicle, lateral wind-induced oscillations of the launch vehicle on the pad were predicted to cause maximum amplitudes of 0.35 g at frequencies of 0.5 to 1.0 Hz. Actuation of launch-vehicle prevalves immediately before engine ignition also caused transient vibratory inputs to the spacecraft, estimated to be:

Axis	Frequency, Hz	Amplitude, g
Longitudinal	11	0.5
Pitch	11	1.25
Yaw	11	1.0

During the launch phase, eight flight conditions caused significant transient vibration: liftoff, transonic buffeting, SRM separation, Stage I ignition, Stage I shutdown, Stage II shutdown and the two Centaur main-engine cutoffs (MECOs I and II). Environments caused by these events were estimated using many thrust-time histories available from previous Titan and Centaur flights. These were applied as forcing functions to the spacecraft mathematical model, and the maximum response time history for each flight condition was calculated at the VO-VLC adapter-truss tie points. This technique was used to estimate the environment in the frequency range below 40 Hz, for which modal properties of the spacecraft structure could be modeled with confidence (fig. 18).

For the frequency range above 40 Hz, the estimate of the environment at the spacecraft was based on a review of flight data from a wide range of large launch vehicles, including Thor, Saturn, Atlas/Centaur, and Atlas/Agena (ref 11 through 14). In the judgment of the test team, the most applicable flight data came from the Mariner Mars 1969 and Surveyor programs.

The acquired transient vibration data were transformed to "equivalent" sinusoidal levels using the following approach:

1) The response shock spectrum for each transient event was computed using Q = 20, the amplification factor used previously in analyses of Mariner and Surveyor data;

2) The assembly of shock spectra was enveloped with a single curve (fig. 19);

3) The envelope was modified for uncertainties, as described below;

4) The modified envelope was divided by Q.

JPL developed this technique, and it was used on subsequent NASA/LRC-managed space programs such as Lunar Orbiter (ref 14).

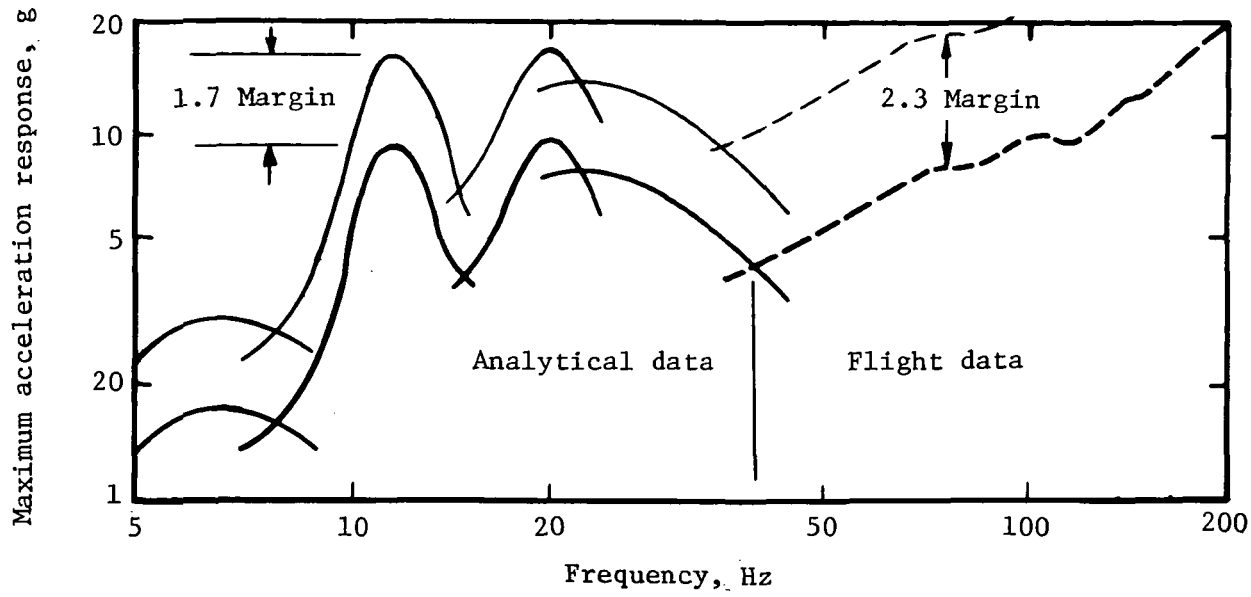

Figure 18.- Enveloped shock spectra from analytical and flight data.

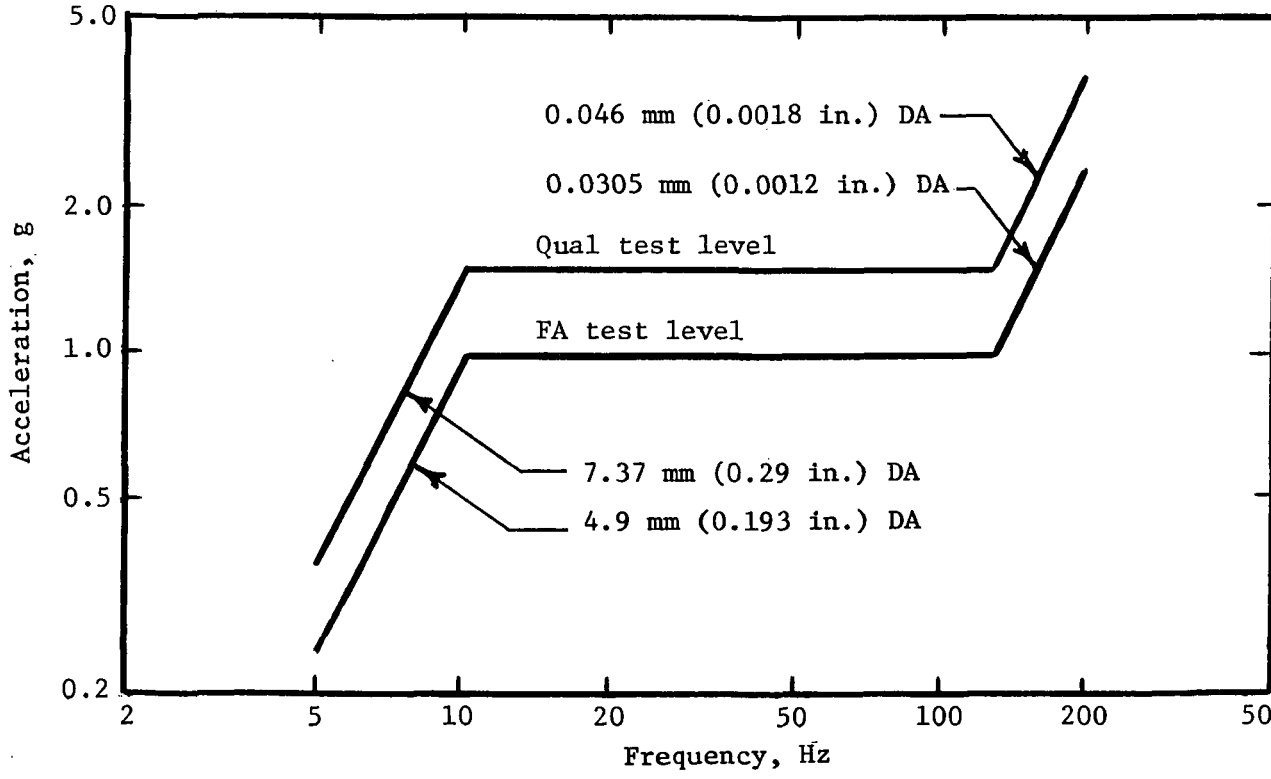

Figure 19.- Viking Spacecraft sinusoidal test spectra.

The shock spectra were modified to account for a number of possible sources of error by evaluating the degree of uncertainty associated with each source, then combining the various effects. This process was carried out separately for the analytical data (<40 Hz) and the measured flight data (40 to 200 Hz), as discussed below. The team selected uncertainty factors strictly on the basis of their experience and engineering judgment.

Analytical data:

1) Test mechanization tolerances--A sine test tolerance of ±10% is commonly used; to allow for the possible 10% undertest, a margin of 1 dB (12%) was used.

2) Damping factor assumptions--The value of damping selected for use in the sine-vibration/shock-spectrum equivalence directly affects the sine-test level. A margin of 3 dB (41%) was allocated to this source.

3) Modeling uncertainty--Because the mathematical models used were in their early development stages, a margin of 3 dB (41%) was included.

4) Boundary conditions--Flight transients simultaneously excite the spacecraft in all six degrees of freedom; however, the test is conducted one axis at a time. Also, the impedance of the test fixture differs from that of the launch vehicle. To account for these differences, a 3-dB margin (41%) was selected.

   The RSS combination of these random percentage errors yields an overall uncertainty of 72% on the analytical data, giving a factor of 1.72.

Flight data:

Uncertainties associated with flight data include the effects of test mechanization tolerances and damping-factor assumptions discussed in 1 and 2. The following sources also contribute:

5) Spatial variations within the spacecraft--Flight measurements from previous spacecraft were assumed to represent the most severe environment based on the spatial variation of accelerations measured on Mariner '69; a margin of -0, +4 dB (treated as 30 ±30%) was used.

6) Flight-to-flight variations--Flight data were obtained from a limited number of flights, with no assurance that they represent the environmental extreme. Inspection of flight data scatter indicates that a reasonable margin would be -0 +3 dB; this was treated as 20 ±20%.

7) Structural differences between Viking and reference spacecraft--A 3-dB margin (41%) was included for these differences.

8) Instrumentation tolerances--A margin of 2 dB (25%) was considered reasonable to allow for possible uncertainties in telemetered data.

Combining random flight data uncertainties by root sum squaring yielded an overall uncertainty of 73%. The two constant errors (5 and 6) produced an additive uncertainty of 53%, for a total uncertainty of 126%, or a total factor of 2.26.

As shown in figure 18, the spectrum was modified by increasing the "analytical data" band by a factor of 1.7 and the "flight data" band by 2.3. Division by the amplification factor (20) gave the amplitude of an equivalent swept sine wave, which established the level for the spacecraft Flight Assurance (FA) test. As shown in figure 19, a factor of 1.5 was applied to establish the Type Assurance (TA) or qualification levels.

The sinusoidal environment thus obtained was used as the basis of a system-level swept-sinusoid test. Because this test subjected the components to an environment not covered by other tests, it was necessary to derive appropriate sinusoidal test criteria for the components. In the absence of measured transfer-function data on the spacecraft, analytical modeling was used. The model comprised 2800 structural degrees of freedom, which were collapsed to 240 dynamic degrees of freedom. These were used to calculate mode shapes and frequencies. A normalized acceleration input tuned to each modal frequency was then applied to the model to calculate maximum in-line and cross-axis responses at 22 representative component locations, for a total of 22 x 3 x 3 = 198 transfer functions. Finally, these were used with the specified system-level test input to calculate environments at the component locations.

Pyrotechnic-shock environment.- Because of the many pyrotechnic devices on the Viking Spacecraft and their close proximity to component locations, it was necessary to qualify many components for the high-intensity shock environment caused by the pyro devices. A number of different types of devices--separation nuts, pin pullers, valves, and tube and cable cutters--were used. Each type had different shock characteristics and so affected nearby components differently. Also, the shock environment at each component due to a particular source varied according to its distance from the source and the nature of intervening structure. Thus, specified test criteria for components had to be adequate to cover all sources affecting the components.

Component environments were derived using the following approach:

1) Identify pyro sources and their relationship to component locations--this includes shock path distance, type of structure, and number of joints between source and component;

2) Establish shock spectra for various pyro sources;

3) Calculate distance attenuation effects on first component;

4) Calculate joint attenuation effects on first component;

5) Draw attenuated shock spectrum at first component for each pyro source--envelope these spectra with a single shock spectrum;

6) Repeat for all other components.

Source shock spectra were established for the various pyro devices on the basis of test data acquired at Martin Marietta and elsewhere. Figure 20 shows the source spectra used for separation nuts, ordnance valves, pin pullers, and tube and cable cutters. It was found that better data consistency was obtained by measuring source environments at a point 10.2 to 12.7 cm (4 to 5 in.) from the pyro device, rather than on or immediately next to it. This is now standard Martin Marietta testing procedure.

Due to several effects, pyrotechnic shock is attenuated as the shock passes through the structure. Considerable attenuation is a function of shock path distance, at a rate depending on the type of structure. There is additional attentuation at mechanical joints in the structure. Although other conditions like redundant shock paths, abrupt changes in cross section, and changes in material are part of the overall attenuation picture, their separate contributions are difficult to identify and are ignored in this approach. Consideration is thus restricted to the effects of distance and joints.

Reference 15 describes a thorough investigation of the distance attentuation phenomenon, drawing on test data from many sources to show curves of attenuation versus distance for several types of structure. The curves in figure 21 are those most applicable to the V-S/C structure. Using this figure, the source shock spectrum is modified in two steps to account for distance effects. In the first step, the ramp or straight-line portion of the spectrum is lowered by an amount shown as a function of shock path distance. In the second step, the spectrum peak is reduced as indicated. A new spectrum is then fitted to these reduced values, and finally adjusted for joint attenuation effects.

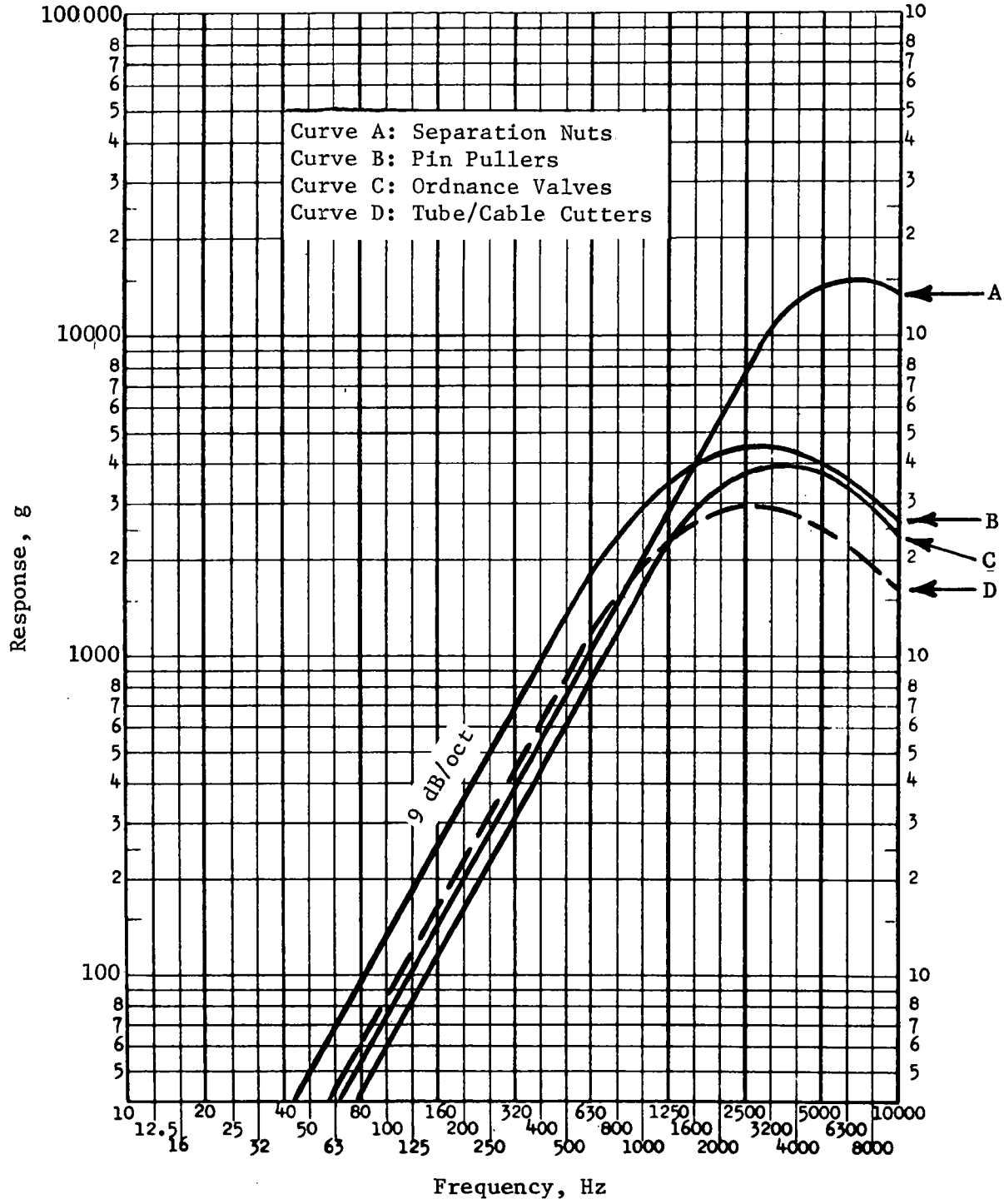

Figure 20.- Source shock spectra for Viking pyrotechnic devices.

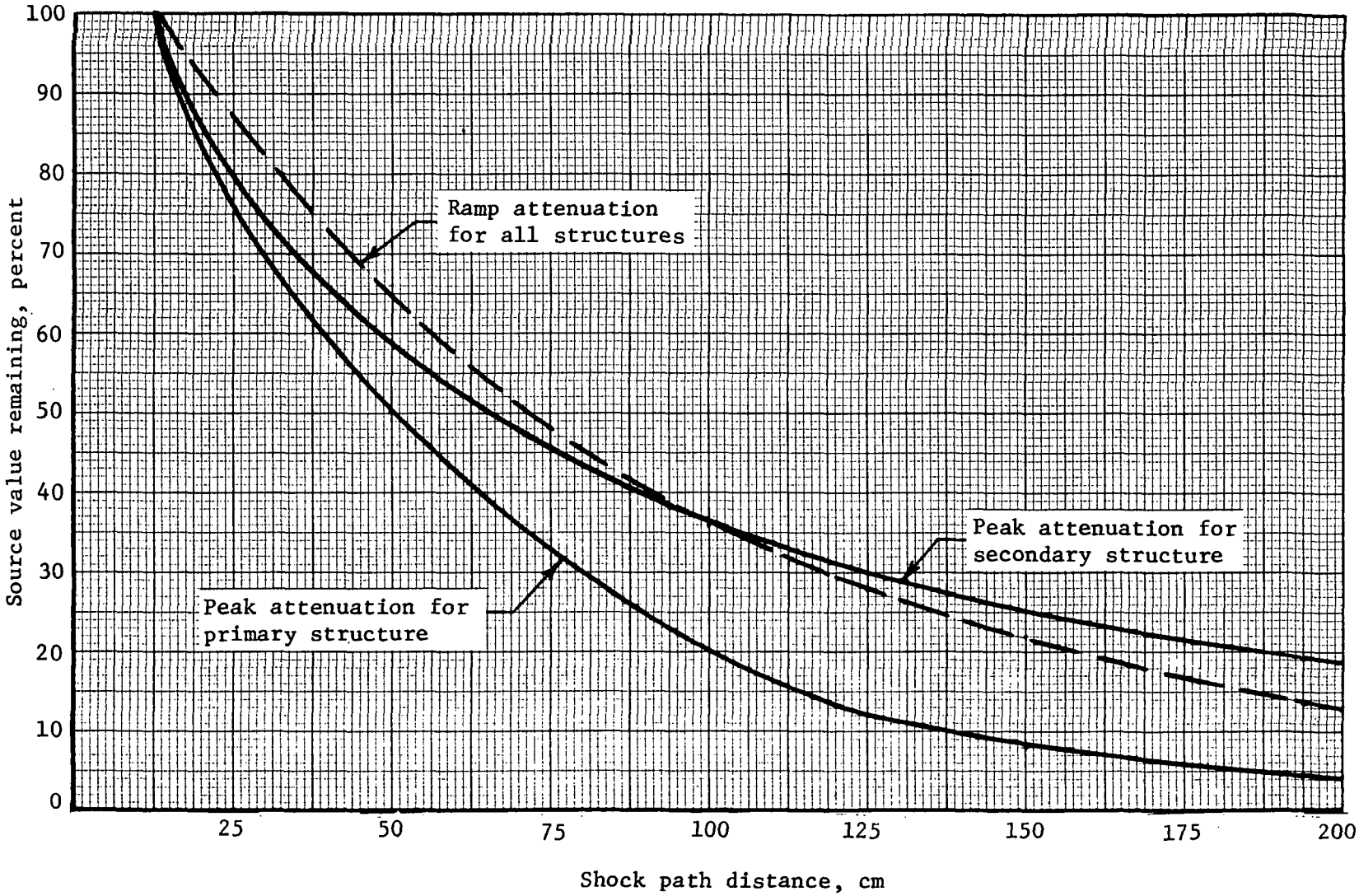

Figure 21.- Distance attenuation curves for pyrotechnic shock.

Tests performed shortly after the start of the Viking Project (reported in ref 16) indicated that when a shock wave passes across a bolted joint, the peak of the input shock spectrum is reduced by 40 to 70%. The effect on the ramp of the spectrum was not consistent, so to ensure adequate conservatism, an attenuation of 40% on the spectrum peak for each joint (up to a maximum of three joints), was selected, with no attenuation applied to the ramp of the spectrum. This approach was used to predict pyrotechnic environments at all VLC component locations.

The prediction technique was later evaluated using data measured on the Pyro Shock Test Bed (PSTB)--a full-scale model Lander body containing mass-simulated components. Pyrotechnic devices were mounted on the PSTB and fired. The resulting environment was measured at four component locations. The data acquired were compared with predicted values at the same locations (fig. 22). It can be seen that the prediction technique gave good results for the four locations investigated. Peak values of the shock spectra are predicted quite well, but acceleration levels in the middle frequency range (100 to 1000 Hz) tend to be overestimated. For the Viking Project, this was considered an acceptable margin. However, because most components will have natural frequencies in this range, the degree of overtest introduced may be unacceptable on future programs.

Data for further checks on the prediction technique were obtained from the system-level base-cover separation test on the Proof Test Capsule (PTC), described in a later section. Figures 23a through d show predicted environments and corresponding measured spectra at four points on the PTC. The results of this comparison supported the preliminary conclusions that the peak value of the shock spectrum is predicted quite well but the middle frequency range is overestimated. Figure 23a relates to a point on the structure that has no joints in the shock path; Figures 23b, c and d involve one, two, and three joints, respectively. Figures 23c and d show an increasing margin in the middle frequency range. This behavior is further discussed in the section on the Applications to Future Payloads.

Landing shock environment.- The magnitude of the landing shock environment experienced by VLC components and structure could only be predicted in probabilistic terms because it was very dependent on such randomly varying parameters as the slope and roughness of the surface at the landing site, as well as descent velocity and VLC inclination angle. Obviously, these can only be estimated within a fairly wide range of values and will be subject to random fluctuations.

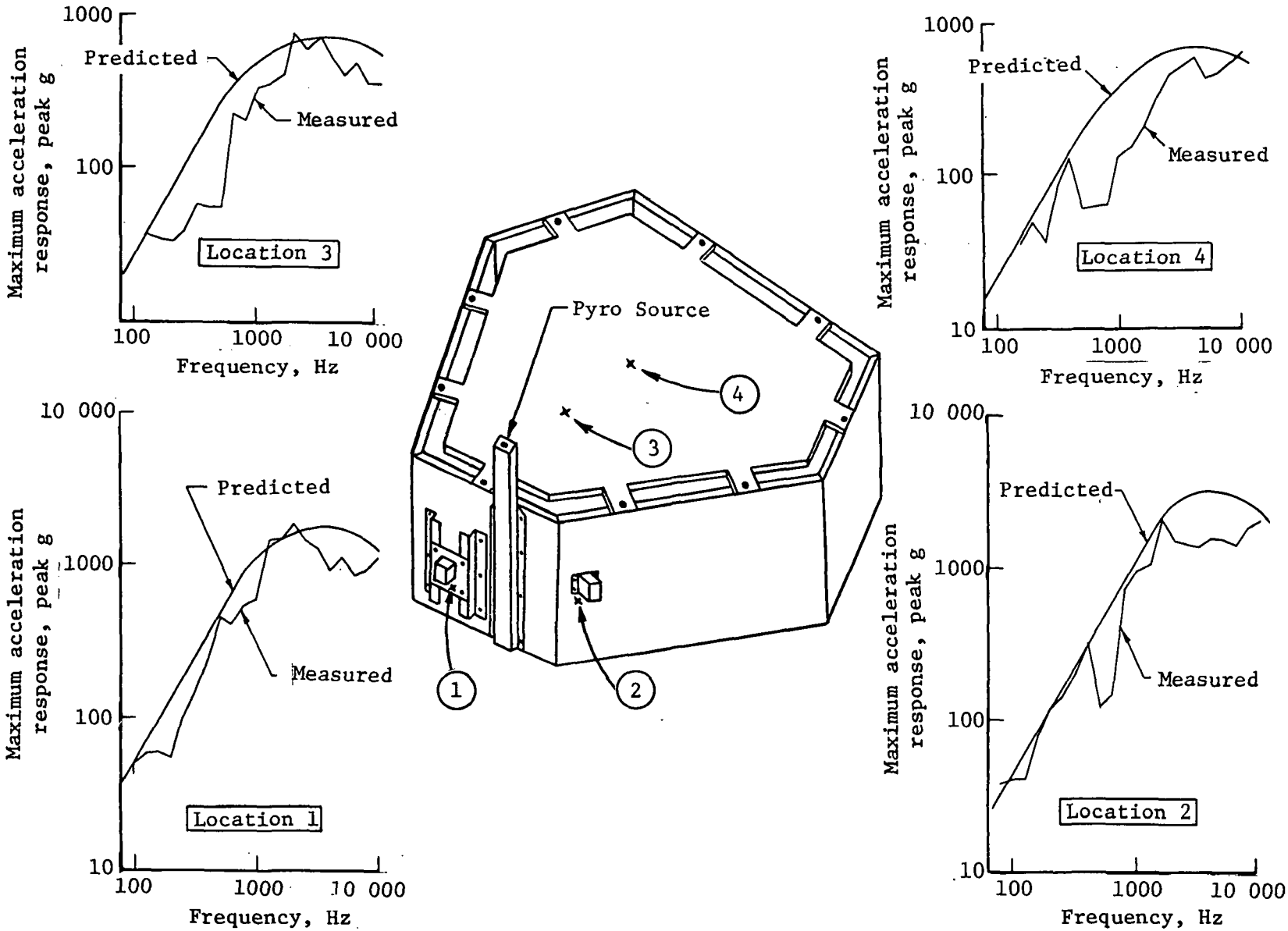

Figure 22.- Comparison of predicted versus measured pyro shock environments on the Pyro Shock Test Bed.

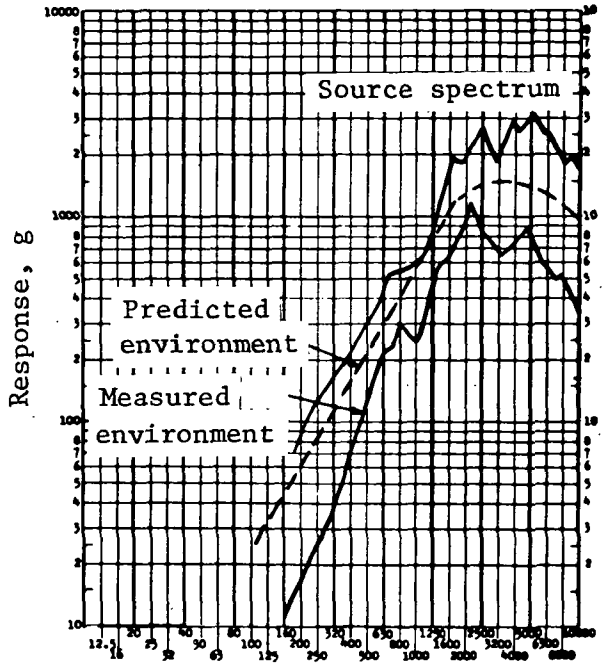

a. No joints

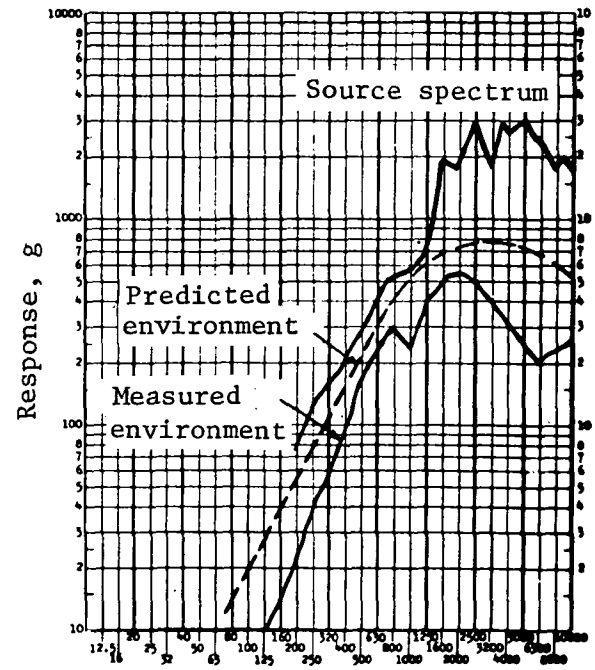

b. One joint

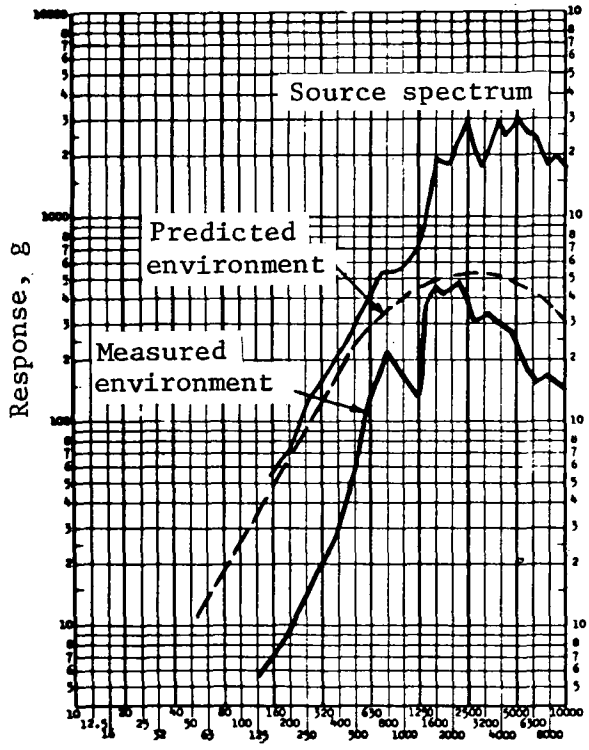

c. Two joints

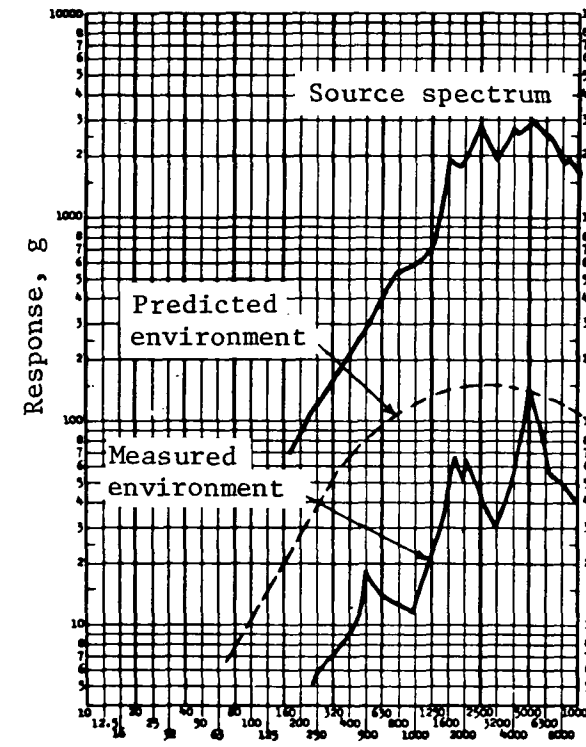

d. Three joints

Figure 23.- Comparison of predicted versus measured pyro shock environments on Proof Test Capsule.

To calculate the range of possible landing shock environments resulting from combinations of touchdown parameters, a Monte Carlo technique was used to randomly select values of these parameters from a population of 300 landing events. Statistical characteristics for the parameters (mean, standard deviation, etc) were derived from the Guidance and Control System specification values. A Monte Carlo population of 300 events was selected so that the extremes observed in the sample results would consitute design limit values; i.e., they would have a probability of nonexceedance equal to the mean plus 3σ probability level (0.997) for normally distributed (Gaussian) populations.

The sample population of 300 sets of initial condition values at touchdown were input to a rigid-body landing-dynamics program to generate landing-gear forces and terminal-descent engine thrust forces as functions of time. These forces were then used to drive an elastic-body model in the time-domain landing transient-response analysis.

Confidence in the analytical model and response prediction techniques for the landing event was established by correlation studies performed after the Lander drop test series in early 1973. Good comparisons of analytical and experimental forcing functions, response time histories, and acceleration shock spectra confirmed the adequacy of the methods.

Landing-gear strut loads computed for the sample of 300 Monte Carlo landing events were used to excite the elastic Lander math model to predict acceleration time responses at selected mass collocation points. These points represent either component mass cg locations or structural mass collocation locations at or near the mounting interface of components on the structure.

The time response analysis used a total of 70 modes (6 rigid body + 64 elastic), with scaled elastic modal frequencies from about 32 to about 164 Hz. A value of 2% of critical damping was used for all modes. This was expected to yield generally conservative (high) response accelerations because ground vibration survey test data indicated nominal damping values of 2.5 to 3.5% for most of the structure. The assumed damping was known to be extremely conservative for components mounted through nonlinear shock isolators (Tape Recorder, Inertial Reference Unit and Terminal Descent/Landing Radar antenna), but the analysis was not amenable to using the "correct" damping because mode shapes for these components were not uniquely separable from general structural modes, and because the degree of damping was highly dependent on the magnitude of the applied acceleration.

As part of this analysis, maximum and minimum accelerations for each response degree of freedom were sorted out of all time slices of all landings. In addition, the extreme accelerations of the time-consistent vectorial combination of the translational-response degrees of freedom at component cg points sorted out of all time slices from all landings were defined to be design-limit load factors for the landing event.

Acceleration time responses at the selected component and interface degrees of freedom were spectrally analyzed for all 300 landings. This was done to determine the comparative severity, in the frequency domain, of the component environment imposed by the Mars landing versus that imposed by the component landing shock qualification test (30-g peak, 22-ms half-sine input).

The technique used to make this determination was a standard shock spectrum analysis in which a series of mathematical single-degree-of-freedom oscillators, each "tuned" to one-third-octave frequencies between 10 and 200 Hz, were base excited by the acceleration time histories computed for the selected response degrees of freedom. A comparison of shock-response spectral curves resulting from different transient time histories thus indicates the relative severity of the acceleration time histories at each spectral frequency.

The resulting peak response accelerations for each degree of freedom for all 300 landings were enveloped to identify the maximum peak value at each spectral frequency. Landing-shock spectral responses were computed using 5% damping (Q = 10).

Figures 24 and 25 show typical shock spectrum plots from the analysis. Each plot includes four curves, identified as the enveloped shock spectra for the X, Y, and Z axes, and, for comparison, the shock spectrum corresponding to the 30-g 22-ms half-sine pulse used for the component qualification test. Figure 24 indicates that the Biology Mechanical Subsystem (MSS) was adequately qualified by the 30-g test, whereas figure 25 shows that this test was not adequate across the full frequency range for the Terminal Descent Engine because its Y-axis spectrum exceeded this test spectrum from 80 to 160 Hz. For this case, the landing shock test would have had to be increased; however, it was shown that this frequency band was adequately covered by the component sine qualification test.

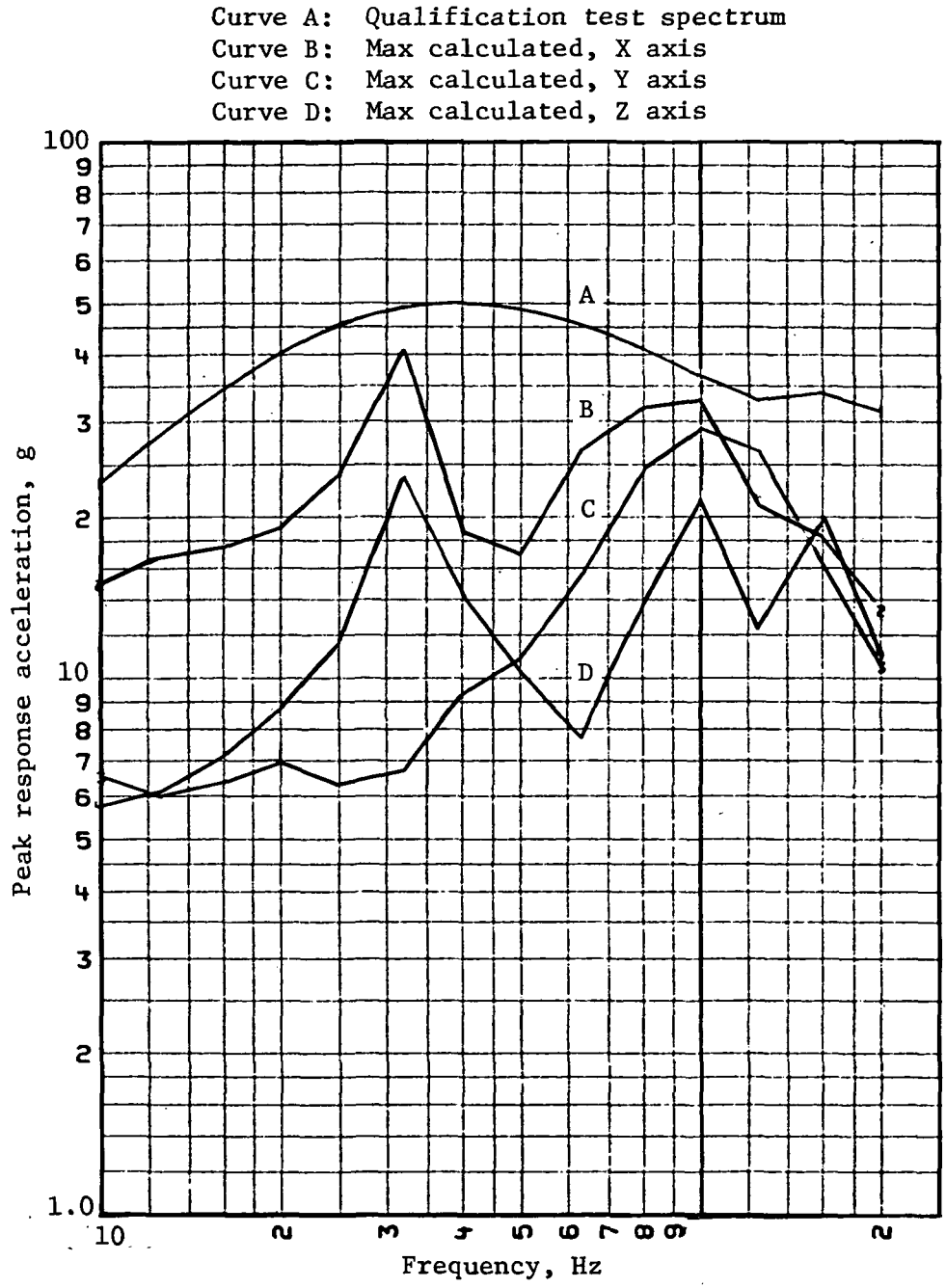

Figure 24.- Comparison of maximum calculated landing shock spectra with qualification test spectrum for biology instrument.

Curve A: Qualification test spectrum
Curve B: Max calculated, X axis
Curve C: Max calculated, Y axis
Curve D: Max calculated, Z axis

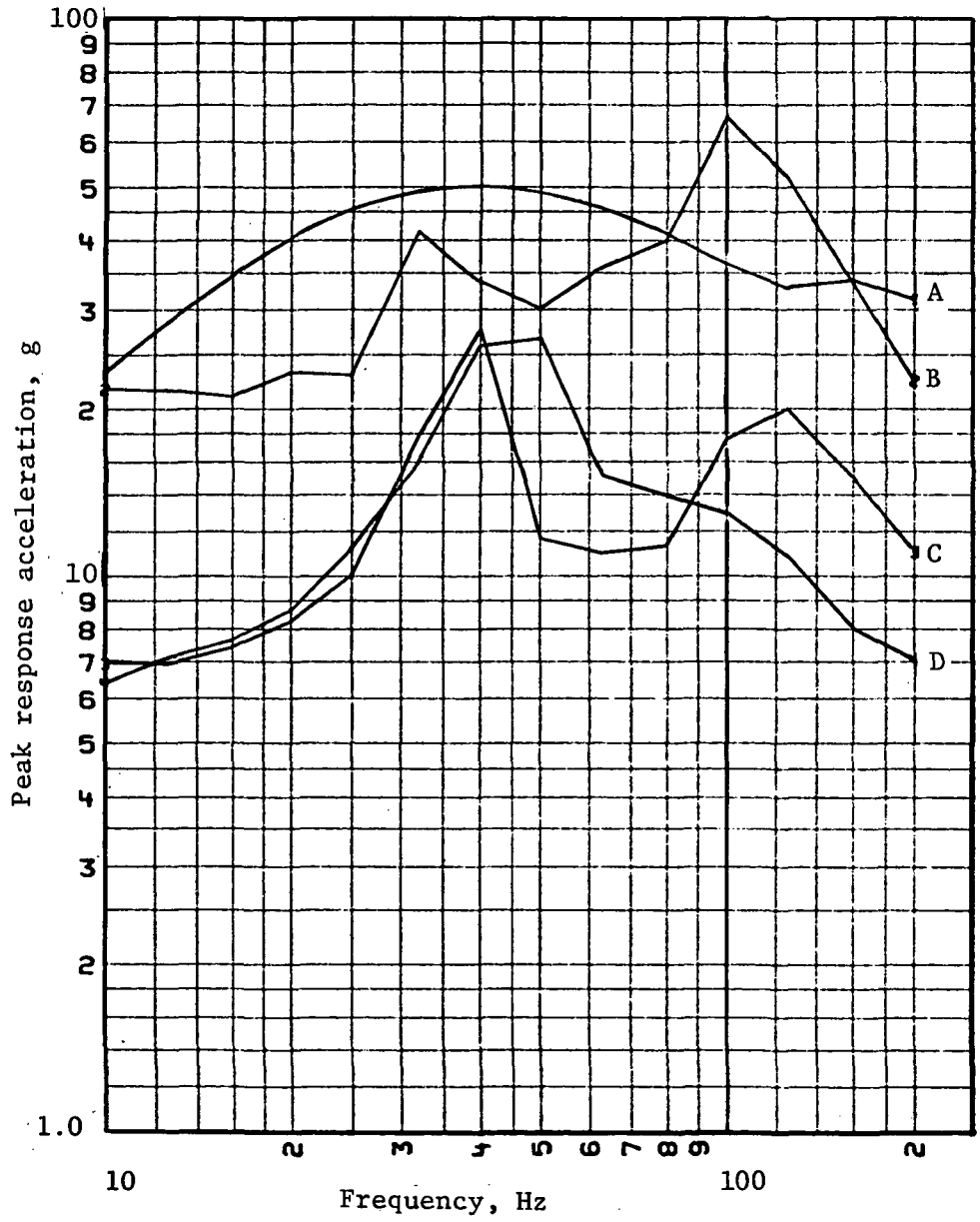

Figure 25.- Comparison of maximum landing shock spectra with qualification test spectrum for terminal descent engines.

Loads Analysis

Loads analysis is the name usually given to the analytical process used to define design and flight loads in the spacecraft structure caused by low-frequency, steady-state, and transient inputs from the launch vehicle. However, for the Viking Project, other environments like landing on the Martian surface were necessarily included in the general group of loads analyses. Early in the project, specific hardware items were designated as primary structure, to be designed by loads analysis.

In general, these were parts of the structure whose failure during flight could have a critical effect on the mission. For the Orbiter, the following items were selected (see fig. 3):

A) The upper plane truss, which carries loads from the fuel and oxidizer tanks into the main Orbiter bus:

B) The propulsion module structure, consisting of the propulsion motor, fuel and oxidizer tanks, and the truss connecting the motor to the tanks;

C) The outrigger trusses supporting the scan platform, on which various scientific instruments are mounted;

D) The top and bottom rings and connecting longerons on the main Orbiter bus;

E) The solar panel spars and outrigger trusses attaching the panels to the bus;

F) The VLC adapter truss connecting the Orbiter to the Lander;

G) The VSC adapter truss connecting the spacecraft to the launch vehicle;

For the Viking Lander loads analysis, the corresponding items were (see fig. 4 and 5):

H) The equipment plate, which is the hexagonal machined plate on which many electronic components and experiments are mounted;

J) The Lander body side beams, which form the long sides of the hexagonal body below the equipment plate;

K) The aeroshell and adapter ring;

L) The deorbit tank trusses, which mount on the aeroshell;

M) The terminal descent tank trusses, mounted on the side beams;

N) The landing-leg main support fittings, which carry the landing loads into the Lander body;

O) The equipment-plate support fittings connecting the equipment plate to the Lander body;

P) The bioshield base struts, used to stiffen the very light bioshield skin;

R) The struts by which the TDLR antenna is supported from the equipment plate.

From the beginning of the Viking Project, it was realized that the spacecraft would be weight critical and therefore required a design philosophy that matched minimum gage, for the lightest structure, with proof of a positive margin of safety. This philosophy implies that each part of the primary structure is designed to carry its maximum predicted load, with some small positive margin. However, practical considerations limit the application of this approach in the strict sense. For example, a multimembered truss structure will be designed for the highest analytical load in any one member, but because each member is loaded differently in any flight event some members will inevitably be overdesigned.

Generally speaking, most loads analyses applied to the launch or boost events. This was particularly true for the Orbiter structure. On the other hand, the Lander was required to enter the atmosphere and land on the Martian surface, resulting in additional load environments. Table 4 lists 17 different events for which loads analyses were performed. Each organization generated detailed finite-element mathematical models to obtain the required structural loads. As the design evolved and test data became available, the complexity of the models gradually increased. For example, the Orbiter mathematical model used in one of the earlier analysis cycles included 32 225 elastic degrees of freedom (DOF), 920 dynamic, and 459 interface DOF. A typical early Lander mathematical model had 20 000 elastic, 600 dynamic, and 180 interface DOF.

TABLE 4.- LOADS ANALYSIS OF VARIOUS EVENTS

Events	No. of forcing functions or conditions
Ground conditions	6
Stage 0 ignition	21
Airloads	5
Stage 0 max acceleration	1
Stage I ignition	12
SRM separation	1
First-mode longitudinal oscillations	1
Stage I burnout	29
Stage II ignition	3
Stage II burnout	19
Centaur main-engine start I (MES I)	1
Centaur main-engine cutoff I (MECO I)	1
Centaur main-engine start II	1
Centaur main-engine cutoff II (MECO II)	1
Entry deceleration	1
Mortar fire	1
Landing	1

As can be seen by the many degrees of freedom associated with the spacecraft structural models, it was necessary in most cases to reduce the size of the substructure models. The general approach was to model the structure in logical pieces and use the techniques of modal coupling (ref. 17) to mathematically combine the pieces. For example, this approach was used to combine the VLC and Orbiter for the complete Viking spacecraft model used for the loads analysis. Once the spacecraft model was completed in modal coordinates, it was combined again by modal substitution coupling techniques with the Centaur/Titan IIIE model for the final model for each loads analysis event. Figure 26, from ref. 18, illustrates the data flow and responsibilities associated with the launch and boost loads analysis.

However, even with reductions in substructure degrees of freedom, the final coupled models were still quite large. Therefore, to reduce model size, some modes associated with each model were truncated. This required close cooperation among the five participating organizations to ensure that the integrity of the coupled models was maintained. Because most low-frequency environments mentioned above are important in the frequency range below 50 Hz, it was felt that the models should be accurate up to at least 50 Hz. The approach taken on the Viking Project was to truncate all modes above 50 Hz. The reasoning was that, because those modes were higher in frequency than the forcing function, they would not be excited significantly and would therefore not contribute to the response. This assumption is not always

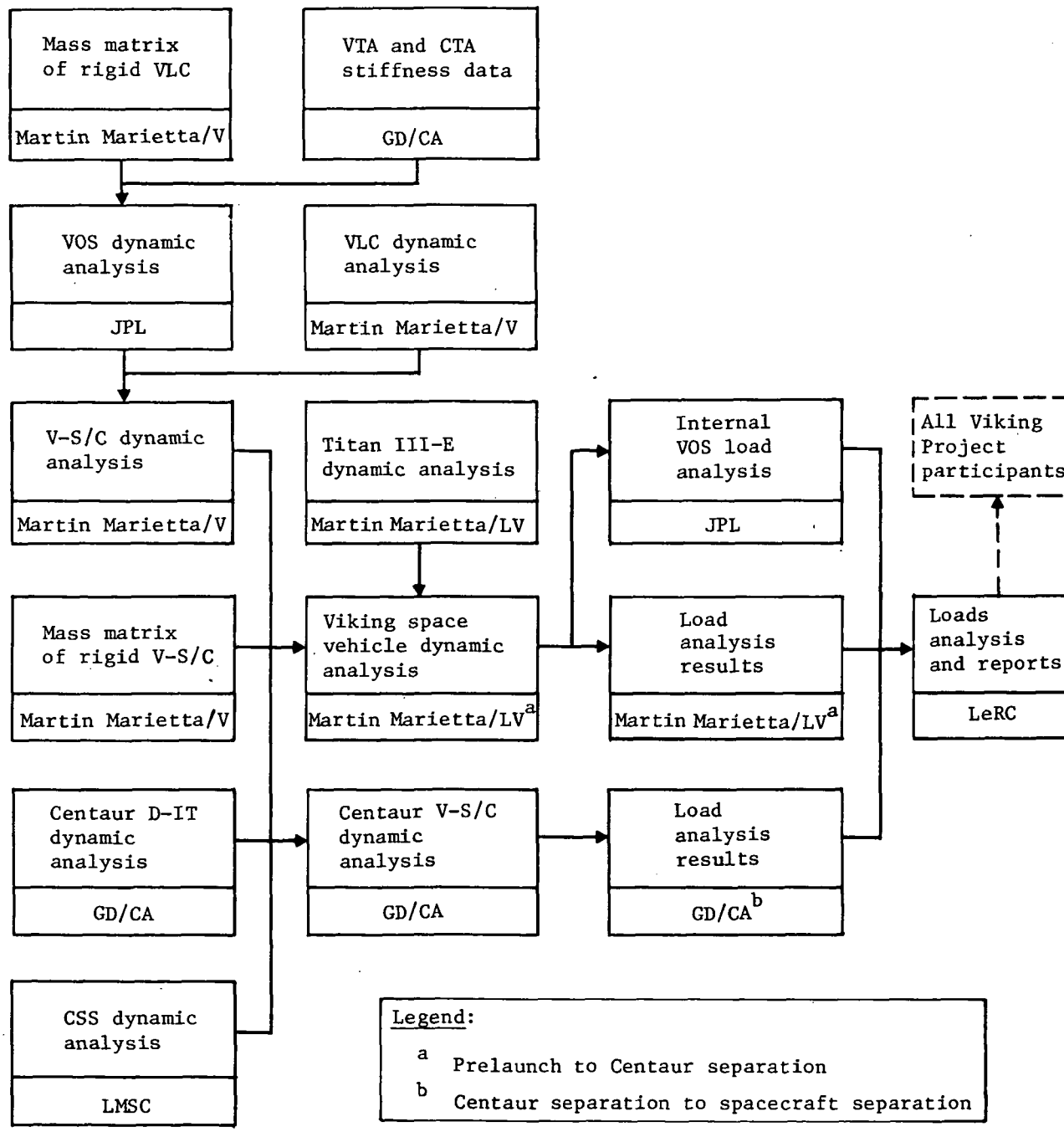

Figure 26.- Data flow for loads analysis.

correct. To ensure the validity of the responses, careful selection of modes is necessary.

Loads analyses for Viking (table 4) were performed in the time domain for the uncoupled modal equations of motion for the various events. Once the modal accelerations were calculated, discrete accelerations for inertial load factors and internal loads from discrete loads transformations were obtained for design loads.

To account for variations in flights and other uncertainties, launch and boost loads were handled statistically. For example, a complete loads cycle (consisting of taking a given forcing function, solving the equations of motion, then calculating discrete responses) was completed for all 21 Stage 0 ignition cases. This resulted in 21 sets of loads for each group of primary structures listed at the beginning of this section. The mean and standard deviation (σ) for each primary structural member for all 21 cases were calculated along with the "mean $+3\sigma$" load for the Stage 0 ignition condition. This load was then used to design for a positive margin of safety.

One problem associated with handling the data in this manner stems from lack of knowledge of the actual probability distribution. For example, using the mean $+3\sigma$ value ensures that any number calculated will be less than the mean $+3\sigma$ number 99.85% of the time for a Gaussian distribution. However, with only 21 cases, it is difficult to determine what kind of distribution existed, so the actual value of the probability of exceedance on the Viking loads analysis remains unknown.

An essential part of the modeling and loads analysis process was feedback of test data into the mathematical model so that any necessary corrections could be made. Both Martin Marietta and JPL, with responsibilities for the Lander and Orbiter, respectively, took great care in determining the correct dynamic properties of the structure. For each major design change, a new math model was generated. Therefore, there were a number of different coupled models; however, complete new loads analyses for the boost events were conducted for only three different Viking spacecraft models.

Discrepancies were generally not large. For example, during the LDTM terminal descent GVS test, an error was discovered in the equipment-plate modal frequency. The discrepancy was caused by an incorrect estimate of how much effect the Lander dust cover had on the stiffness of the equipment-plate mode. The changes that were necessary generally consisted of scaling frequencies and assuming no change in the mode shapes themselves. The validity of this assumption varied from case to case. It is obvious that, if there is a discrepancy between test and analysis, there

should be a change in the model properties (i.e., mass and/or stiffness) to correct the error. However, in most cases, to remodel was impractical. Parametric eigensolutions to determine the overall impact of the changes are also usually impractical during the design phase. The true criterion of the model and/or model change should be its effect on the energy in the system, as described by a given mode. For example, for the equipment plate, because most of the energy associated with that mode was in the plate itself, adding the stiffness of the dust cover changed the boundary conditions only slightly and did not redistribute the energy significantly. In this case, the frequency was scaled to account for the added stiffness, but the mode shape was not changed.

In both organizations, the criteria for evaluating the models and test data were primarily frequency comparisons and orthogonality checks. Selected key mode shapes were also reviewed. Table 5 compares calculated and measured modal frequencies, taken from the Orbiter loads analysis described in ref. 18. The average error was +6%, with a maximum of +11.4%. A criterion commonly used to check the quality of the modal test data is the orthogonality check, in which off-diagonal terms should vanish in the matrix product

$$\left[\phi\right]^T \left[M\right] \left[\phi\right] \tag{12}$$

When this check was conducted on the Orbiter test data, the maximum off-diagonal term was 6.2%, with only three terms exceeding 5%, out of a total of 66 terms. Development of the Orbiter dynamic model and its correction with test data are described in detail in ref. 19.

TABLE 5.- COMPARISON OF MODAL FREQUENCIES FOR VIKING ORBITER

Mode	Frequency, Hz		
	Analysis	Test	Error, %
1	4.35	4.51	3.5
2	4.40	4.63	5.0
3	7.48	7.87	5.0
4	7.83	8.30	5.7
5	10.92	11.51	5.1
6	13.36	14.09	5.2
7	14.64	15.35	4.6
8	17.95	19.49	7.9
9	18.81	19.83	5.1
10	23.42	24.85	5.8
11	26.18	29.54	11.4
12	24.28	26.49	8.3

Test Program

Component-Level Tests

In general, dynamic testing at the component level was restricted to random vibration, transient vibration, pyrotechnic and landing shock. Although several components were judged to be potentially susceptible to acoustics because of their large surface area and low-density configurations, the only one to receive a separate acoustic test was the Terminal Descent and Landing Radar (TDRL) antenna. The remainder were qualified for acoustics by the system-level acoustic test. Components were not tested for steady-state acceleration environment, although selected electronic piece parts and devices were subjected to steady-state acceleration testing during their qualification program, to levels from 10 000 to 30 000 g.

Two types of tests were performed on the components; namely, Flight Acceptance (FA) and Qualification (Qual) tests. In addition, most components received some degree of development testing, which was generally similar to a Qual test in severity but less formal.

Margins between FA and Qual tests were different for each environment, as discussed in the following paragraphs. Because it was desirable to have a consistent philosophy with regard to test margins for the various areas of responsibility on the spacecraft, the margins that evolved included a number of compromises on the part of LRC, JPL and Martin Marietta--each of which had initially favored its own individual approach.

Random vibration tests.- FA test levels were based on predicted flight environments calculated by the techniques discussed in the section on environments and criteria, with the additional requirement of satisfying the Simpkinson criterion that the overall acceleration level should not be less than 6 g_{rms}. The corresponding Qual test spectrum was obtained by applying a margin of 3 dB to the FA spectrum. Figure 27 shows typical test spectra for components mounted on the Lander equipment plate.

The duration of exposure to random-vibration FA test input was established by defining the acoustic environment as significant whenever the overall level was within 6 dB of the peak value. After reviewing a number of past Titan flights, this led to a conservative estimate of 60 seconds. For the Qual test duration, a factor of five was applied to the FA test duration.

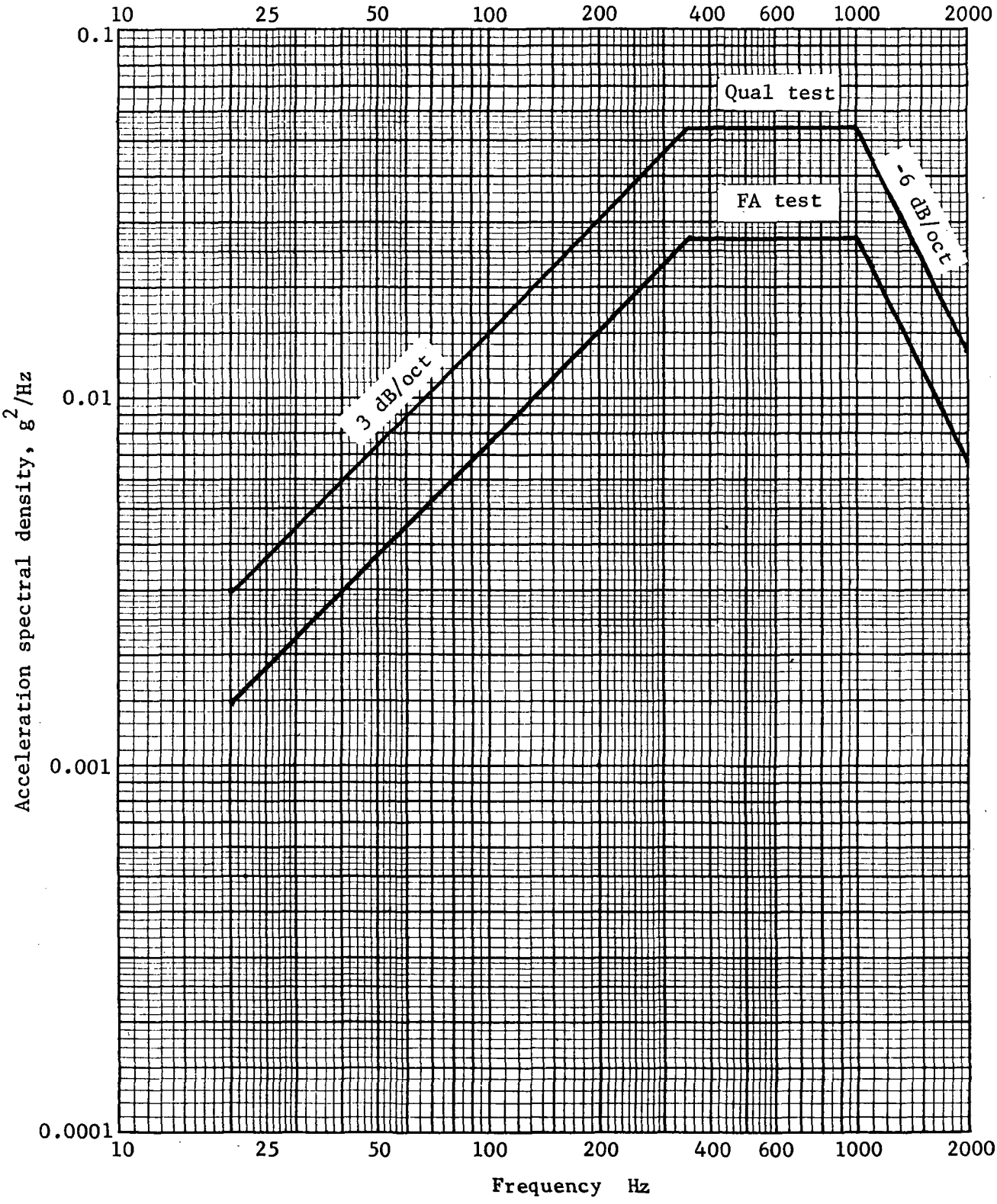

Figure 27.- Random-vibration test spectra for components mounted on VLC equipment plate.

Random vibration input was generally the same for all three axes. In a few cases, where test data indicated that a particular axis should be relatively quiet, advantage was taken of this to specify a lower test level in that axis.

Transient equivalence tests.- Analytically predicted responses to the system-level sine test were used to define preliminary test environments for components. Most individual responses showed a rapid roll-off above 60 to 70 Hz. However, because this is the frequency range in which the analytical model becomes less reliable, specific reductions for individual component test levels could not be justified until system-level test data became available.

After the system level tests, results showed that, with very few exceptions, component test inputs could be reduced above 50 Hz. This reduction was applied on an individual basis. To ensure that the FA test would be adequate to demonstrate proper assembly and workmanship, a working minimum accleration level of 1.7 g was established. A Qual/FA margin of 1.5 was used, leading to a minimum Qual test level of 2.5 g. These minimum criteria applied above 20 Hz.

Landing shock considerations influenced the input reduction process to a secondary degree. The envelope of shock spectra derived from the analytical population of Mars landing transients was predicted to exceed the qualification landing-shock test for a few components. The decision to require the component sine test to cover these isolated spectral deficiencies therefore imposed an additional constraint on the allowable degree of input reduction.

Figure 28 shows a typical component sine test spectrum obtained by the above procedure, with a plot of the environment measured at the component location during the system-level test. Sweep rates of 4 oct/min and 2 oct/min were specified for the FA and Qual tests, respectively.

Pyrotechnic shock tests.- Two different method were used to test components for the pyro shock environments, and the corresponding test criteria were somewhat different. One method was to use a shaker to apply a complex wave to the test article three times in each axis. After shock spectrum analysis, the complex wave was required to match a specified shock spectrum for the component within tolerances of +6, -0 dB. Below the frequency of peak response, three points were allowed to be as high as +9 dB and three as low as -3 dB from nominal.

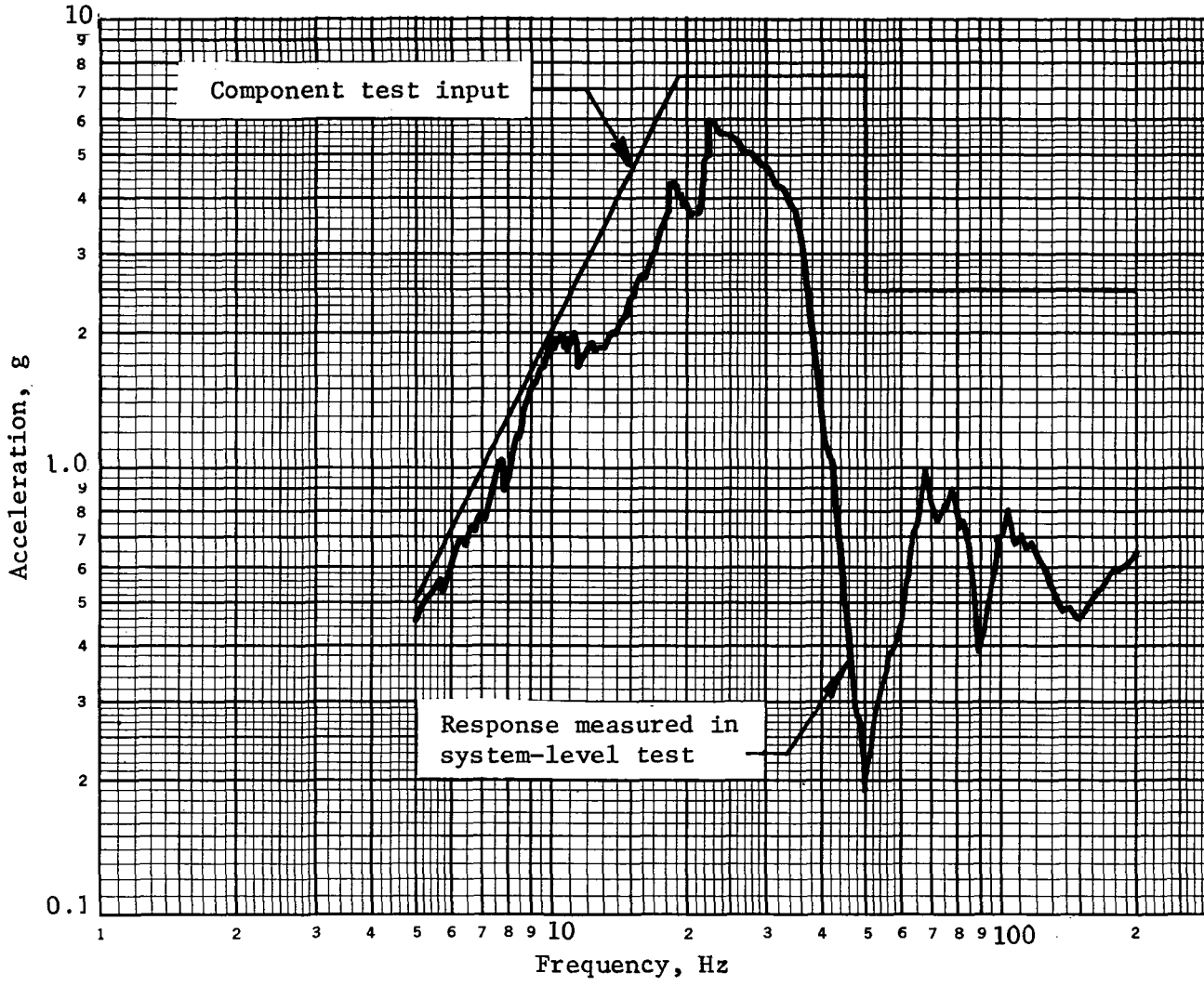

Figure 28.- Qualification sine-test input for typical component.

The second test method was to mount the test item on the Lander Pyro Shock Test Bed (PSTB), attach ordnance devices to the PSTB structure, and fire them for a minimum of six shots. Because some scatter in the data always results from repeated ordnance firings, the tolerance on the resulting shock spectrum at any one-third-octave-band center frequency was ±3 dB about the average of all data points at that frequency. Consideration was also given to the effects of structural characteristics of the PSTB on the response spectrum.

To minimize the number of different shock spectra that had to be specified, a zoning approach was used, so that, for example, components mounted on the equipment plate were tested to the spectrum shown in Figure 29. No FA tests were performed for the pyro shock environment, only development and qualification tests, which included a factor of 1.2 over the maximum predicted spectrum levels.

Landing shock tests.- Input for the landing shock test was specified in terms of a half-sine acceleration pulse, rather than a shock spectrum. An important parameter associated with the pulse was the velocity change represented by the area under the pulse shape. Most components on the VLC were qualified to a 30 g x 22 ms (14 fps) half-sine pulse. A few items mounted on the landing legs were qualified to higher levels to account for the possible condition in which the vehicle initially landed on two legs so that the third leg, on which the item was mounted, would rotate about the initial impact point with a resulting high final impact velocity. Figure 30 shows typical test pulses.

The landing shock qualification test was coordinated with the sine vibration test to ensure full spectral coverage of these two low-frequency environments. Thus, even when the landing analysis indicated that a particular component could be qualified to a level considerably below the basic 30 g pulse, this level was retained as a working minimum. A qualification factor of 1.2 was included in the test inputs. No FA tests were performed for the landing shock environment.

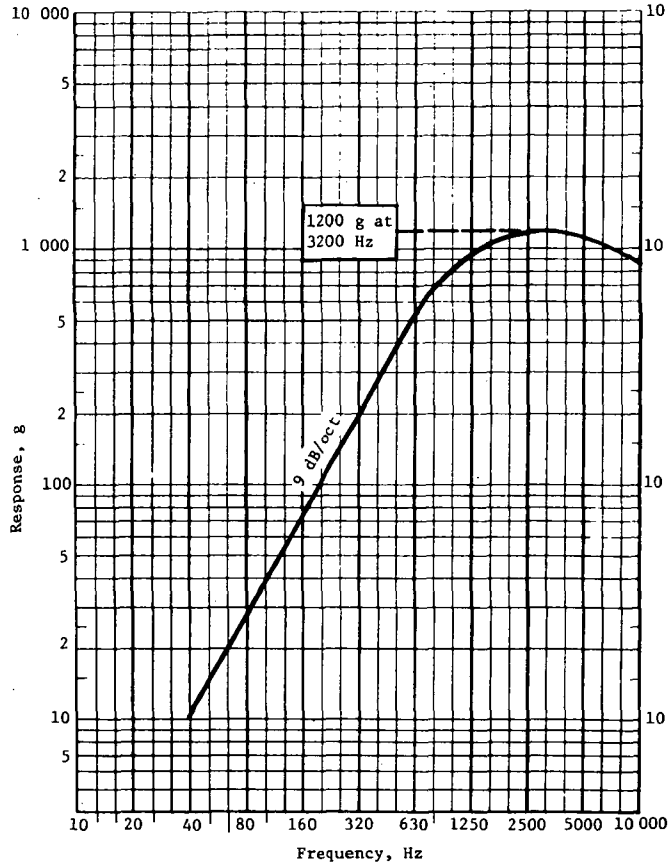

Figure 29.- Input spectrum for pyrotechnic-shock qualification test for components mounted on VLC equipment plate.

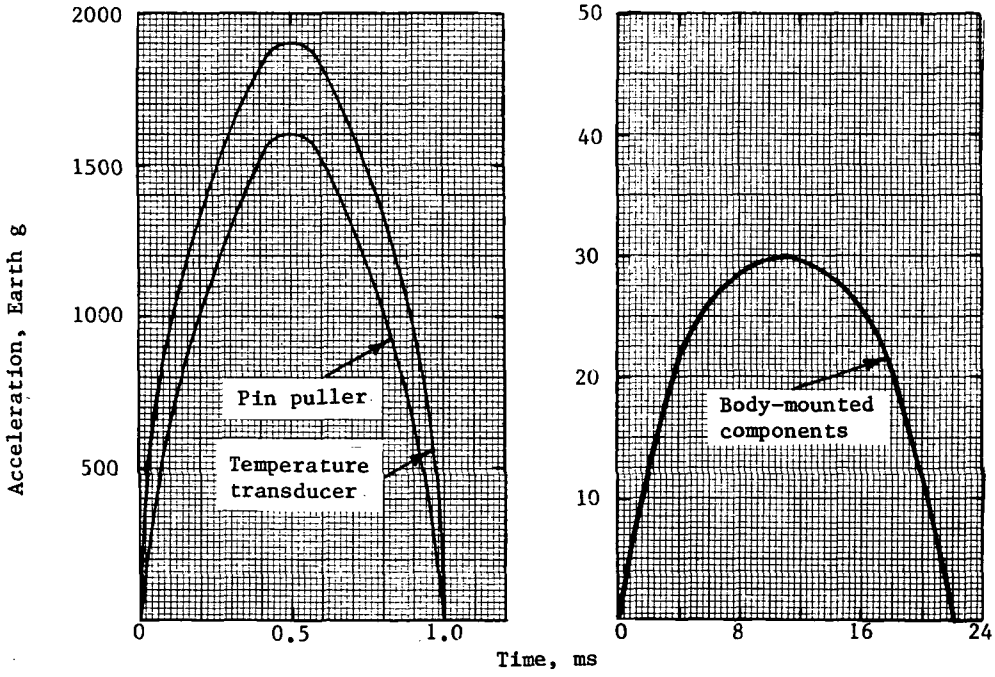

Figure 30.- Landing-shock test pulses.

System-Level Tests

The system-level test program evolved from the *Viking Structural Verification Plan*, a document generated to establish the detailed steps to be accomplished to verify the integrity of the spacecraft structure. The plan included a description of the analyses and tests to be accomplished and their interrelationships. Consequently, considerable pretest planning went into the preparation, including definition of test objectives, measurement requirements, major fixture/suspension-system requirements, and hardware schedule flow.

As a result, system-level tests were performed for the following dynamic environments:

1) Acoustics;

2) Launch transients (simulated by sine vibration tests);

3) Pyrotechnic shock;

4) Separation events;

5) Mortar fire;

6) Landing leg deployment;

7) Landing shock;

8) Ground vibration survey (GVS);

9) Aeroshell dynamic capability.

In addition, ground vibration survey (GVS) tests were performed for a number of different configurations.

The test articles used for the system-level test program were:

1) Lander Dynamic Test Model (LDTM);

2) Proof Test Capsule (PTC);

3) Orbiter Dynamic Test Model (ODTM);

4) A combination of the LDTM and the ODTM.

The LDTM was a complete Viking Lander Capsule made up of flight-type primary and secondary structure with, in general, mass-simulated components. The PTC was also a complete Lander Capsule, constructed with updated flight-type structure and using almost a full set of flight components. The exceptions (mass simulators) were the Radioisotope Thermoelectric Generators (RTG) and the Viking Biology Instrument (VBI). The ODTM was similar to the LDTM in that it consisted of flight structure and simulated components.

This section summarizes the objectives and general results of the system-level tests. Detailed results are recorded in the test reports describing the individual tests (see Bibliography). The tests are grouped according to type (i.e., acoustic, sine vibration, etc) rather than being presented in the chronological sequence in which they were conducted.

Acoustic tests.- Tests were performed on the LDTM and the PTC for acoustic environments. The two sets of tests occurred approximately 9 months apart. In the interim, the estimated launch acoustic environment was revised using data measured during flight tests.

The LDTM test was conducted in two phases, exposing it to acoustic levels simulating predicted mission environments (with appropriate qualification margins) during launch and the transonic phase of Mars entry. The objectives of the test were to:

1) Evaluate random vibration environments induced by launch and transonic entry acoustics at VLC component locations;

2) Confirm the ability of the secondary structure (component support bracketry) to sustain random vibration resulting from critical-design ultimate acoustic loads;

3) Evaluate any coupling and amplification between the acoustic input and VLC structural response, particularly for the transonic entry test;

4) Serve as a precursor test for developing test techniques for use during the PTC acoustic test.

Figure 31 shows the test configurations.

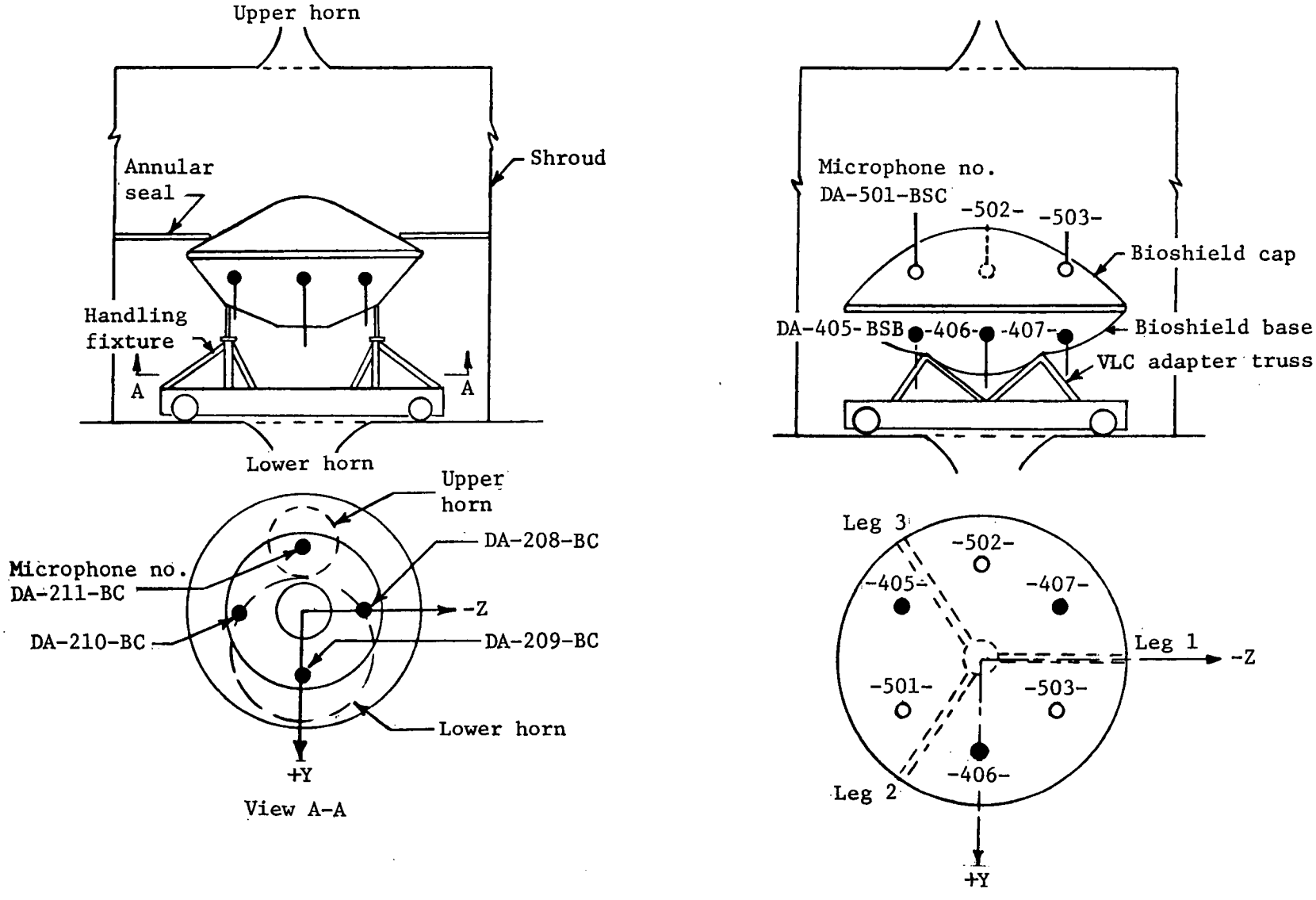

a. Entry acoustics

b. Launch acoustics

Figure 31.- Acoustic test configurations.

For the entry test, the test article consisted of the Lander body (including the decelerator system), base cover and aeroshell. It was supported on three adjustable jacks. The aeroshell propellant tanks were off-loaded to the mission entry weight condition. To obtain the specified acoustic field adjacent to the base cover, it was necessary to install a plywood collar just above the base-cover/aeroshell interface to seal off the lower part of the acoustic chamber, as shown in figure 31a.

Four control microphones were mounted on floor stands below the base cover. Three additional microphones were mounted above the aeroshell, and five microphones inside the test article. Twenty-three accelerometers were used to measure vibration responses.

The test article for the launch test was made up of the Lander body (including decelerator system), base cover, aeroshell, bioshield base and cap. The assembled LDTM was mounted on a VLC adapter truss, supported by the VLC dolly. Input environment was controlled by using a set of six control microphones surrounding the test article, as shown in figure 31b. To obtain information on the acoustic transmission characteristics of the VLC, an additional nine microphones were mounted inside the VLC. The vibration environment was measured by 70 accelerometers on the test article.

Figures 32 and 33 are plots of input acoustic spectra. The entry test lasted 250 s. To evaluate any effects of bioshield pressure on vibration response, the total duration of the launch test was divided into three parts. Bioshield pressures of 690 N/m^2 (0.1 psig) and 5171 N/m^2 (0.75 psig) were used for two 100-second runs. An additional 100-second run was then performed with the bioshield pressurized to 2070 N/m^2 (0.3 psig).

Transonic entry test results revealed that random vibration levels would not be a significant design or test condition for components. The highest overall acceleration level measured was less than 1 g_{rms}.

Acceleration responses measured during the launch-configuration test were compared to equipment Qual test spectra. Good agreement between measured data and the specification was found for the equipment plate. However, a number of areas exceeded specifications (particularly on the aeroshell and payload support ring), and all random vibration criteria were extensively reviewed.

Vibroacoustic data obtained during this test program, together with vibration data acquired during a terminal propulsion system verification test and the Viking proof flight formed the basis for specification revisions discussed in a later section of this report.

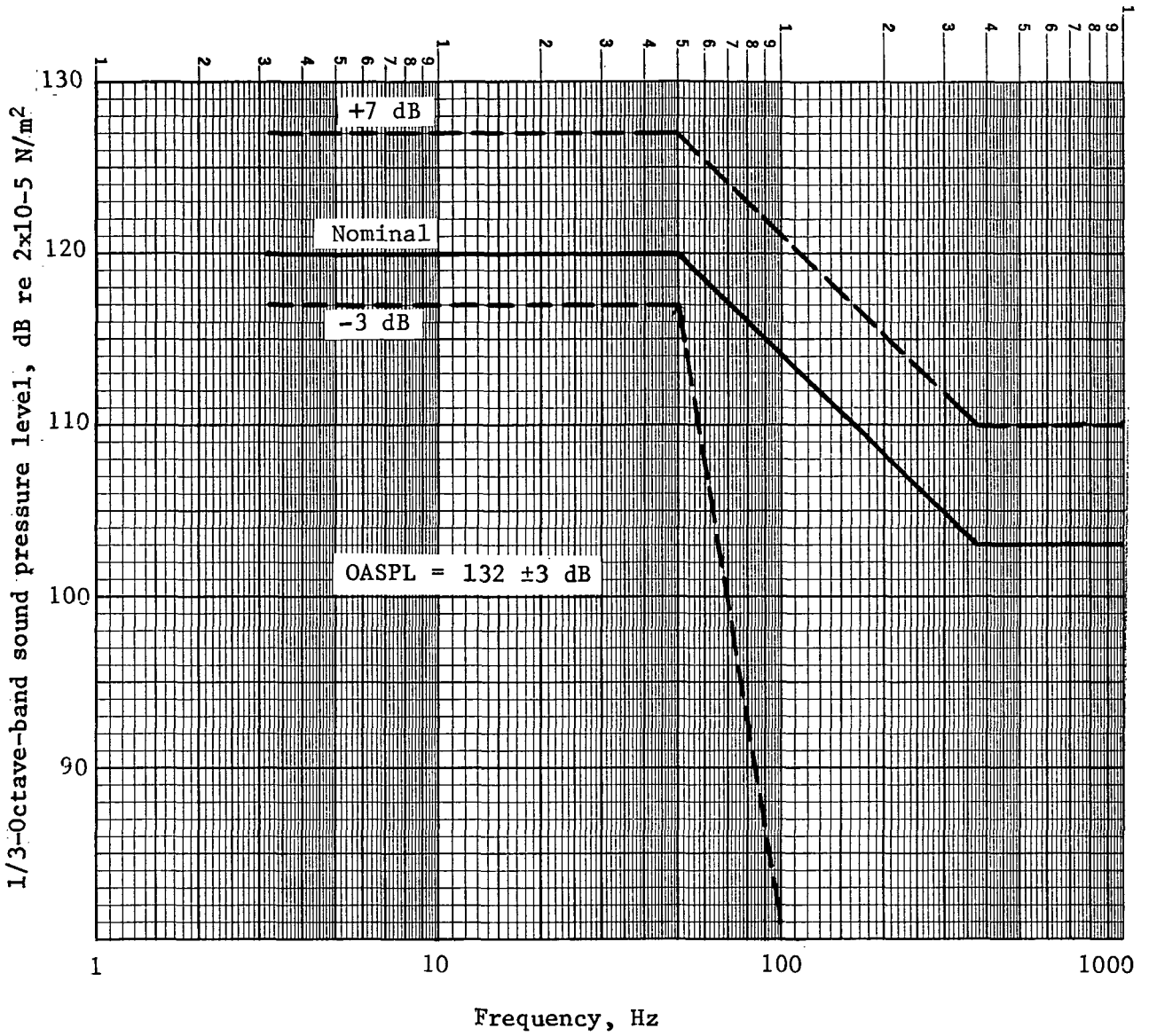

Figure 32.- Entry acoustics test spectrum.

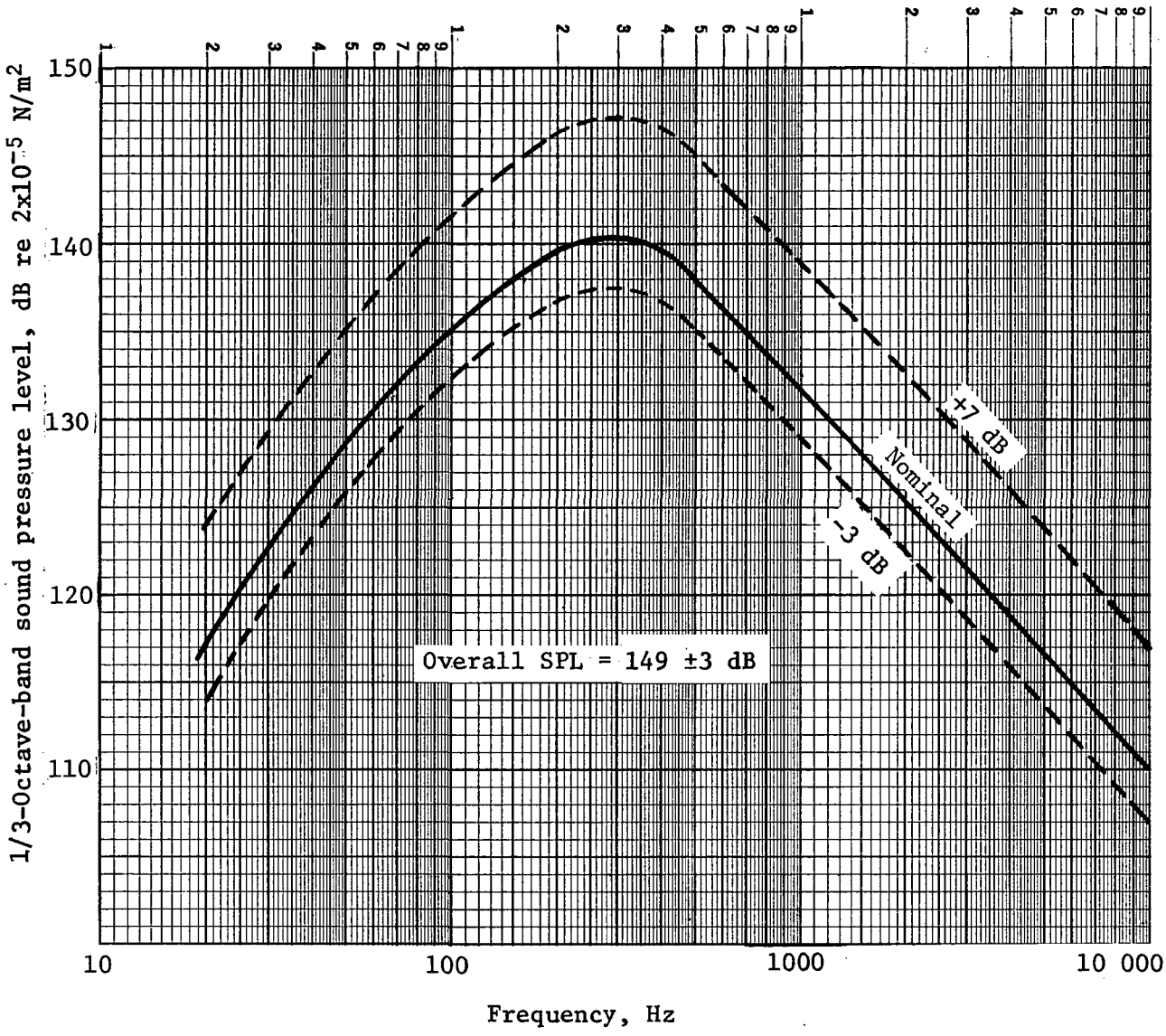

Figure 33.- Launch acoustics test spectrum.

A posttest inspection of the LDTM structure revealed a number of small fatigue cracks in the aluminum panels around the periphery of the base cover. In every case, the cracks appeared to have started at rivet holes. No cracks were detected in the fiberglass panels. A redesign effort was initiated after the cracks were discovered. The "fix" used was to install washers beneath the rivet heads, which relieved the stress concentration. No damage occurred in a later retest.

All test objectives were met. Enough data were obtained to evaluate and modify component test criteria, and all component support bracketry survived the test without damage. No amplification of acoustic levels was detected inside the test article, and noise reduction through the various structural layers was close to the predicted values.

The PTC was subjected to FA and Qual level acoustic tests to:

1) Verify the operation of selected systems before, during, and after exposure to the acoustic environments;

2) Verify that acoustic environments did not cause failure or malfunction of selected operating systems;

3) Determine response at selected locations to correlate with analyses and criteria.

The test was conducted in two phases, the precursor test and Qual test. The precursor test was run at the flight acceptance level (137-dB OASPL) with the bioshield unpressurized. The Qual test was run at 143 dB with the bioshield pressurized to 2070 N/m^2 (3.0 psig). Instrumentation-channel limitations precluded running functional checks on all components simultaneously; therefore, the Qual test was conducted in two time segments, and half of the components were monitored during each segment.

For all tests, the PTC was mounted on the VLCA truss supported by the VLC dolly. The acoustic spectrum was controlled by averaging the signals from six external microphones. Figure 34 compares a nominal qualification test spectrum to the tolerance band. The acoustic environment inside the test article was measured by four internal microphones, and vibration responses were measured at 43 accelerometer locations.

Qual test inputs were within specified tolerances, and no visible structural degradation occurred. Overall acceleration responses were generally less than the comparable LDTM responses by a factor of 2 to 3. This was expected because the qualification level was reduced from 149 to 143 dB after a review of data obtained from the Viking Proof Flight (discussed in a later section), which occurred between the LDTM and PTC tests. In some

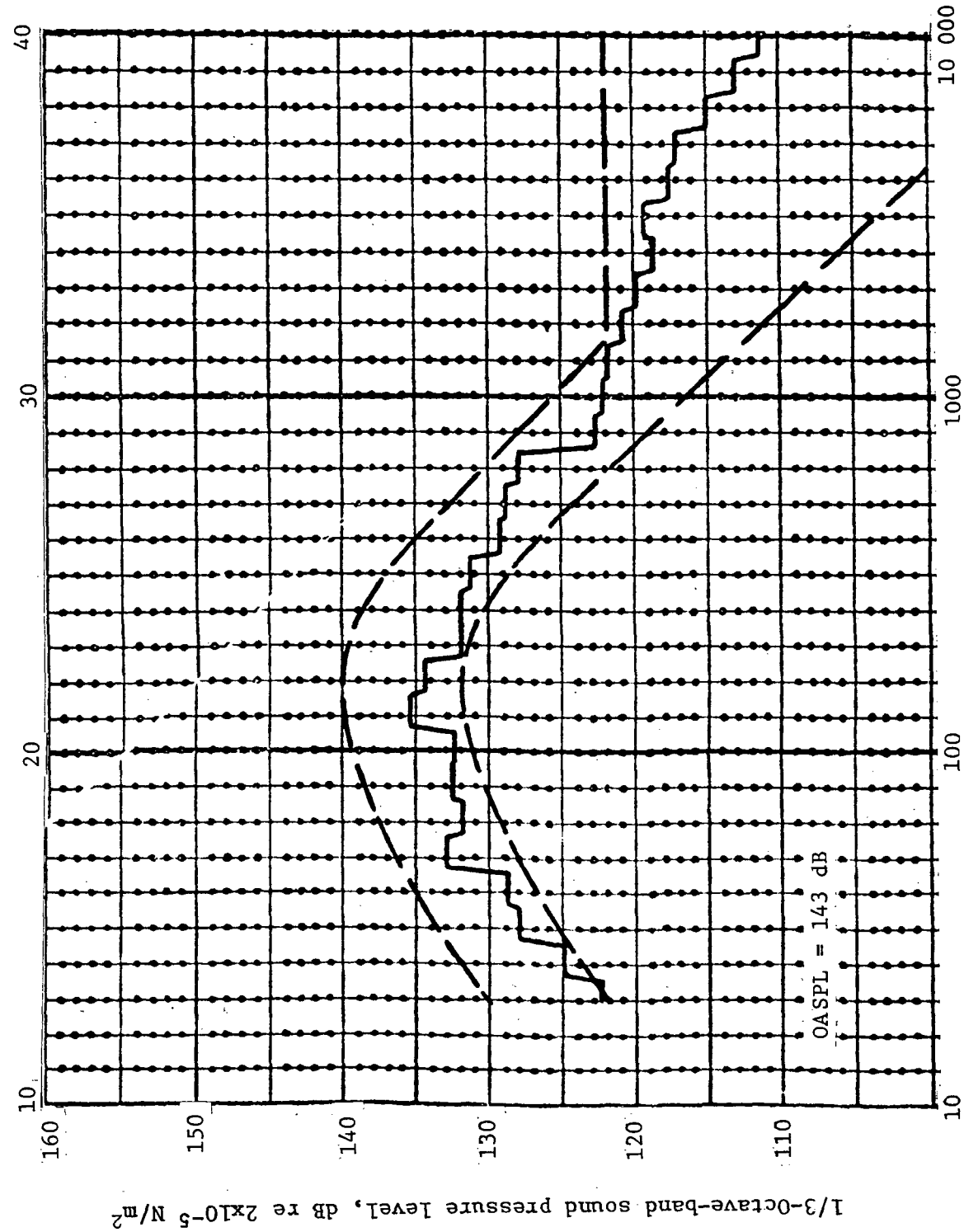

Figure 34.- Input acoustic spectrum for proof test capsule qualification test.

cases, vibration response spectra measured in the qualification tests exceeded predicted levels at certain frequencies. For example, the environment measured at the Upper-Atmosphere Mass Spectrometer (UAMS) exceeded the Qual test level for the instrument at certain frequencies. The UAMS also displayed functional performance anomalies during the test. Appropriate steps were taken to revise the qualification requirements and provide satisfactory solutions for the components affected, including retesting where necessary.

Sine qualification tests.- System-level midfrequency sine vibration tests were performed to qualify the spacecraft for launch transients. Initial tests were performed on the LDTM, followed by a more complex test on the LDTM/ODTM assembly, and final verification testing on the PTC.

From August 8 through October 12, 1973, the LDTM was subjected to vibration tests over the frequency range from 5 to 200 to 5 Hz (up and down sweeps) in three orthogonal axes. The objectives of the test were to:

1) Evaluate sinusoidal qualification levels for the various components;

2) Establish controls and techniques for the PTC and flight-article tests;

3) Verify the adequacy of secondary structure;

4) Obtain data for controlling the LDTM/ODTM (stack) midfrequency tests.

The test specimen consisted of the Lander body, aeroshell, base cover, bioshield and VLCA truss, assembled on a test fixture coupled to the vibration exciter. For the longitudinal (X) axis tests, as shown in Figure 35, the vibration fixture was restrained laterally by four sets of mechanical flexures and Teflon safety pads, reacted by four support-column assemblies. For this test series, the exciter trunnions were unlocked, resulting in a trunnion resonance of approximately 15 Hz.

For the lateral (Y, Z) axes, as shown in Figure 36, the test specimen was attached to an aluminum slide plate restrained by eight hydrostatic bearings supported by a base assembly rigidly attached to a seismic mass. The exciter trunnions were locked during the lateral axis tests.

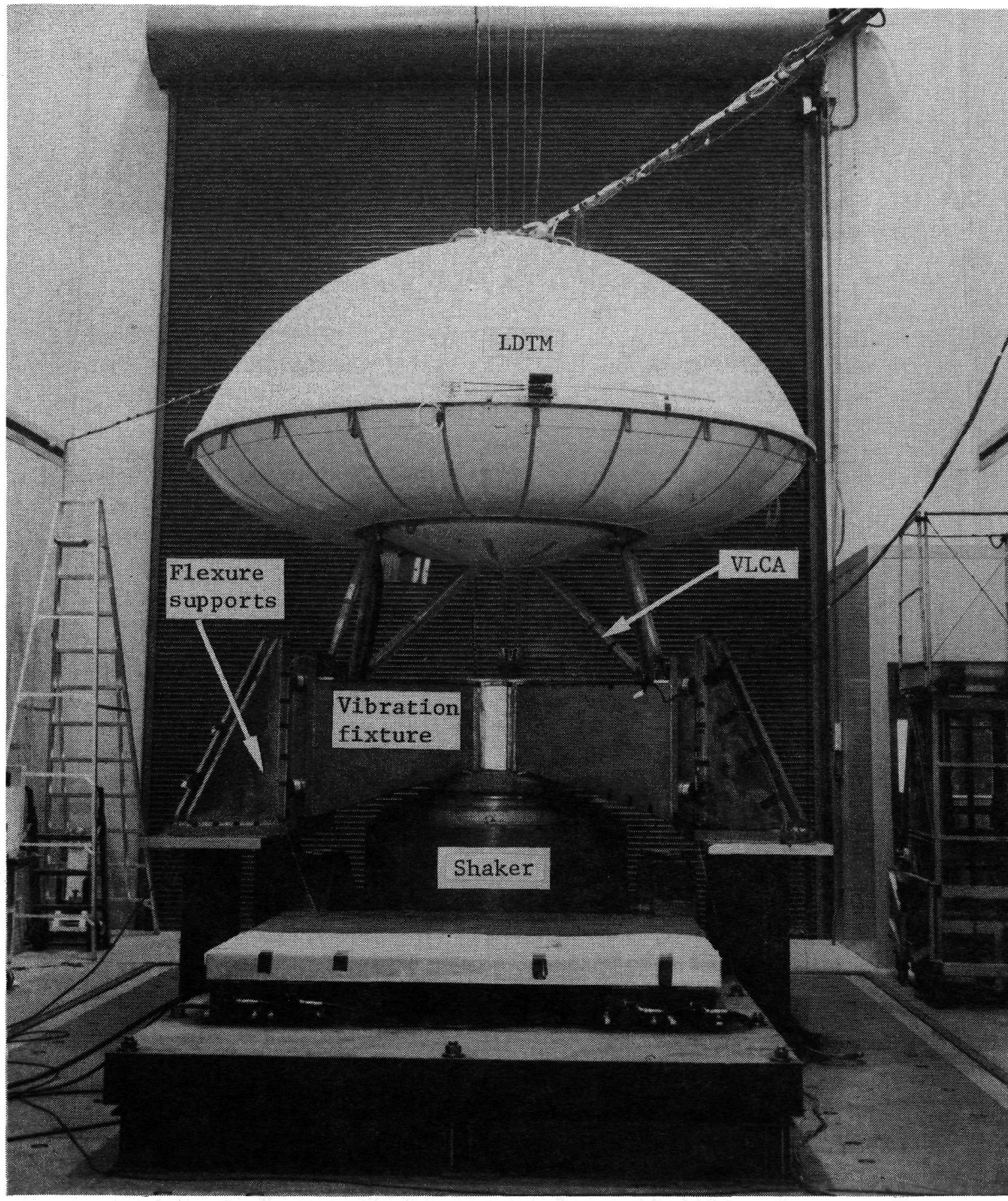

Figure 35.- Longitudinal-axis test setup.

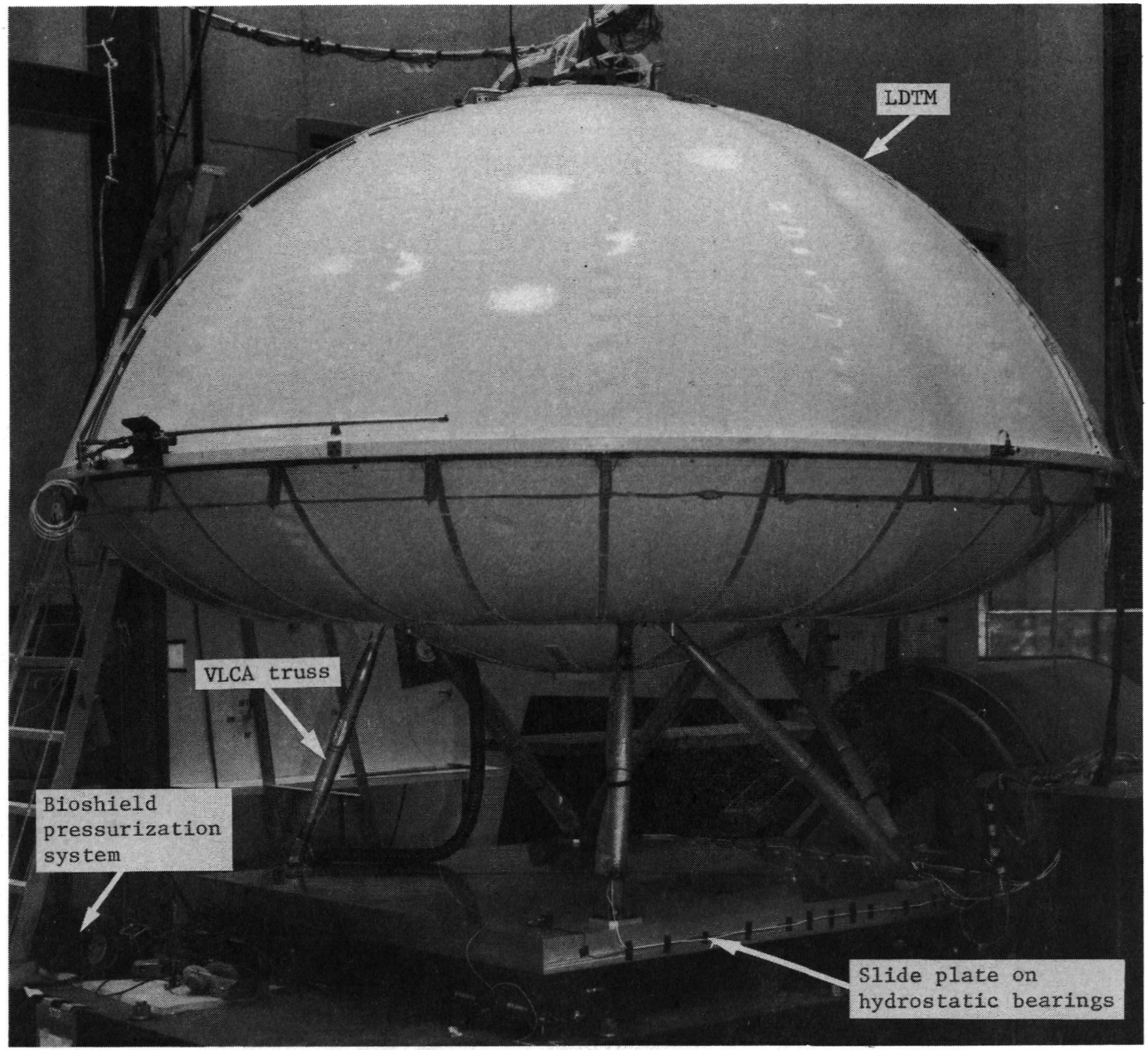

Figure 36.- Horizontal-axis test setup.

Each axis of testing consisted of low-level precursor tests followed by FA (1.0 g peak) and qualification level (1.5 g peak) tests. After each level of testing, the data were reviewed and changes to response control and abort channels were made as necessary until adequate data were obtained to select the control/abort and response measurements for the Qual tests. Specification test levels were controlled at the four VLCA/fixture interface points except in the frequency ranges where responses were limited by primary structural members. In general, the four fixture accelerometers controlled at frequencies below 10 and above 50 Hz, and primary structure limited responses between 10 and 50 Hz.

Test results are summarized as follows.

1) The adequacy of the secondary structure to withstand the dynamic environments not imposed by other tests was verified.

2) Response data were obtained to evaluate previously specified qualification levels for Lander components.

3) Guidelines, controls, and test techniques were established for later use in the PTC test, and data for controlling the LDTM/ODTM midfrequency test were obtained.

In November and December 1973, the combined LDTM/ODTM was subjected to sine vibration testing at JPL's dynamic test facility. This became known as the "Stack Test." FA and Qual or Type Approval (TA) test levels were applied to the spacecraft structure in a longitudinal test configuration using a 133 440 N (30 000 lbf) shaker. The two lateral axes were tested at lower levels using four 667 N (150 lbf) shakers.

The objectives of the stack test series were to:

1) Evaluate the effect of Lander/Orbiter interaction on responses at subsystem/component locations;

2) Evaluate the adequacy of the LDTM/ODTM secondary structure;

3) Serve as a precursor to the Proof Test Orbiter (PTO) forced vibration test, and evaluate PTO test levels;

4) Evaluate component sinusoidal test levels;

5) Obtain data for comparison to analytical results.

Significant pretest analytical effort was expended to provide assurance that test-peculiar failures of primary structure would not occur, and to aid in test implementation, because the complexity, scope, and tight schedule of the stack test left no time for surprises or emergencies. The analyses were divided into four categories: test fixture, overturning moment, response analysis of the test setup, and fatigue damage.

Analysis of the preliminary test fixture design revealed a torsional mode at 36 Hz. The proposed test setup was therefore considerably modified, including addition of a pair of V-type hydrostatic bearings.

Early in the program, because of the stack height coupled with the spacecraft cg offset, it became apparent that the longitudinal test buildup would be subject to large overturning moments. This setup is shown in figure 37. Estimates of these moments ranged from 5 650 000 to 11 300 000 N-cm (500 000 to 1 000 000 lb-in.) applied to the Viking Transition Adapter (VTA)/test-fixture interface.

For this analysis, the Orbiter elastic model was coupled to a rigid Lander. This combination was in turn mated to a rigid longitudinal fixture model restrained at three locations by hydrostatic bearings of known stiffness. The results of the analysis offered the first positive indication that the stack test could be implemented. Angular deflection limits of the shaker armature, a source of concern, were shown to be no problem.

In addition, reaction forces on the hydrostatic bearings and forces applied to the fixture were computed and used to perform a stress/fatigue analysis of the fixture and check bearing adequacy. These same moment reaction forces were applied to the piers supporting the bearings to check the stability of the piers.

The response of the test setup was analyzed to estimate the member loads and find the critical response points at which to locate acceleromters. Shaker force requirements and control levels were evaluated, and reaction forces estimated for use in fixture design. The analysis followed an evolutionary pattern and was accomplished in phases because both LDTM and ODTM elastic models were being revised and upgraded.

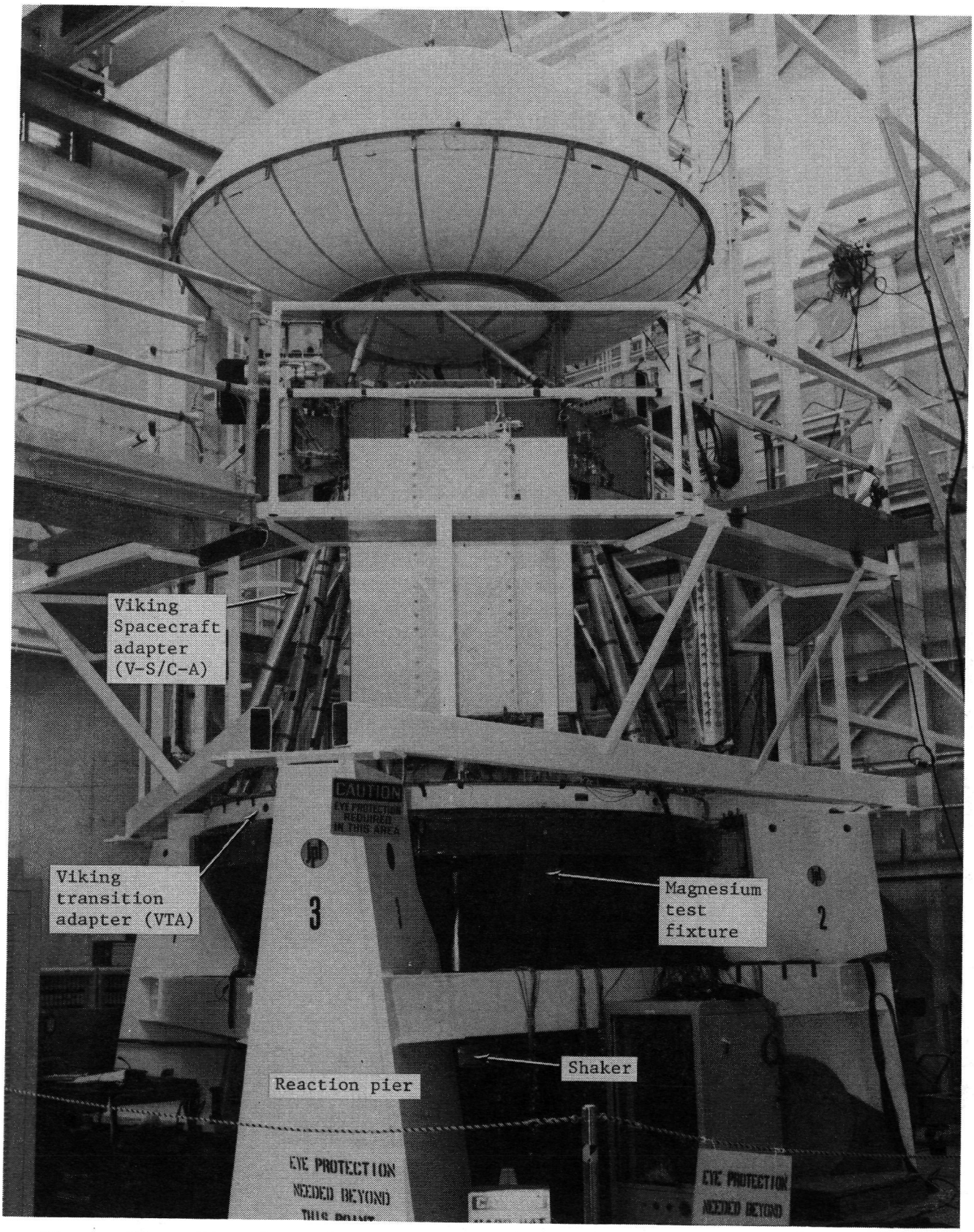

Figure 37.- View from floor of Viking 75 LDTM/ODTM longitudinal-axis (Z) test setup.

Simulation of lateral-axis excitation was noteworthy because of a change in test philosophy. Preliminary analysis had indicated strong coupling of the lateral and torsional modes of the spacecraft due to the combination of spacecraft cg offset and application of unrestrained driving forces at the bus main longerons. Therefore, an intermediate analysis using restrained or guided input forces was performed. It appeared to solve the coupling problem at all but the lowest frequencies (5 to 10 Hz). In this bandwidth, analysis indicated that the required driving forces were so small that control might be difficult to achieve. However, there were objections to the restraint of spacecraft torsional motion due to the massive lateral test fixture connected to the shaker. The fixture was to be constrained by hydrostatic bearings to move only in one plane. As a result, the test team was directed to seek a lateral driving scheme with minimum restraint. The final choice consisted of using four 667 N (150 lb) shakers.

The objective of the fatigue analysis was to monitor and permit prediction of possible fatigue damage so that vibration test levels could be controlled to prevent cracks from forming in the ODTM primary structure. The analysis, performed in two phases, consisted of the following basic steps:

1) Identification of critical primary structure;

2) Survey of parts for material, notch-sensitive areas;

3) Compilation of S/N curves, derivation of curve fitting equations;

4) Definition of loading spectrum (predicted or test);

5) Computation of cumulative damage ratio (CDR).

To be conservative but consistent with general practice in the industry, a CDR $\leq$ 0.20 was selected. Loads were computed using the analog system shown in figure 38.

The net result of the fatigue analysis was that the ODTM possessed substantial margin to withstand a moderate number of FA- and TA-level vibration sweeps without exceeding the CDR of 0.02. This provided considerable confidence in the conduct of the test because earlier approximate analyses had indicated potential problems in the VLCA and bus main longerons. This confidence was borne out when a rigorous posttest dye-penetrant examination disclosed no fatigue cracks.

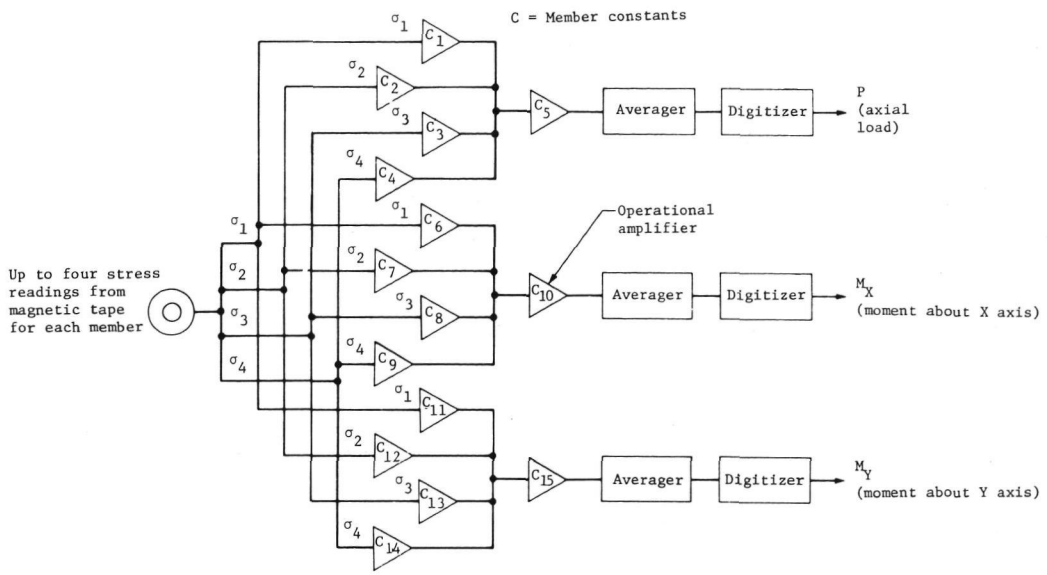

Figure 38.- Analog computation of loads.

The test article consisted of the LDTM, ODTM, VLCA, a Viking Spacecraft Adapter (VSCA), and a Viking Transition Adapter (VTA). Major assemblies comprised flight-configured hardware where possible, while most components were mass simulated. The bioshield and propellant tanks on the LDTM contained referee fluids and were pressurized for the test. The ODTM propulsion model was pressurized.

For the longitudinal axis test, excitation was provided by a vibration exciter with an output force rating of 133 440 N (30 000 lb).

The combined weights of the LDTM/ODTM and the test fixture (more than 4500 kg, 10 000 lb) would have prevented normal operation by excessive deflection of the shaker armature. Pneumatic springs with a resonant frequency of approximately 2 Hz were mounted on the shaker body at 120° intervals. A position control servo regulated the springs' air volume and positioned the shaker armature at the center of its stroke under static conditions.

Experiments with the shaker indicated a trunnion resonance of approximately 12 Hz when the shaker was suspended on its isolation pads. Blocking the shaker or lifting the trunnions off the isolation pads increased this frequency to 35 Hz. Further experiments and analysis demonstrated the potential danger of sweeping through the trunnion resonance (i.e., undesirable coupling of the spacecraft and fixturing could occur). Therefore, for all tests below 25 Hz, the shaker was blocked by inserting shims between the shaker body and steel posts hard-mounted to the seismic mass. For testing above 25 Hz, the shims were removed.

The LDTM/ODTM was excited in the two lateral axes with four electrodynamic shakers, each rated at 667 N (150 lbf). The shakers were pendulously supported from crane hooks and chain and attached to the ODTM bus main longerons through adjustable "stingers" and mechanical fuses (flexures).

Low-level test runs were made before full-level testing, (tables 6 and 7). From these precursor runs, the responses of critical structural elements or components were evaluated by analysis of oscillograph plots, X-Y tracking filter plots, and the analog computer program that generated ODTM member loads. Comparison of these data with response analysis predictions provided confidence in the test structure to withstand full loading.

TABLE 6.- FORCED VIBRATION TEST LEVELS, LONGITUDINAL (Z) AXIS

Level	Amplitude, g peak					
	25-7 Hz	22-8 Hz	22-10 Hz	200-20-200 Hz	128-20-128 Hz	200-128-200 Hz
Precursor	0.5	--	--	0.5	--	--
Flight acceptance	--	1.0	--	--	1.0	0.00305 cm (0.0012 in.) double amplitude
Type approval	--	--	1.5	--	1.5	0.00457 cm (0.0018 in.) double amplitude

TABLE 7.- FORCED VIBRATION TEST LEVELS, LATERAL (X,Y) AXES

Level	Text Axis	Amplitude, g peak	
		200-5-200 Hz	200-8-200 Hz
Precursor	Y	1.5 (311)*	--
Full	Y	--	1.5 (556)
	X		

*Numbers in parentheses indicate force level (N) for each of the four shakers.

Longitudinal vibration input was controlled with a 36-channel peak select system, which continuously monitored the output signals of 12 input control accelerometers on the ODTM bus structure main longerons (fig. 39) plus a 24 channel mix of strain gages and accelerometers.

Acceleration input to the test structure was controlled on the transducer whose output signal matched its peak select setting. Figure 40 is a functional diagram of the control system.

A 59 channel peak limit system was used. This safety circuit terminated the output of the vibration exciter without transient if the instantaneous peak magnitude of any of the 59 peak limit settings exceeded a preset value. Because of test philosophy and hardware differences, peak limited signals assigned to the LDTM were passed through a 200 Hz filter before reaching the protection module. Channels used for ODTM peak limiting were conditioned with 800 Hz filters. Figure 41 shows the instrumentation flow.

Lateral axis testing, in which four separate shakers were used, was controlled in a manner similar to that used for the longitudinal test. The four shakers and associated power supplies were married to the peak select control system. Because individual shakers were carefully matched with their transformers, it was decided to control the force input on all four shakers by connecting them in series and using the armature current output signal from just one of the four shakers. This technique was very successful.

Control accelerometers mounted on main longerons			
Acc ID	Upper ring	Lower ring	Direction
2-3 Top L	✓		Long.
2-3 Top R	✓		Radial
2-3 Bot R		✓	Radial
7-8 Top L	✓		Long.
7-8 Top R	✓		Radial
7-8 Bot R		✓	Radial
10-11 Top L	✓		Long.
10-11 Top R	✓		Radial
10-11 Bot R		✓	Radial
15-16 Top L	✓		Long.
15-16 Top R	✓		Radial
15-16 Bot R		✓	Radial

Additional positions			
Acc ID	Upper ring	Lower ring	Remarks
4-5 Bot tri		✓	Accel to be mounted on blocks attached to chassis face by No. 8 shear-plate fasteners
15-15 Bot tri		✓	
1-16 Bot tri		✓	

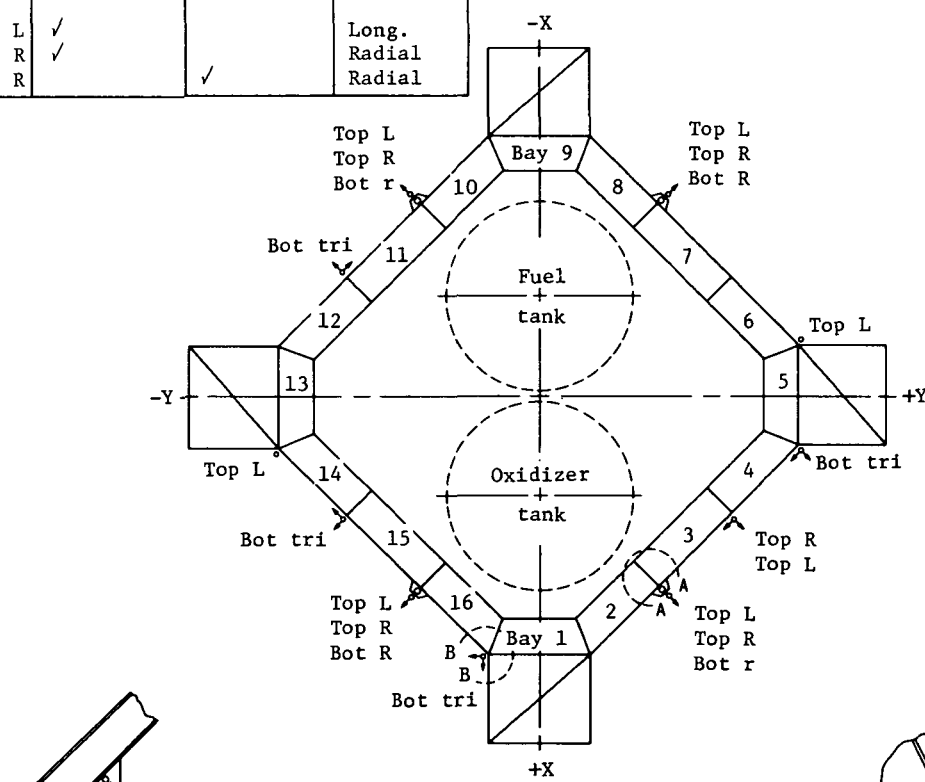

10-32 Keensert
top and bottom rings

Detail A-A
separation boss

Notes:

(1) Top - Upper ring
(2) Bot - Lower ring
(3) L - Longitude
(4) R - Radial
(5) Tri-triaxial

1/4-28
Keensert

Detail B-B
upper and lower
ring (corners)

Figure 39.- Input control accelerometers.

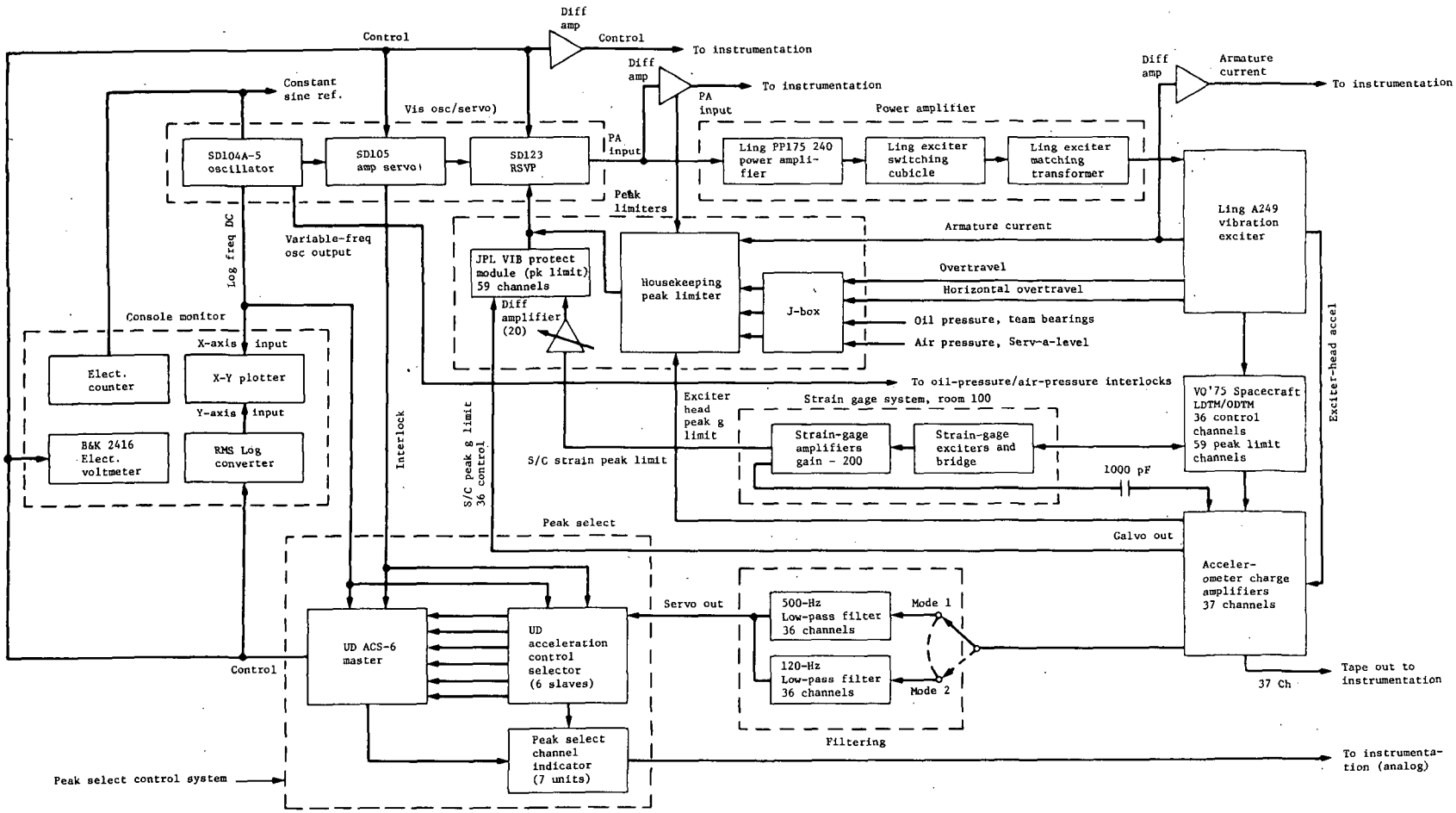

Figure 40.- Schematic of longitudinal-axis control system.

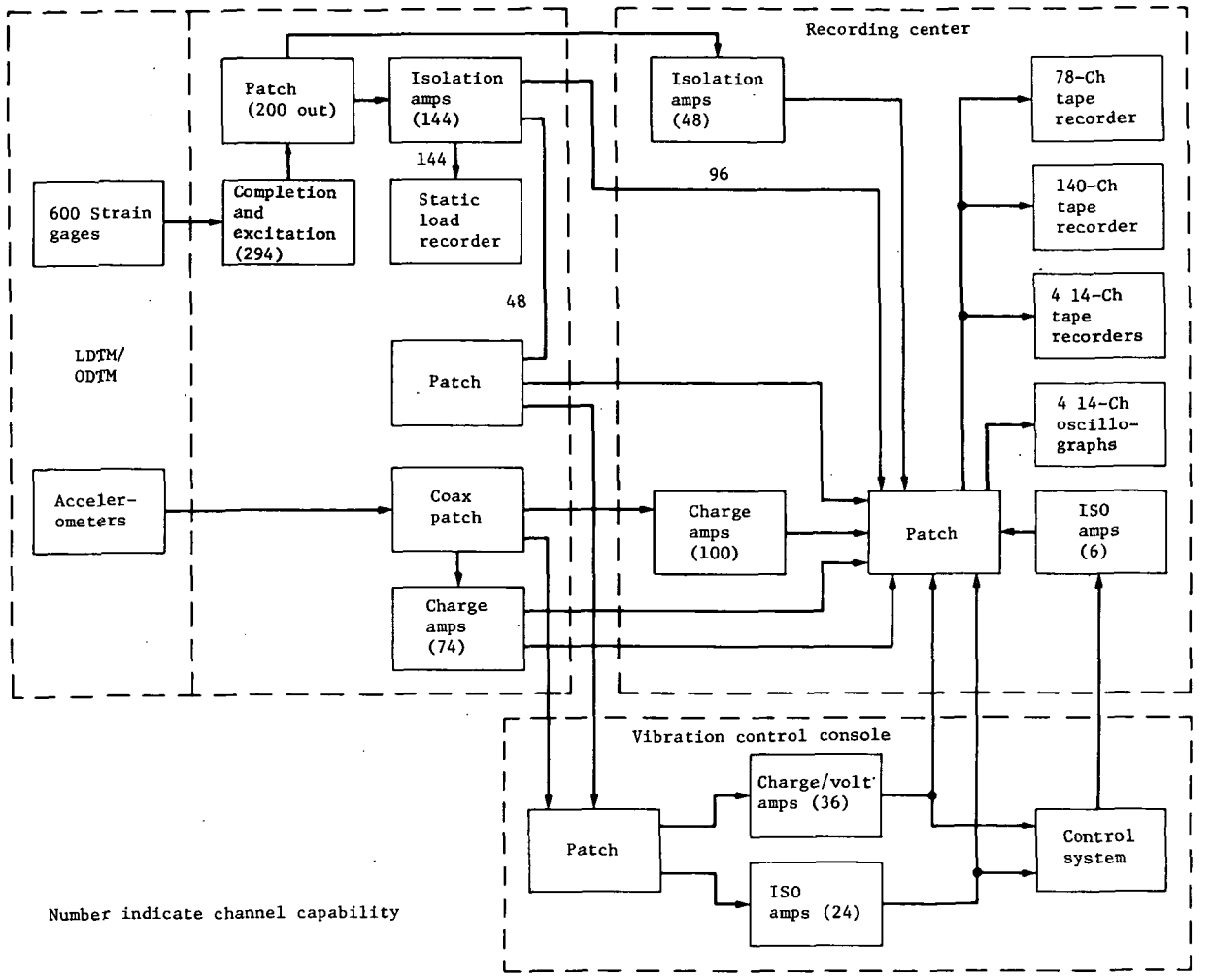

Figure 41.- Instrumentation flow.

Test results revealed a number of interesting facts about response control of complex test setups. Because of control-system and load limitations combined with the response characteristics of the LDTM/ODTM (narrow bands with high amplitudes), the servo control was unable to maintain a constant input acceleration at any one of the 12 control accelerometers. This was not unexpected because similar behavior had been observed in earlier spacecraft testing. In addition, studies at the dynamic test facility using instrumented cantilevered beams and the proposed control hardware disclosed that control might be difficult at frequencies below 17 Hz. That is, during switching from one control channel to another, overshoot errors could occur, resulting in a possible overtest. Overshoot is the maximum observed test amplitude greater than the desired peak select control level.

Two basic sources contribute to overshoot: RC time constant of ac-dc conversion, and deadband. The time constant is simply the time required to convert the ac signal from the transducer into a dc voltage. This was done in two places: the ACS-6 (peak selector), and the servo. The time constant is a function of frequency and is longer at low frequencies than high. Deadband is the amount that one signal must exceed another to cause a switch of the ACS-6 output from the latter to the former. Of the two overshoot sources, the RC time constant was the more significant.

Although a definitive model of control system capability was not available, the overshoot appeared to be dependent on the following parameters:

1) Resonant frequency;

2) Slope or Q of the resonance;

3) Sweep rate;

4) Direction of sweep (up or down).

Significant overshoots were observed during the test runs. Low-level test runs were made and the peak select control levels carefully monitored to evaluate this phenomenon. Examination of on-line oscillograph records of response-control strain gages disclosed initial amplitudes 1.00 to 1.52 times the peak select level established for these transducers. Stress values from these low-level test runs were used to derive internal loads in ODTM structural members. Peak limit and peak select load values were established based on these low-level runs and applied to full FA and TA test levels.

All forced vibration test runs on the LDTM/ODTM were controlled by ODTM bus input accelerometers or by various strain-gage/accelerometer response measurements. Figure 42 illustrates a typical run showing the effects of response control on the input levels at the ODTM bus. Figures 43 through 45 are examples of comparison of analytical and measured response values.

The response analysis of the coupled LDTM/ODTM math models was very helpful in estimating potential response control channels. Typical measured load values were compared with their analytical counterparts. Based on the comparison, 50% of the measured frequencies were higher than predicted and 50% lower. Approximately two-thirds of the measured loads were somewhat lower than predicted values. This was not unexpected because of the tolerances used in establishing peak limit/select values (i.e., analysis limits did not include test tolerances).

Examination of typical response accelerations reveals that measured frequencies were usually higher than those predicted by analysis. Amplitudes were generally lower than predicted, by approximately the amount established by test tolerances.

Results of the Viking 75 LDTM/ODTM test were:

1) Test implementation went better than anticipated, due in large part to the pretest analyses and careful preparation leading up to the test;

2) Forced vibration qualification levels were successfully imposed on the LDTM/ODTM structure. Load levels generally did not reach design load limits attained in static testing because of control-system test tolerances;

3) Test predictions based on the Viking mathematical model correlated reasonably well with test data. In general, test frequencies were slightly higher than analytical predictions and amplitudes lower. This further demonstrated that the coupled Viking spacecraft mathematical model had no major errors;

4) Precision in determining exactly when a control accelerometer would take over (other than for rigid-body modes) was beyond the capability of the analysis. This is particularly true when actual control system constraints are considered (i.e., overshoots, time constants, etc).

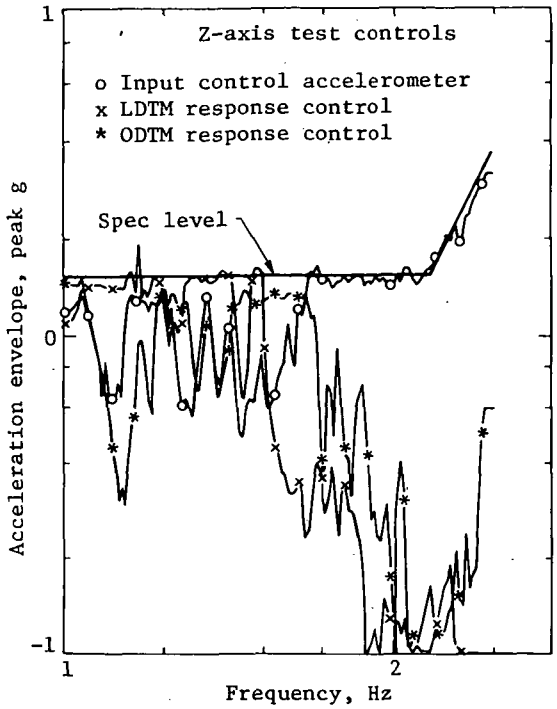

Figure 42.- LDTM/ODTM stack test, TA-level downsweep controls.

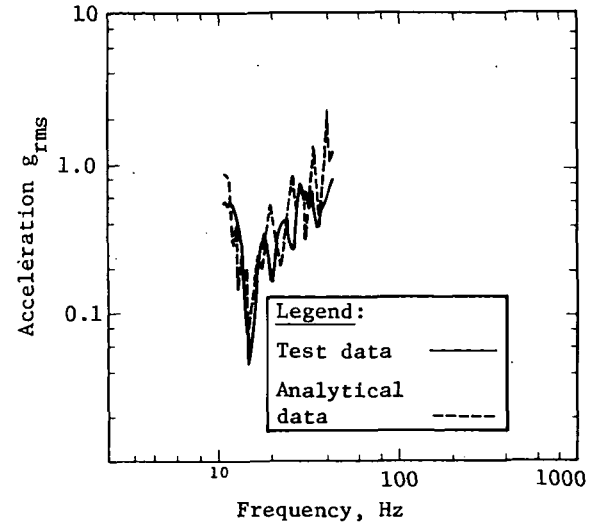

Figure 43.- Comparison of test and analytical data at VTA/VO interface.

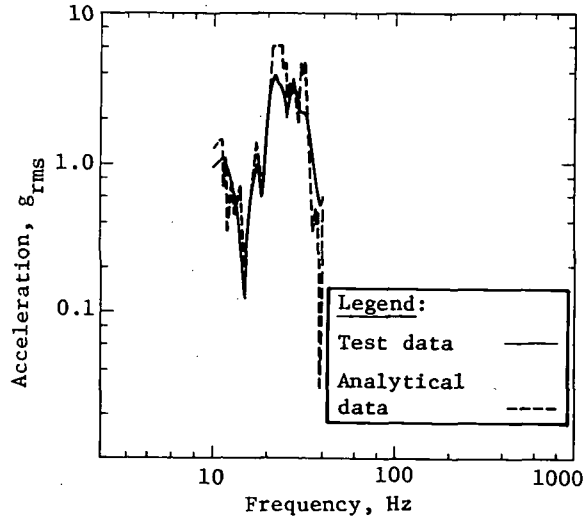

Figure 44.- Comparison of test and analytical data at lander equipment plate.

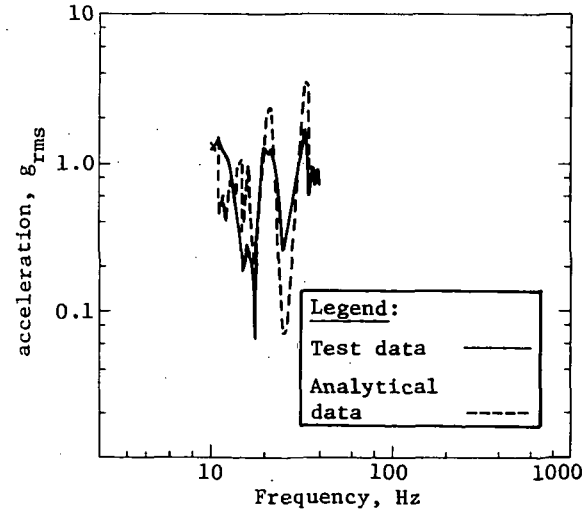

Figure 45.- Comparison of test and analytical data at Lander terminal descent engine.

The primary objectives of the sinewave vibration test of the PTC were to verify that the simulated launch vibration environment would not cause intermittent failure of selected operating systems, and to measure responses at a number of critical component locations.

The PTC, attached to the VLCA truss, was installed on a magnesium fixture attached to a vibration exciter. The fixture included flexures for lateral and torsional stability. The input to the VLCA truss was controlled by a digital system that monitored the outputs of selected transducers and adjusted the shaker input to keep the responses within specified tolerances so that design loads in primary structure would not be exceeded.

Sinewave sweeps were conducted as follows:

Type	Frequency range, Hz	Level, cm (in.)	Sweep rate, oct/min
Precursor	5.0-7.1	0.49 (0.193) DA	4
	7.1-200	0.5 g pk	(up only)
Flight acceptance	5.0-10.0	0.49 (0.193) DA	4
	10.0-128	1.0 g pk	(up and down)
	128-200	0.00305 (0.0012) DA	
Qualification	5.0-10.0	0.74 (0.29) DA	4
	10.0-128	1.5 g pk	(up and down,
	128-200	0.0046 (0.0018) DA	twice)

During each test, data were recorded from 75 accelerometers and 12 strain gages. After each test run, all data were played back on oscillograph recorders for quick-look review. Spectral plots of selected data were obtained using a peak detector/narrow-band filter to condition the signals.

The success criterion for the test stated that the fixture accelerometers must control to the specified input levels to within ±2 dB until primary structural limits controlled, where the tolerances were increased to ±3 dB. A posttest data review indicated that the test met this requirement.

During the precursor (0.5 g pk) test, a noisy channel on the equipment plate erroneously exercised control in certain frequency ranges. Before proceeding to the FA test, this problem was corrected by inserting a low-pass filter. During the FA run, an abort occurred because the trigger level had been set too low. The qualification level runs were conducted without any difficulties, and the PTC test was successfully concluded.

Pyrotechnic shock and separation tests.- A series of pyrotechnic shock tests and combined pyro/separation tests was conducted to:

1) Evalute the effects of pyrotechnic actuations on the total system, including the effects of one test sequence on subsequent events;

2) Measure shock environments at critical points on the vehicle resulting from each test event;

3) Demonstrate end-to-end separation and deployment sequences on the PTC vehicle to verify the functional capability of the pyro devices and separation/deployment hardware.

The pyro shock tests consisted of firing the full complement of ordnance devices in proper mission sequence, starting with prelaunch propulsion valves and tube cutters and finishing with devices used to initiate operational status on certain science experiements. These were conducted on the PTC vehicle so that any undesirable effects on component performance could be monitored. The resulting shock environments were measured using the set of accelerometers installed for the preceding acoustic and sinusoidal vibration tests, after appropriate recalibrations of the instrumentation.

No performance anomalies were found in the electronic components, but two mechanisms malfunctioned. A staging connector failed to separate cleanly due to a faulty retention bracket, and a temperature probe did not deploy properly. These were both redesigned and retested successfully.

Separation tests were conducted on both the LDTM and the PTC. The following separations were performed:

LDTM

1) Lander/base cover;

2) Lander/aeroshell;

3) VLC/bioshield cap;

4) VLC/VO;

PTC

1) VLC/bioshield cap;

2) VLC/VO;

3) Lander/aeroshell;

4) Lander/base cover.

The order of LDTM separation tests was dictated by scheduling convenience and hardware availability, whereas the PTC tests were performed according to the mission sequence.

As a result of anomalies revealed by the test program, a number of significant design improvements were necessary. Before the Lander/base-cover separation test on the LDTM, static friction at the shear pins connecting the base cover to the Lander was measured and found to exceed the maximum allowable value. This was corrected by reaming the shear pin holes to a larger diameter. The stiction criterion was met when the measurement was repeated. When the separation test was performed, the assembly bolts were not extracted cleanly when the pyrotechnic separation nuts fired. The bolt retention system, which had been a passive crushable honeycomb shock absorber, was replaced with a spring-loaded bolt extraction and retention mechanism. This functioned satisfactorily in the subsequent PTC test.

During the LDTM VLC/VO separation test, excessively high pitch rates were measured on the separating capsules. After careful measurement of the ball and socket joint locations at the VLC/VO interface, it was concluded that joint misalignment had caused the high pitch rate. Alignment tolerances were tightened, and the problem did not recur on the PTC.

Mortar firing tests.- Three parachute mortar firing tests were conducted using a test article of flight-type VLC primary and secondary structure ballasted with mass simulators representing components. The assembled test article included the Lander body, base cover, aeroshell, flight weight mortar (with dummy parachute pack), and mortar thermal cover.

The test article was supported by a suspension system that included horizontal cable constraints to prevent excessive pendulum motion of the vehicle. A large, ballasted net was used to arrest the motion of the dummy parachute pack.

The first test indicated the need to change the design of the sabot retention system to reduce structural loads and component shock environments induced by the mortar firing. In the modified version, rows of stitching in the webbing retention system were designed to tear out progressively, thus reducing the deceleration shock. For the second test, a flight-type mortar thermal cover replaced the simulator used in the first test, and the redesigned sabot retention was incorporated. Finally, in the third test, a flight-type bridle was added to determine the effects of swivel deceleration on component environments. The second and third tests demonstrated that the design change was successful in reducing shock environments to acceptable levels.

Landing-leg deployment tests.- Landing-leg deployment tests were performed using landing-leg assemblies and Lander/base-cover structures in the configuration representing the Viking Lander System (VLS) at leg deployment as defined in the mission sequence of events. Before deployment, the landing legs were locked in their stowed position inside the base cover. The locking devices were released by pyrotechnic pin pullers, allowing the legs to extend under the influence of deployment springs and gravity--then lock in the down position. The objectives of the test were to:

1) Verify the functional performance of the leg deployment system;

2) Qualify the landing system structure to dynamic design limit and margin deployment loads, and measure leg downlock loads.

The test article was suspended from a parachute bridle simulator, leg deployment was initiated, and the resulting shock environment measured using high-frequency accelerometers. Loads developed in the leg members and in the main support fittings were measured with strain gages.

To impose the margin deployment load condition, a second leg deployment test was performed in a 1.5-g simulated deceleration environment. Simulation of this load condition was achieved by addition of mass to the bipods of each leg.

All test objectives were met. Strain-gage data indicated that deployment loads were close to predicted values and quite repeatable. Accelerometer data showed that shock levels were less than those used for component qualification. The shock resulting from the mechanical impact at downlock was more severe than that caused by the pyrotechnic pin puller.

Landing shock tests.- Landing shock and resulting loads were prime concerns in the design of Viking structure. Therefore, an extensive development program was conducted including component footpad, attenuator, and load-limiter development tests, soil penetration tests, vehicle stability analyses, and 3/8-scale model tests, followed by full-scale drop tests of the LDTM vehicle. Table 8 lists requirements for the landing system at two points during the project.

TABLE 8.- VIKING LANDING-GEAR DESIGN CRITERIA

Parameter	Contract go-ahead	As flown
Vertical velocity	3 ±1.5 m/s (10 ±5 fps)	2.44 ±0.9 m/s (8 ±3 fps)
Horizontal velocity	±1.8 m/s (±6 fps)	±1.22 m/s (±4 fps)
Engine cutoff altitude	3 ±1.5 m (10 ±5 ft)	at touchdown
Engine cutoff sensor	by radar	switches in legs
Stability	all 19° slopes	99.7% stable
Package loads	80 g	30 g
Clearance	22 cm (8.66 in.)	22 cm (8.66 in.)
Coeff of friction	1.0 for stability 0.2 for clearance	1.0 for stability 0.2 for clearance

The final flight configuration of the landing gear, weighing 20 kg (44 lb) evolved from an early design weighing over 45 kg (100 lb). The main features of the final design were the crushable honeycomb main strut attenuators and secondary strut load limiters.

The test article, consisting of the Lander body ballasted with mass simulators representing components, was suspended from a drop sling and release mechanism. A series of drops were conducted, varying the pitch and yaw attitudes so that each of the footpads impacted first, then so that various combinations of two footpads impacted first in order to produce worst-case loading conditions and shock levels at component locations.

The series of tests confirmed the capability of the landing gear and the integrity of the structure to survive the loads imposed by landing shock. Adequate data were obtained to verify the shock environments for components and to establish confidence in the landing dynamics analyses.

Ground vibration survey (GVS) tests.- A series of ground vibration surveys was conducted to obtain natural frequencies, damping and mode shapes of major structural modes, and to measure modal strain transformations to key structural elements, for use in correlation with analysis and to support the static test program. The overall objective of the series was to obtain data to verify the mathematical model used for loads and controls analyses of the various phases of the Viking mission.

Modal survey tests of the postlanded configuration and base-cover and mortar support structure were deleted from the program. Enough data were obtained from the tests conducted so that these tests were not considered necessary.

This section briefly describes testing conducted for the LDTM launch and terminal descent configurations. In general, each test program was conducted in four phases as follows.

1) Wide-band sine sweeps (5 to 200 Hz) were conducted using single or multiple shakers at a constant force level on each shaker. The control signal was stepped over the frequency range in increments of 0.5 Hz. Selected measurements were processed to obtain coincident/quadrature (CO/QUAD) versus frequency plots to identify modal frequencies and provide insight on shaker locations most likely to excite specific modes.

2) Modes were coarse tuned by manually adjusting shaker frequencies near the modal frequencies and monitoring Lissajous patterns. Force distributions and shaker phase relationships were adjusted to optimize mode excitation. Acceleration decays were then obtained to assess the purity of the mode.

3) Each mode was fine tuned by varying the frequency around the modal frequency to obtain the peak quadrature value on selected transducers.

4) Modal dwells and decays were conducted after fine tuning was completed. Outputs from accelerometers, strain gages, and force transducers were recorded and processed to CO/QUAD tabulations.

Data describing 20 elastic modes were considered sufficient for correlation with the analytical model of the launch configuration because very few primary structural members were designed by the launch environment. Modes contributing to loads in these members and to the component launch environment were deemed important. The goal for assessing the validity of the modal data was the commonly used $\leq 10\%$ orthogonality criterion.

During the terminal descent GVS test, 26 test modes were identified. Thirteen of these involved significant overall vehicle response and were recorded on magnetic tape for posttest analysis. The other 13 modes were localized structure modes. As a result of the test data, several deficiencies in the Lander stiffness matrix were identified. To improve the analytical model, terminal descent propellant-tank and engine brackets were corrected.

Aeroshell dynamic capability test.- Data obtained during the boost phase of the first and second Titan/Centaur flights (TC-1 and TC-2) created concern about the strength capability of the Viking aeroshell to withstand the steady-state acceleration combined with the sinusoidal vibration expected during the Titan boost phase. Using the test setup shown in figure 46, a special test program was conducted to verify the structural integrity of the aeroshell for the combined POGO and steady-state acceleration environment.

The program was conducted in two phases. The first, using the LDTM aeroshell, served as a precursor to verify the techniques, procedures, and instrumentation before testing the flight capsule 3 (FC-3) aeroshell in the second phase.

The LDTM aeroshell survived the imposed vibration test without structural damage. However, elastic buckling occurred at the 0.9 g peak test level and recurred on all subsequent higher levels. Figure 47 shows an example of this behavior, as indicated by the notched peaks on the strain gage outputs. Buckling was not evident during the FC-3 aeroshell tests, but, beginning at the 1.3-g level, an audible beat was detected that continued for the 1.4- and 1.5-g tests. The beating is illustrated in figure 48. Attempts were made to isolate the cause of this phenomenon, including runs at reduced levels and thoroughly checking the shaker control and servo systems. It was concluded that the beating was similar to the dynamic buckling observed on the LDTM aeroshell, but occurring in a different mode because of the structural differences between the two aeroshells. Testing continued and the flight-configuration aeroshell survived the 1.5-g vibration test.

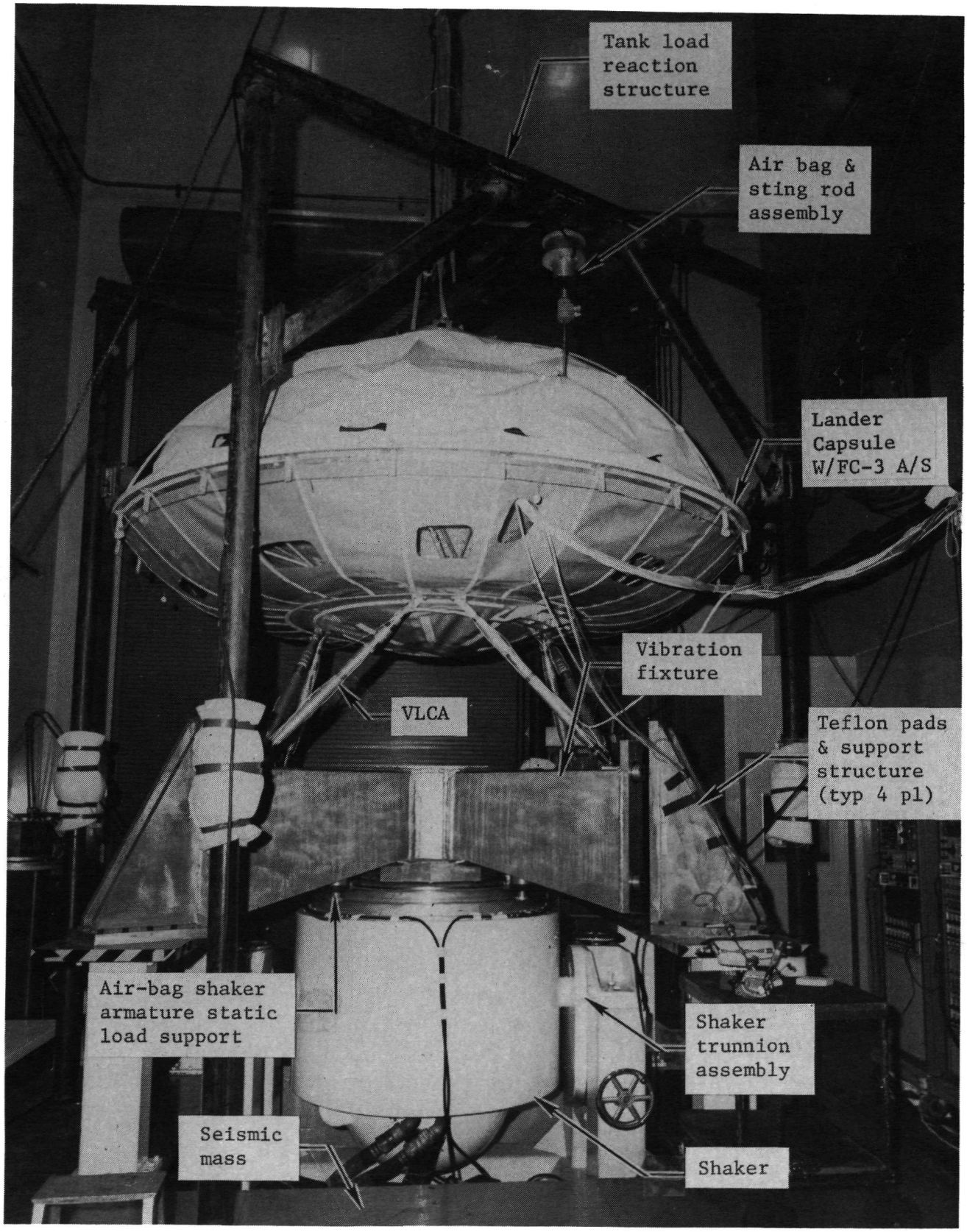

Figure 46.- Aeroshell dynamic capability test setup.

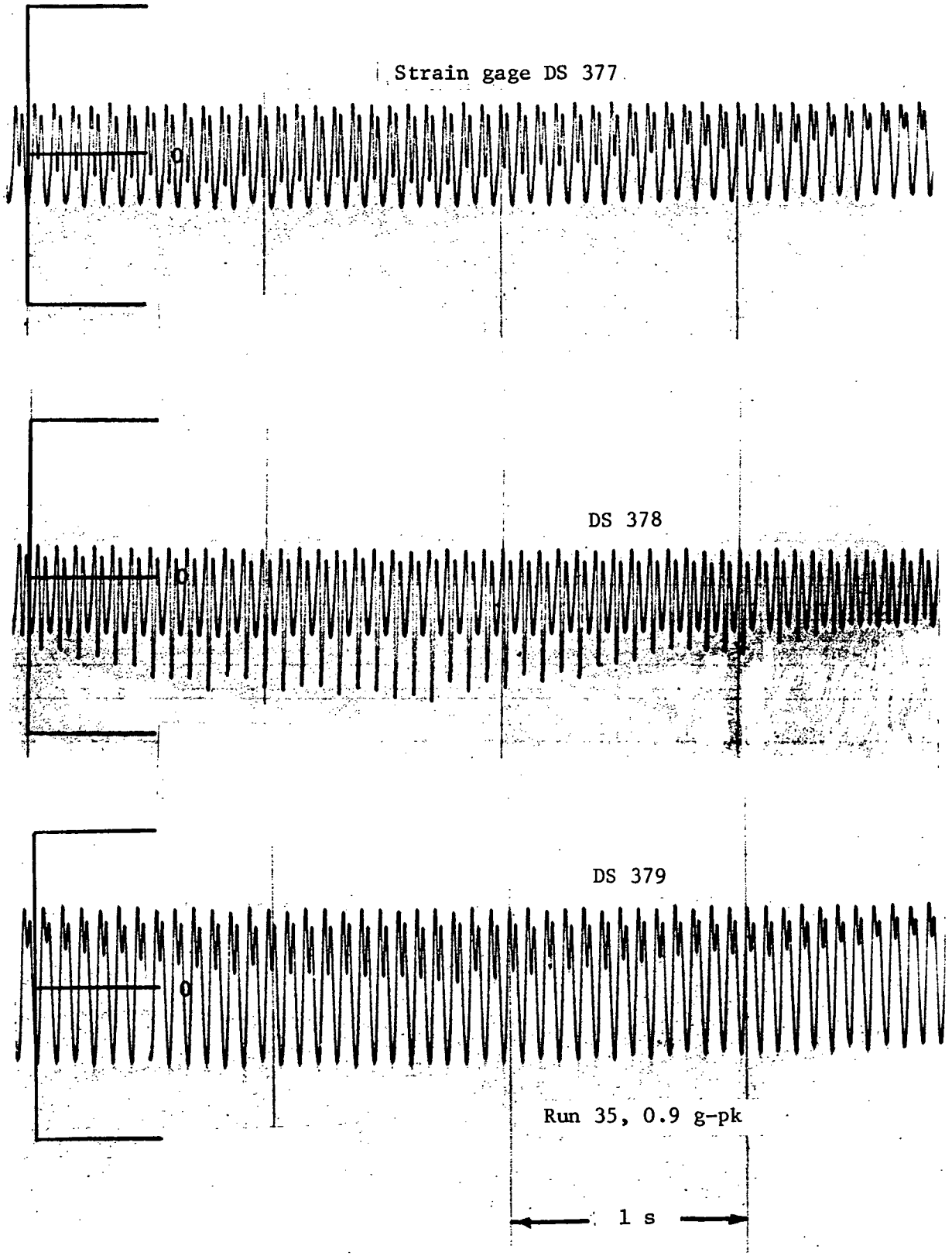

Figure 47.- Aeroshell buckling, run 35.

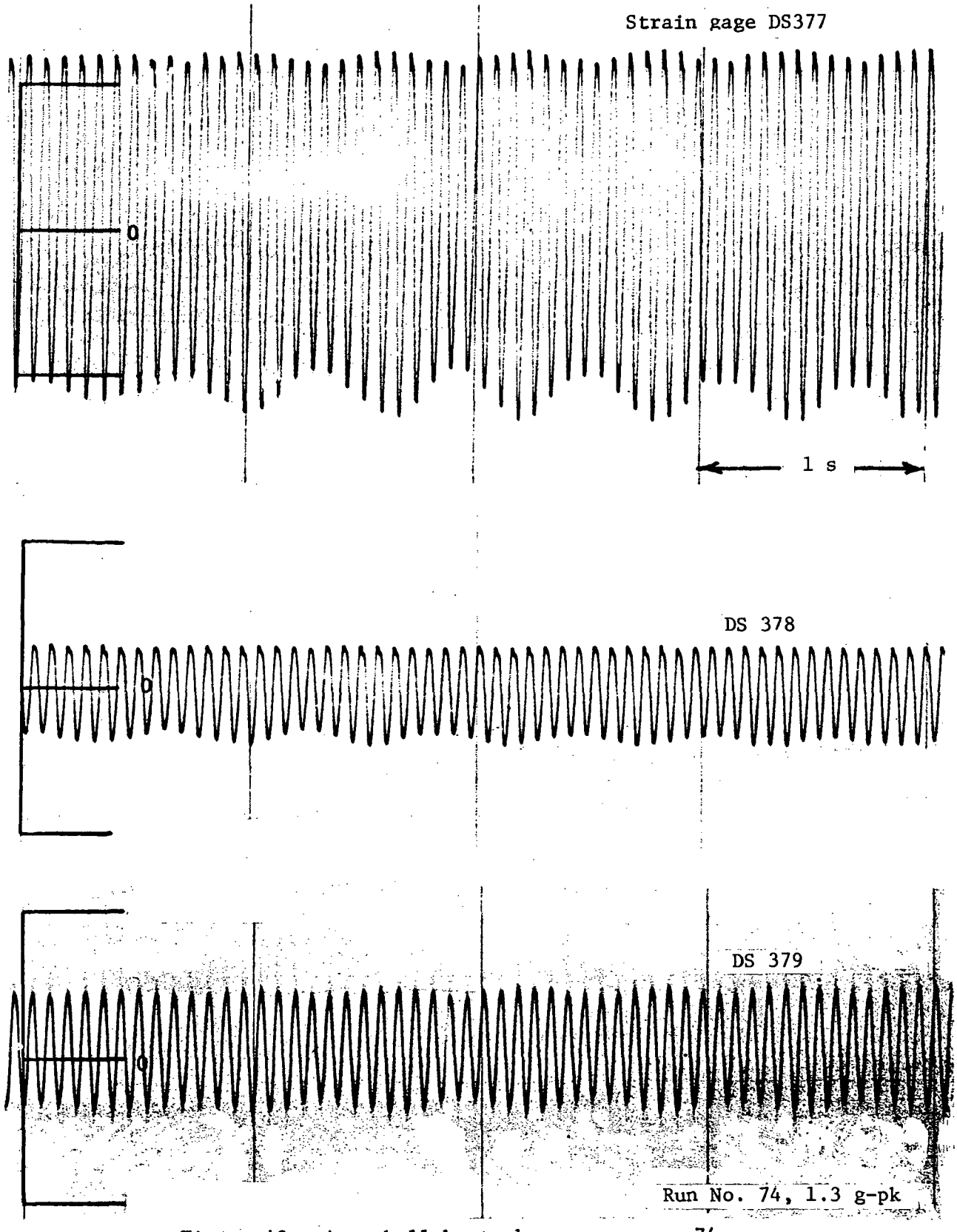

Figure 48.- Aeroshell beat phenomenon, run 74.

Flight Program

The flight program consisted of three launches of the Titan III/Centaur vehicle:

1) TC-1 Viking Dynamic Simulator (VDS);

2) TC-3 Viking B Spacecraft;

3) TC-4 Viking A Spacecraft.

These flights and their sequence afforded Viking structural and component designers an unusual opportunity. In effect, the spacecraft got a practice launch.

The primary goal of the first flight (VDS), the "proof flight" of the new launch vehicle system, was to verify the coupled Titan III/Centaur system. With instrumentation described later in this section, it also provided environmental data for components and verification of analytical techniques used for modal coupling and flight loads predictions. These environmental and loads data are seldom available at a timely point in a spacecraft production schedule for use in checking component test environments and primary structure loads.

The VDS (fig. 49) consisted of inertia simulations of the Lander and Orbiter supported by flight-type trusses. Table 9 lists flight measurements, and figure 50 shows transducer locations. The instrumentation gathered data to meet two major goals: environmental and loads evaluations. The environmental evaluation included measurements of acoustics, random vibration, and transient accelerations, and was accomplished with the listed accelerometers and microphones.

In addition to vibration measurements for environmental evaluation, strain gages and low-frequency (0 to 50 Hz) accelerometers were also telemetered for loads evaluation. As shown in figure 50, the majority of the strain gages were on the Proof Flight Lander Adapter (PFLA) members. Before assembly, these PFLA members were calibrated as axial load cells, allowing the axial loads in the PFLA members to be recorded as a function of time. Inherent in telemetry systems is a phase error from channel to channel when the data are extracted from the carrier signal. Special phase-matched filters and reduction techniques (ref. 20) were used to minimize these phase errors from channel to channel, resulting in time-correlated PFLA loads and VDOS bus accelerations. The PFLA load time histories were then used to:

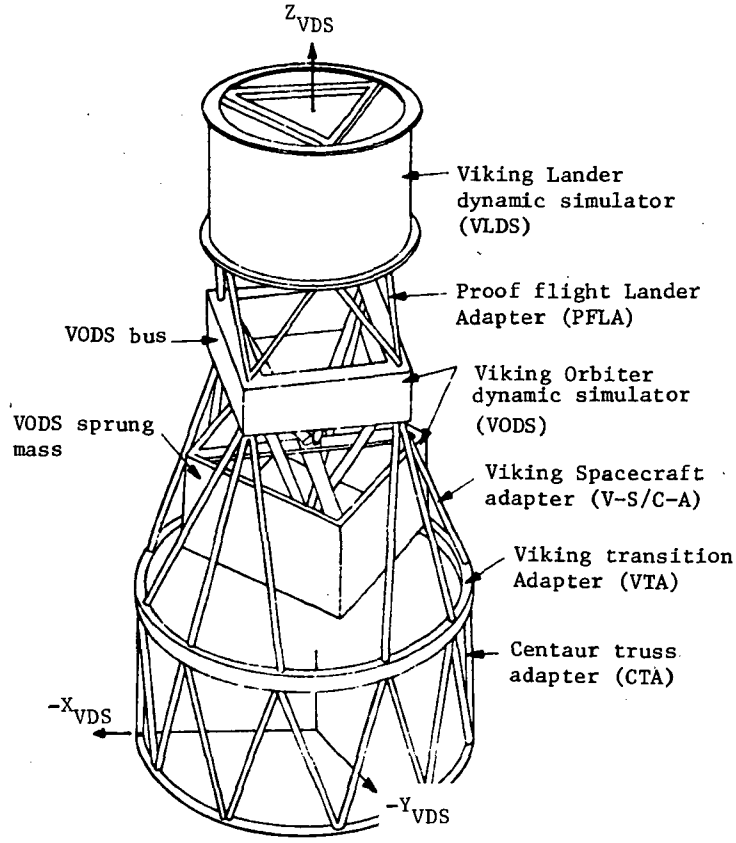

Figure 49.- Viking dynamic simulator configuration (from ref. 20).

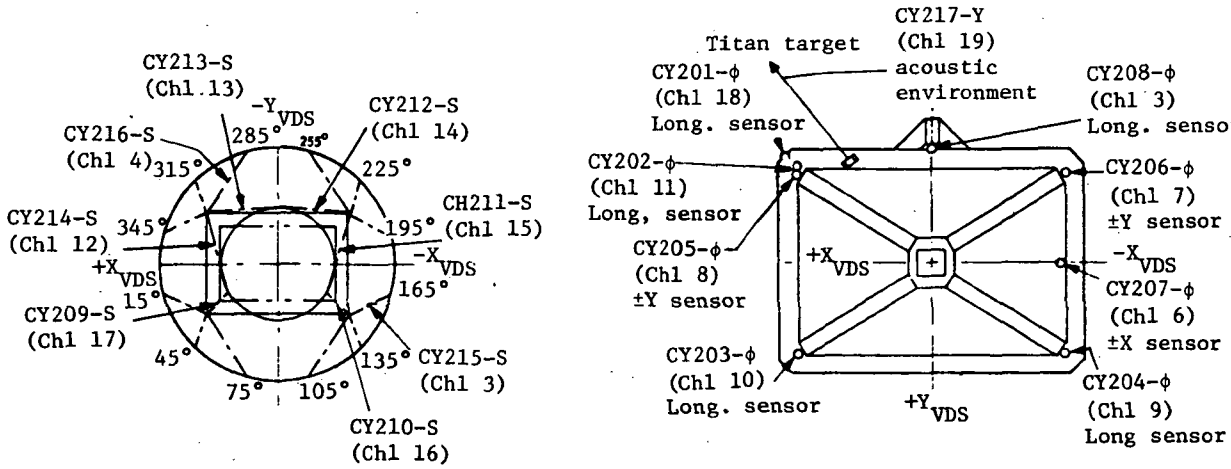

Figure 50.- VDS instrumentation locations.

TABLE 9.- VDS FLIGHT MEASUREMENT LIST

No.	Measurement No.	Description	Full scale range	Data cutoff frequency, Hz
3	CY216-S	V-S/C-A axial load transducer	112.7 kN (25 342 lb)	11.0
4	CY215-S	V-S/C-A axial load transducer	112.67 kN (25 331 lb)	14.0
5	CY208-Ø	VODS sprung mass Z-axis accelerometer	10.0 g	20.0
6	CY207-Ø	VODS bus X-axis accelerometer	10.0 g	66
7	CY206-Ø	VODS bus Y-axis accelerometer	10.0 g	55
8	CY205-Ø	VODS bus Y-axis accelerometer	10.0 g	50
9	CY204-Ø	VODS bus Z-axis accelerometer	20.0 g	46
10	CY203-Ø	VODS bus Z-axis accelerometer	20.0 g	43
11	CY202-Ø	VODS bus Z-axis accelerometer	20.0 g	42
12	CY214-S	PFLA truss axial load, member 202	120.88 kN (27 177 lb)	265
13	CY213-S	PFLA truss axial load, member 203	120.95 kN (27 192 lb)	239
14	CY212-S	PFLA truss axial load, member 204	120.79 kN (27 157 lb)	220
15	CY211-S	PFLA truss axial load, member 205	118.48 kN (26 636 lb)	210
16	CY210-S	PFLA truss axial load, member 206	120.87 kN (27 175 lb)	204
17	CY209-S	PFLA truss axial load, member 201	121.51 kN (27 319 lb)	200
18	CY201-Ø	Piezoelectric accelerometer, Z-axis	40.0 g	1050
19	CY217-Y	Acoustic microphone	150 dB	1400

1) Provide load data for verification of load prediction techniques;

2) Provide time histories of the forces and moments across an interface.

3) Define accelerations of the structure above the PFLA.

As further evaluation, the six servoaccelerometers mounted on the upper plane of the VDOS bus were used to calculate the rigid-body accelerations at the bus cg using an analog computer. These cg accelerations were compared to predicted analytical accelerations.

In general, except for the special reduction techniques described, reduction of the flight data was in the form of time history oscillographs, power spectral density (PSD) plots for steady-state random and shock response spectra for transient events.

At the conclusion of the VDS postflight data analysis, improved estimates of the acoustic and structural loads environment were obtained. VDS data had two major effects. First, measured acoustic levels were lower than predicted, resulting in a reduced environment for the PTC acoustic test, and in revised random vibration criteria for some components. Second, longitudinal oscillations (POGO) measured during VDS flight, and similar data from TC-2, Helios, resulted in concern for the aeroshell's ability to withstand the dynamic loads. As a result, the performance characteristics of the aeroshell were determined in the aeroshell capability test, described in a previous section, and accumulators were installed on TC-3 and TC-4 to alleviate the oscillations.

Originally, the purpose of the Viking spacecraft flight instrumentation was to permit postflight evaluation by comparing measured environments with calculated allowable loads. As a result, the number of transducers and their locations had less emphasis than for the VDS flight. Table 10 lists flight instrumentation for the Viking spacecraft and the Centaur equipment module. Figures 51 through 54 show the locations. However, with the concern about the POGO environment, flight data took on new significance. A Viking Flight Loads Evaluation Team was formed to assess the environments of the first flight. If any anomalies or unexpected conditions had existed, decisions as to what changes, if any, could be made for the second flight. For both TC-3 and TC-4 flights, loads analysis of the VLC and the Orbiter were performed on a limited basis as a postflight structural evaluation.

TABLE 10.- FM/FM TELEMETRY INSTRUMENTATION
(transmitter frequency = 2208.5 MHz; measured accuracy = ±5%)

Meas No.	Description	Range		Units	Response, Hz	FM/FM Channel	JPL Design
		Low	High				
CA886Y	Fwd equip. comp ambient	120	150	db	1395	19	
CY1820	Long. vib, bay 7/8	-30	30	g	1050	18	2001AC1
CY1830	Radial vib, bay 7/8	-20	20	g	790	17	2001AC2
CY1840	Long. Vib, Bay 2/3	-5	5	g	600	16	2001AC3
CY1850	Radial Vib, Bay 2/3	-20	20	g	450	15	2001AC4
CY186S	VLCA 750 strain 1	C-4448.2	T-3558.56	kN	330	14	2001SG1
CY187S	VLCA 751 strain 2	(10 000)	(8000)	(lbf)	220	13	2001SG2
CY188S	VLCA 752 strain 3	↓	↓	↓	160	12	2001SG3
CY189S	VLCA 753 strain 4				110	11	2001SG4
CY190S	VLCA 754 strain 5				81	10	2001SG5
CY191S	VLCA 755 strain 6				59	9	2001SG6
CY192P	VLC bioshield DP	-1723.69 (-0.25)	5171.07 (0.75)	N/m^2 (psid)	14	4	
CY193P	VLC bioshield pressure	(0)	110 316.12 (16)	N/m^2 (psia)	11	3	
CY000Z	Viking reserved				45	8	
CY000Z	Viking reserved				35	7	
CY000Z	Viking reserved				25	6	
CY000Z	Viking reserved				20	5	
	Centaur Vehicle (PCM data)						
CA8950	SCU normal 320°	-10	10	g	100		
CM101A	Axial acceleration	-2	8	g	50		

C - Compression
T - Tension

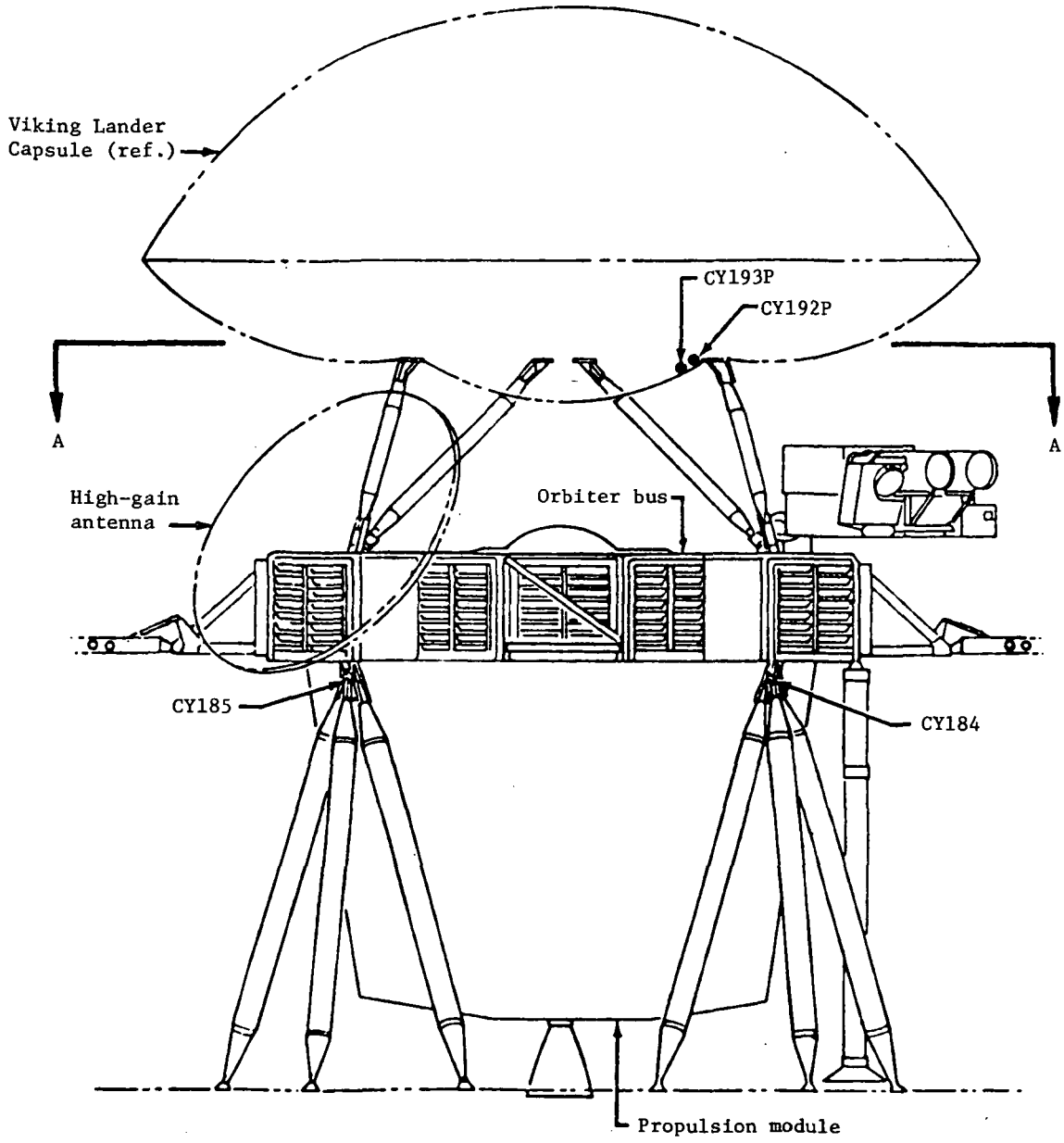

Figure 51.- Flight instrumentation locations.

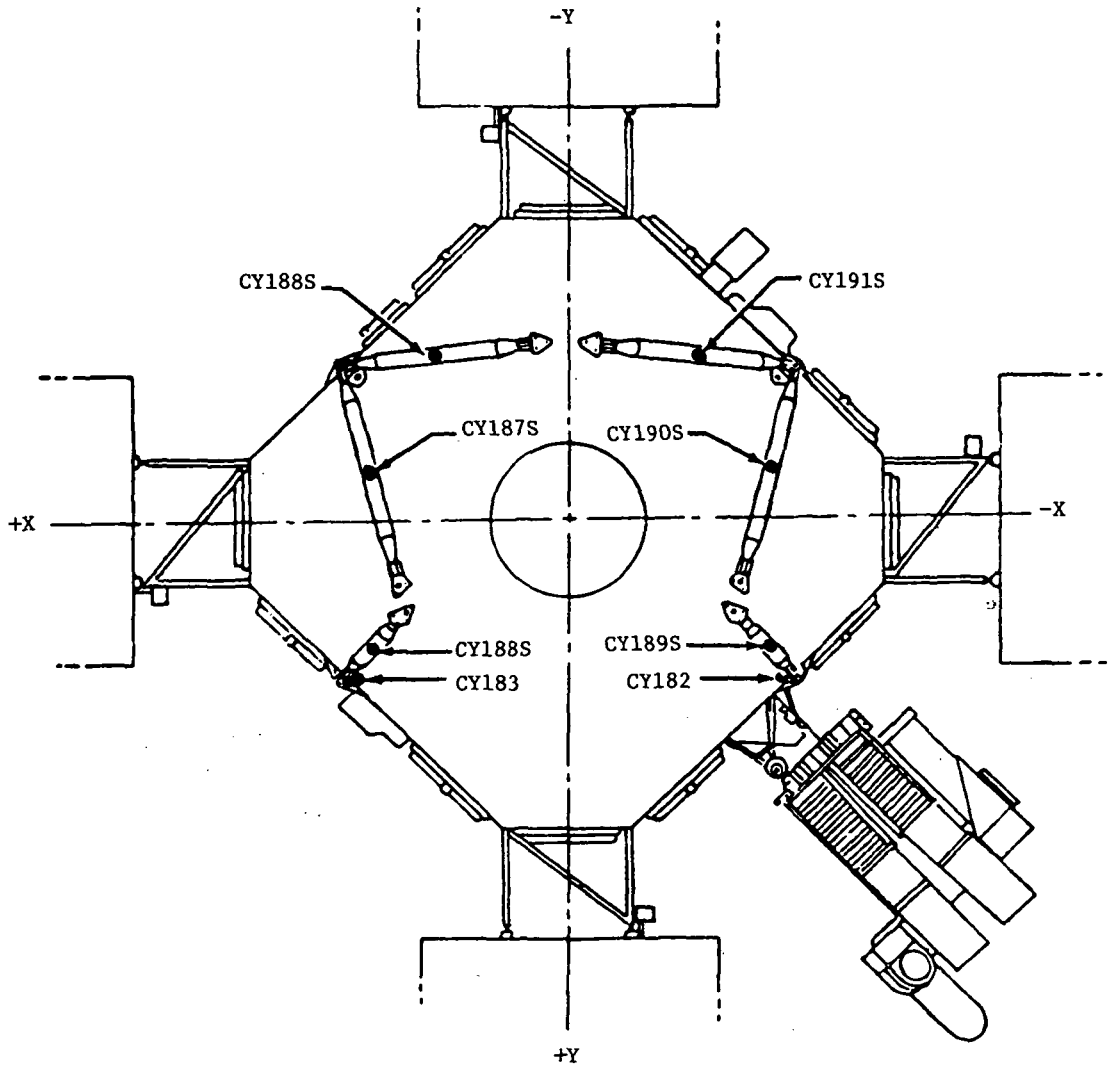

View AA

Figure 52.- Truss strain-gage locations.

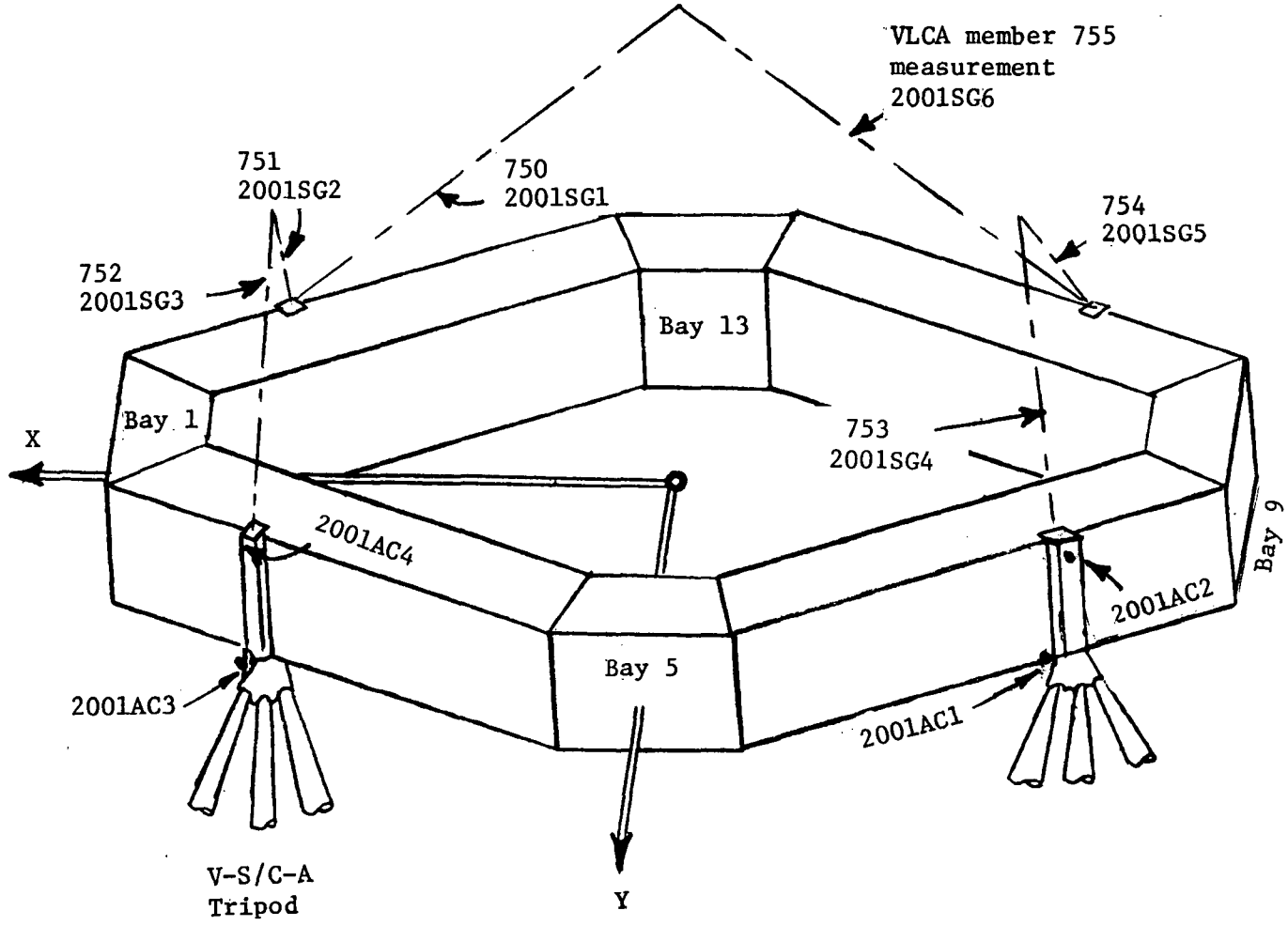

Figure 53.- Viking flight instrumentation on Orbiter bus.

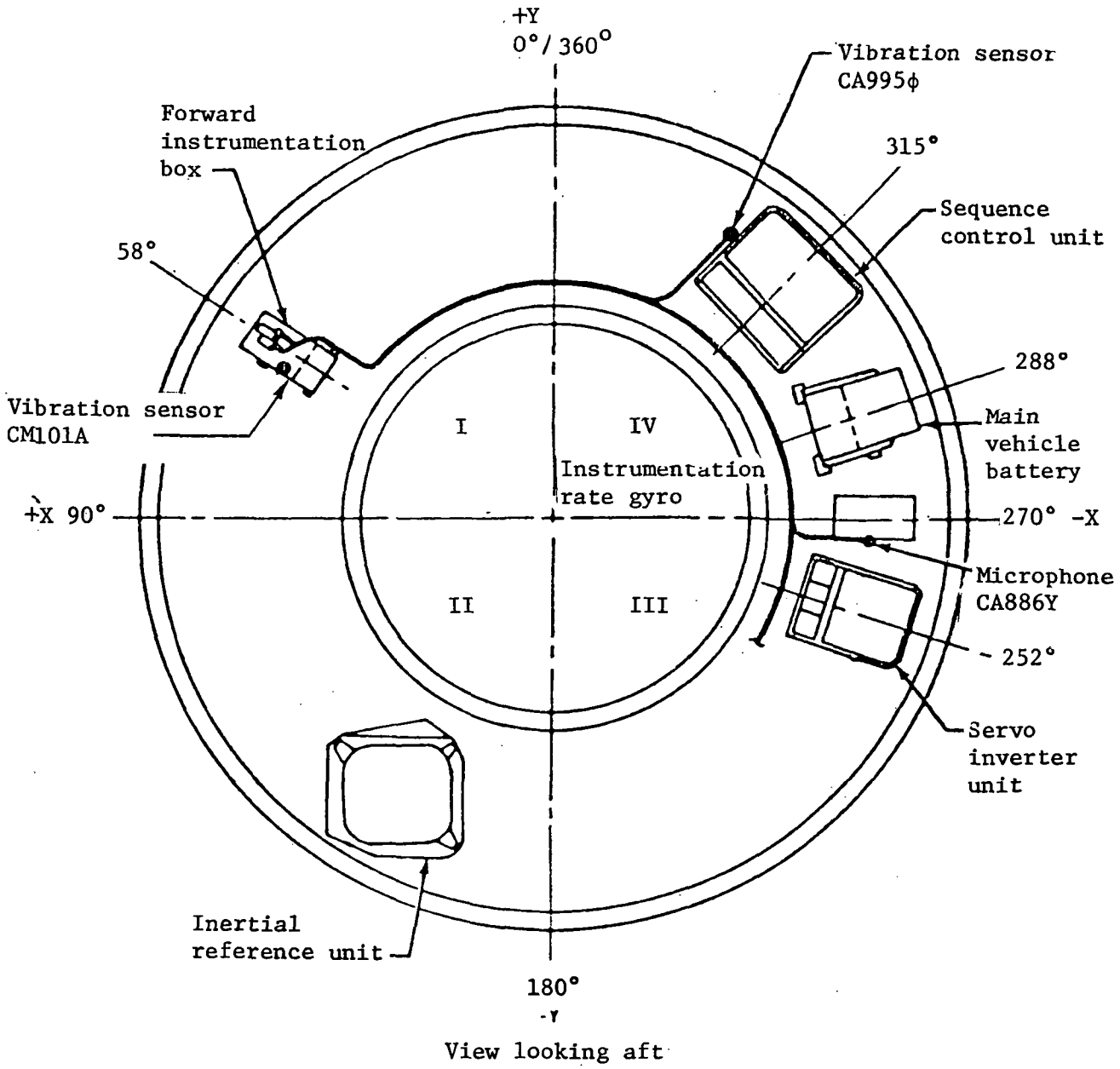

Figure 54.- Centaur equipment-module instrumentation.

The extensiveness of flight data and data analysis for Viking was a direct result of the design philosophy. The Viking spacecraft was very weight critical. Therefore, a safety factor of 1.0 was used to design both the Lander and Orbiter structures, resulting in a somewhat less conservative design in some areas. This approach strongly influenced the test and flight measurement programs.

Page intentionally left blank

A broad spectrum of missions, configurations, and performance requirements will be associated with future payloads. The Space Shuttle program alone exemplifies the wide range of components, experiments, and spacecraft that will present new problems in structural dynamics. Included are such factors as:

1) Reliability requirements for single-mission spacecraft and experiments compared to multimission, repairable spacecraft;

2) Commonality and standardization of parts, components, and subsystems, and qualification by similarity of components with previous flight use;

3) Cost effectiveness of protoflight versus the prototype system-level tests for different types of payloads and mission requirements;

4) The relatively broad range of test factors used throughout the industry for different types of dynamic environments.

In this section, experience gained during the Viking Project is used to suggest improvements for future payloads

Environments and Criteria

Vibroacoustics

Accurate definition of the acoustic environments for future payloads and improved techniques for predicting vibration response to the acoustic environment are needed to minimize changes to specifications and retest requirements. For example, figure 55 compares the revised acoustic spectrum measured on the Viking proof test flight to the original predicted spectrum. To account for uncertainties associated with the limited number of flight measurements, the revised spectrum included a 7 dB margin across the full frequency range.

Figures 56 and 57 show examples of changes to random vibration criteria resulting from the updated acoustic spectrum and ground test data. These are extreme cases, indicating both large increases and decreases to the vibration spectra based on original predictions. It is emphasized that this problem was not unique to Viking, but has been encountered on a number of other programs. For instance, on Apollo, initial estimates of the vibration environment were found to be low by as much as 10 dB, and many components had to be requalified (ref 21).

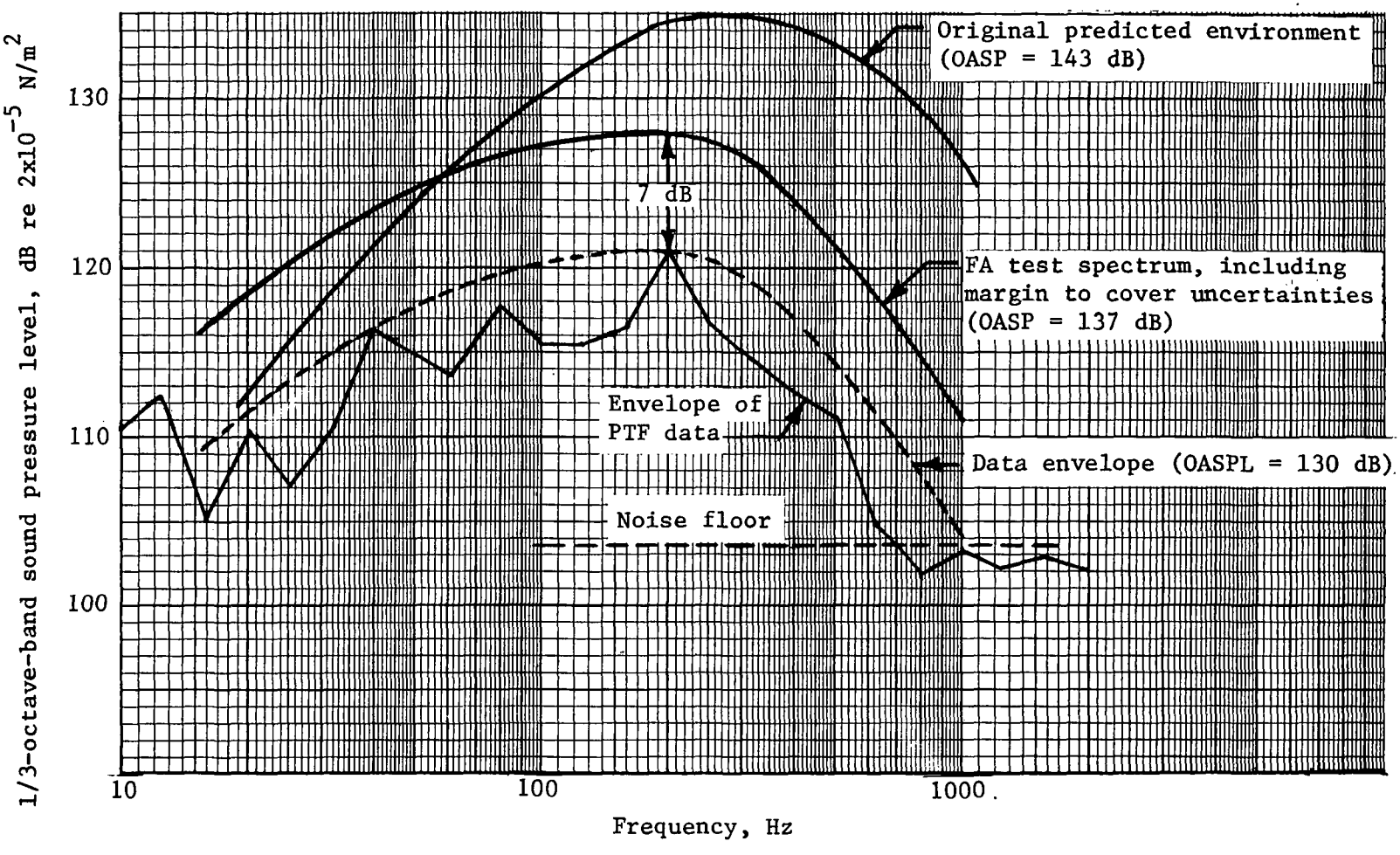

Figure 55.- Comparison of predicted acoustic environment with flight measurements.

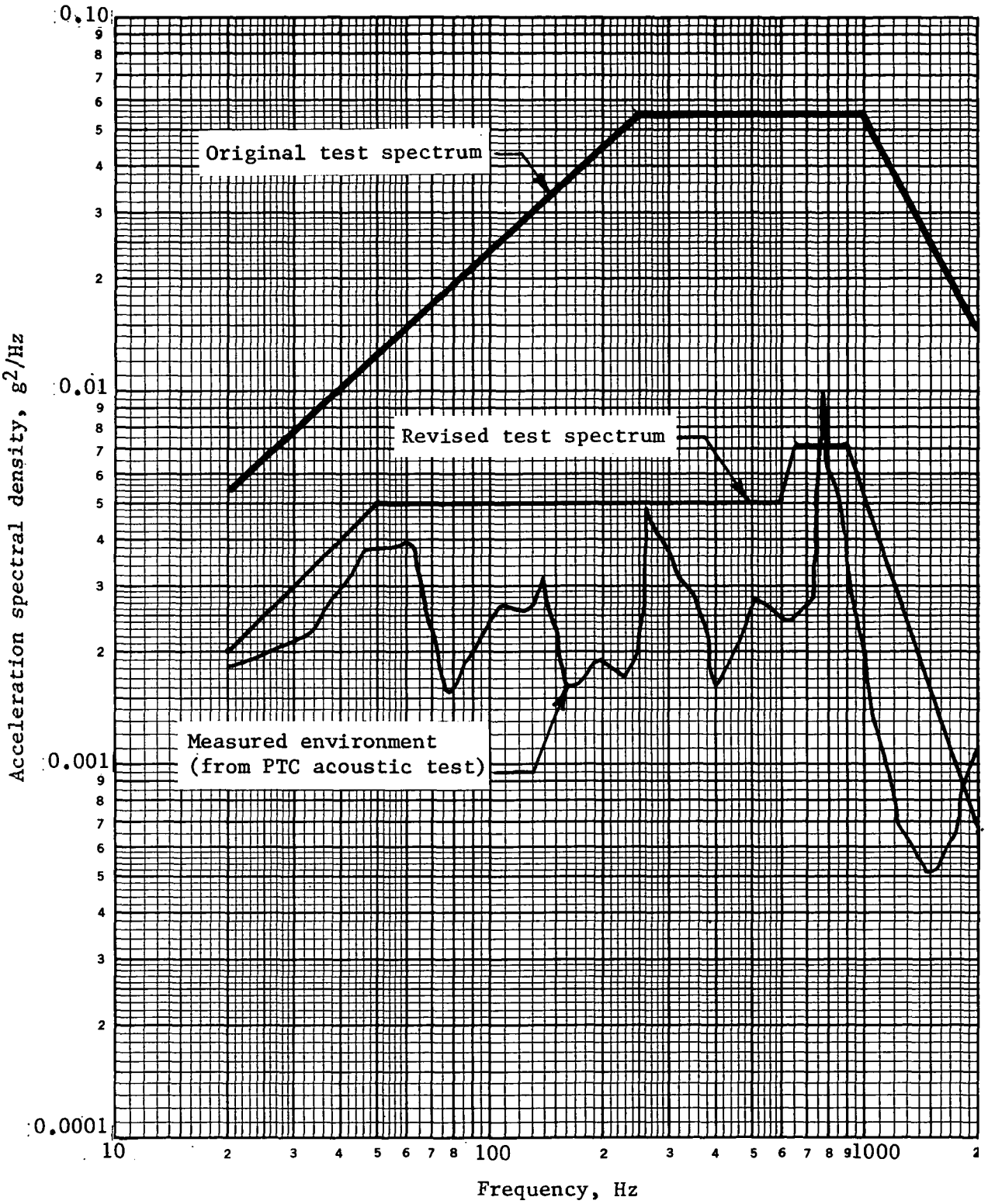

Figure 56.- Random vibration spectra for UHF low-gain antenna.

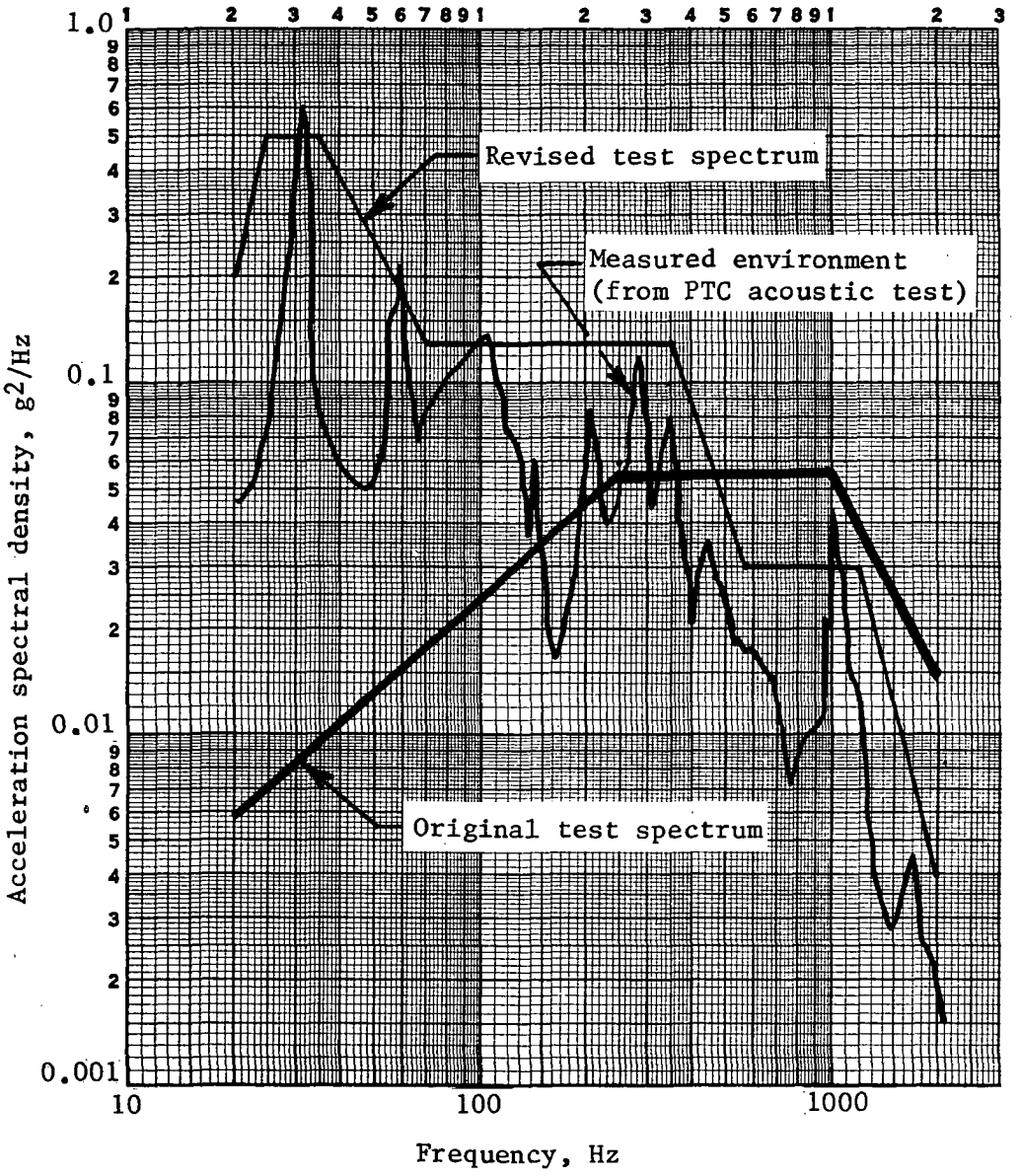

Figure 57.- Random vibration spectra for bioshield power assembly.

For future payloads, ground test and flight measurement programs should be planned and coordinated to minimize the uncertainty factors and establish the spacecraft acoustic environment with statistical confidence as early as possible. Also, improved analytical and empirical techniques are needed to define vibration spectra resulting from the acoustic environment acting on different types of structures. The techniques should include the ability to account for component and subassembly mounting stiffness and mass effects on both amplitude and frequency.

Predictions of the acoustically induced random vibration environments were derived by using established empirical prediction methods, primarily the method developed by Barrett (ref. 6). In its original form, this method provided a set of standard response spectra associated with various types of structures like heavy trusses, beams, light unstiffened panels, light stiffened panels, and bulkheads. It assumed that the shape of the input acoustic spectrum would be similar to the launch spectrum generated by Saturn I, on which the empirical data were measured. For application to Viking, the basic response spectrum shapes were modified to account for differences between the Saturn I and Titan III launch acoustic spectra. In general, this gave acceptable results when compared to ground test data. However, as shown in figure 58, for the Lander equipment plate, which was quite heavily loaded with components, the environment was underestimated. The estimate was based on the "forward bulkhead" and "stiffened panel" curves in ref. 6 and was factored downward to account for mass-loading effects. The degree of extrapolation required to account for the heavily loaded plate was obviously too great.

The curves shown in figure 59 were generated using response data measured at 24 locations on the Lander equipment plate, with two different acoustic inputs. The abscissa is in terms of an "Acoustic Mobility Function (M)," defined as

$$M = 10 \log \left[\frac{A(f)}{P(f)} \cdot w \right]^2 \quad (dB) \qquad (13)$$

where:

A(f) = rms acceleration in 1/3-octave band, g;

P(f) = rms acoustic pressure in 1/3-octave band, psi;

w = average surface density of loaded panel, psf;

f = center frequency of 1/3-octave band, Hz.

M is plotted against the ratio (frequency/fundamental frequency of loaded plate).

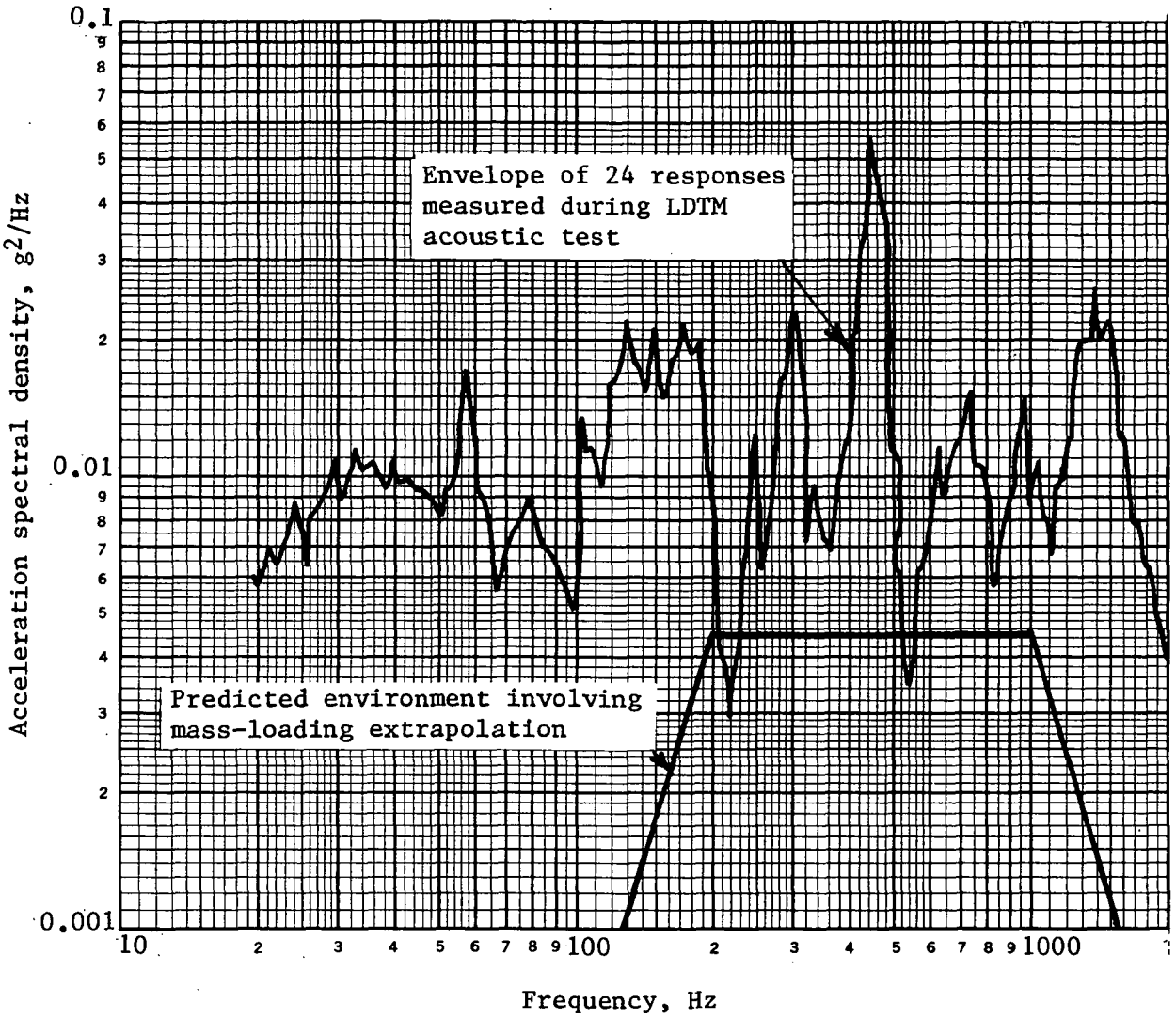

Figure 58.- Comparison of predicted versus measured random-vibration environments on Lander equipment plate.

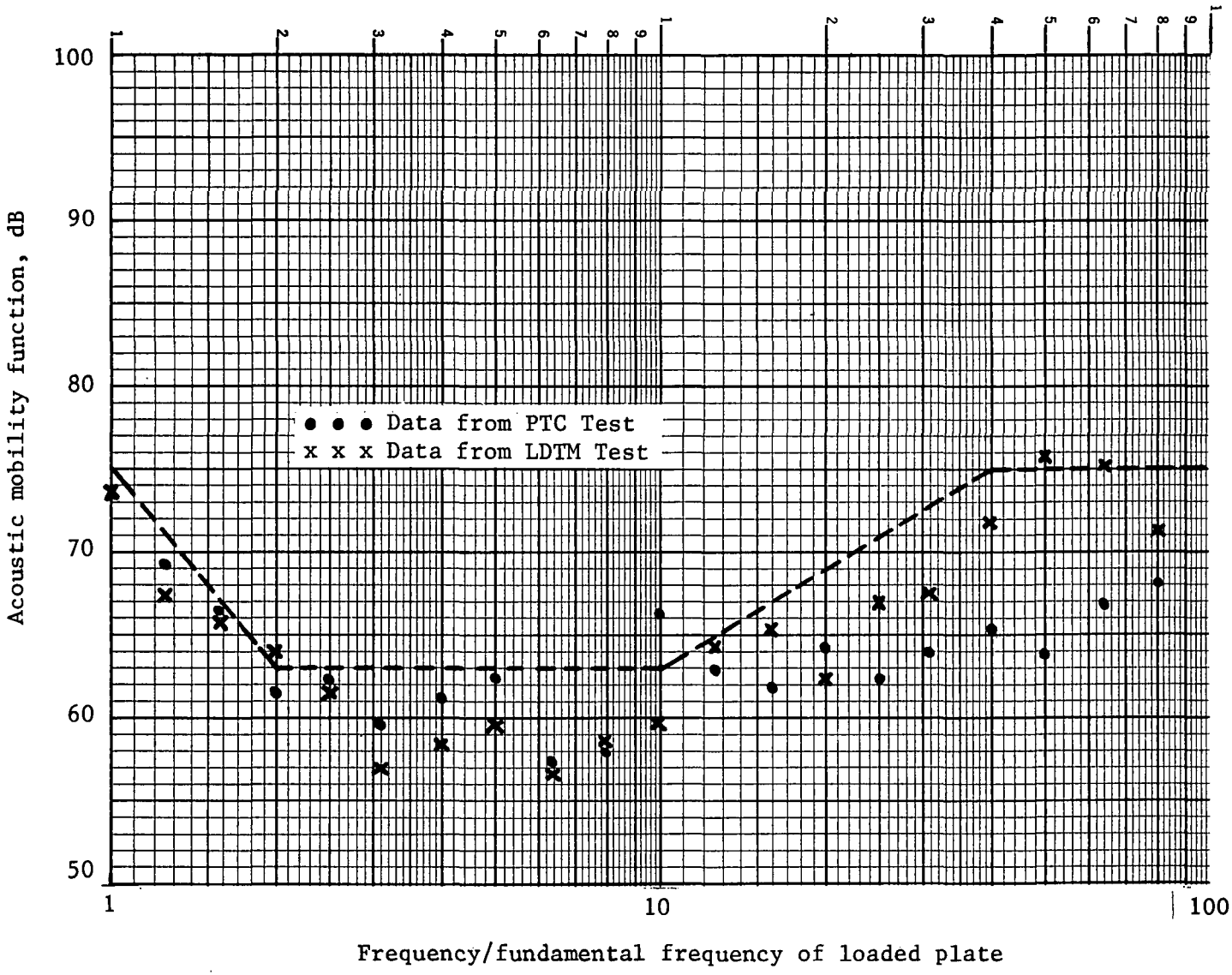

Figure 59.- Acoustic mobility data derived from Viking tests.

The two curves were enveloped to obtain the dashed response prediction curve in figure 59 and redrawn in figure 60. This is proposed for making a preliminary estimate of the acoustically induced random-vibration environment on a heavily loaded plate subjected to a known acoustic spectrum. This would apply to a plate with a total surface density of 500 N/m^2 (10 psf) or more.

To check the conservatism in the enveloping, the prediction curve was applied to the equipment plate using the LDTM and PTC inputs. The calculated response PSDs were compared with the measured PSDs, which indicated that the prediction curve is reasonably close to the measured data over most of the frequency range.

Damping

One of the most significant parameters involved in vibration analysis is damping. Damping in subsystem attachments and small parts that make up components is particularly important because it provides the only limiting effect on the magnitude of resonant response in these items. Because the vibroacoustic environment during launch is basically broad-band random, the great majority of items will be driven to resonance or near resonance, which will usually provide the critical design loads. Information on damping in typical structures and subassemblies is very scarce, so conservative values for Q are usually assumed for use in analysis. On the Viking Project, the following approach proved to be successful and, in general, not overly conservative.

1) For damping in primary structures, assume Q = 33, corresponding to a damping ratio of 1.5%. This was used in initial dynamic analyses of the Lander until test data became available.

2) Use Q = 5 to calculate input environments to components mounted on complex substructure. This was originally derived from a review of Titan data and found to give good results during Viking system-level sine tests.

3) To calculate the response of parts mounted inside components, use Q = 10 to 30, relative to the component base input, with the actual value dictated by the engineering judgment of the analyst. This range was generally adequate when used on Viking. However, it was exceeded in a number of cases. Table 11 lists response data measured inside various Viking components. The average Q was 14, and most values were less than 30, although in one case Q = 60 was measured. It is clear that more test data are needed so that generalized guidelines can be established to give the designer some idea of the peak responses to be expected inside his component.

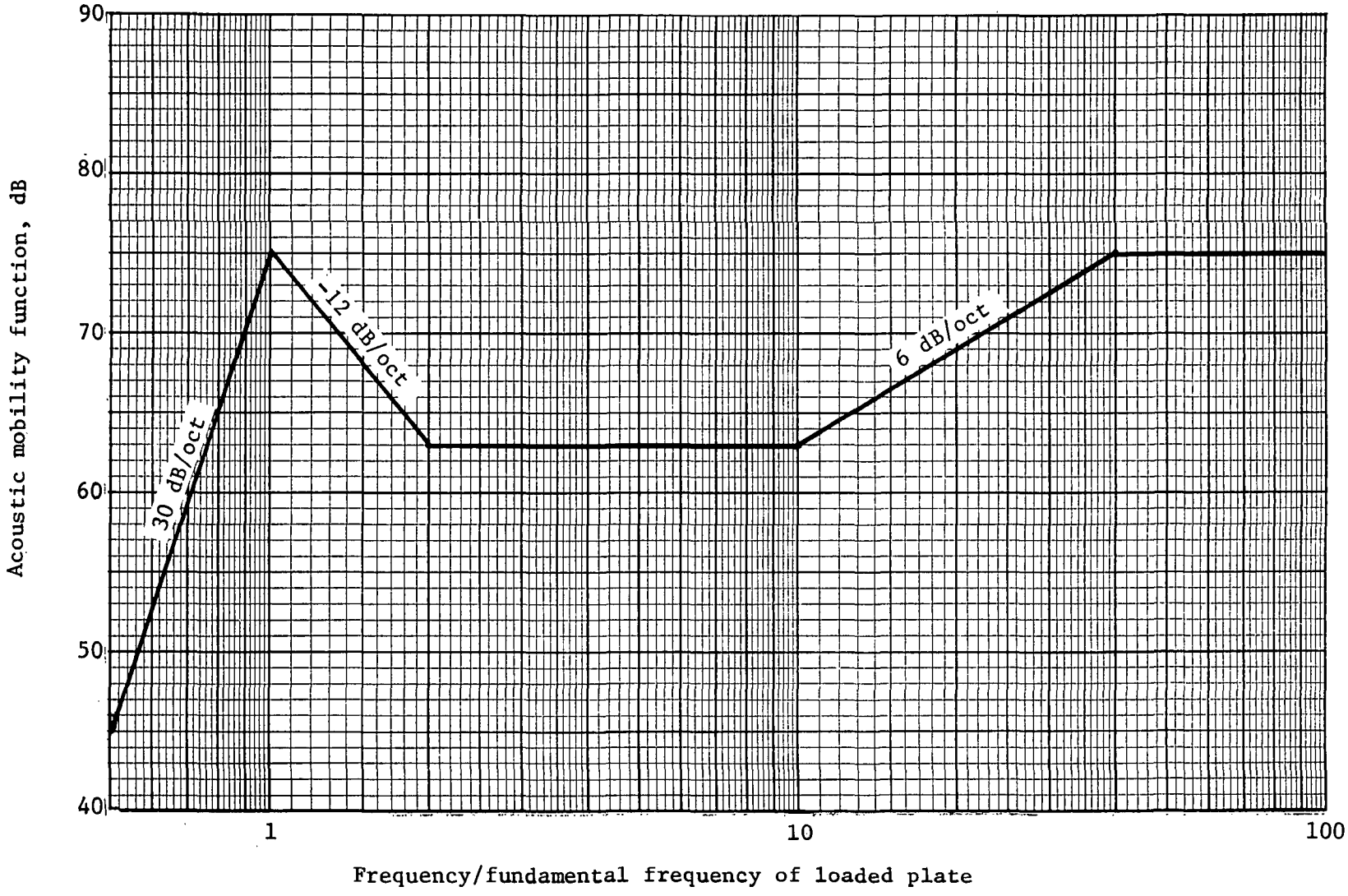

Figure 60.- Prediction curve for heavily loaded plate.

TABLE 11.- LOCAL VIBRATION RESPONSE DATA FROM VIKING COMPONENT TESTS

Source	Type of structure or device	f_n	Q
Viking lander biology instrument (VLBI) dev test	Machined magnesium plate, densely loaded with small components	280	4.5
	Similar plate, different mounting location in VLBI	280	6.0
	Similar plate, different mounting location in VLBI	285	3.4
	Spherical helium tank, 15.24-cm (6-in.) dia, truss mounted	185	5.0
	Spherical tank, liquid filled, 15.24-cm (6-in.) dia, truss mounted	150	6.0
Guidance control & sequencing computer (GCSC)	Machined magnesium cover plate, unloaded	239	60.0
	PC-board support frame	230	32.7
	Box structure, above mounting feet, in axis parallel to mounting bolts	330	8.0
Camera	Internal mechanisms	1000	26.6
		950	10.6
		220	4.0
		83	31.6
		230	11.2
		230	21.9
Gas chromatograph mass spectrometer processing & distribution assy (GCMS/PDA)	Internal mechanisms	96	5.6
		100	4.0
		105	8.4
		105	14.1
		105	11.2
		77	5.6
		79	7.5

Damping in printed circuit boards.- Most aerospace electronics assemblies contain PC boards, usually made of fiberglass or phenolic. The resonant response of the PC boards during severe dynamic excitation is often a cause for concern because excessive displacements can cause the board to crack, while high accelerations can lead to parts failure. The primary effect limiting the resonant response is the damping in the PC board, so that it would be highly desirable to be able to estimate Q with confidence.

Steinberg (ref. 22) has suggested that maximum transmissibility for a PC board at resonance can be calculated by $Q = K\sqrt{f_n}$, where f_n is the fundamental bending frequency for the board and K varies from 0.5 to 2.0, taking lower values for low-frequency $\left(f_n < 100 \text{ Hz}\right)$ boards. Data from vibration tests of Viking components, supplemented with data from references 23 and 24, were used to evaluate this approach; the result is plotted in figure 61. No attempt was made to account for different boundary conditions, on the assumption that the natural frequency would reflect these effects.

Of the 86 data points plotted in figure 61, 38 fell outside the region bounded by the two values of K. The "least squares" regression line was calculated for the data, assuming, like Steinberg, the relationship between f and Q to be in the form $Q = Kf^n$, or $\log Q = \log K + n \log f$. This yielded the result $\log Q = 4 \log f - 8.2$, or $Q = 7 \times 10^{-9} \times f^4$.

This is plotted as a dashed line in figure 61. It is obviously not a useful indicator for predicting damping. The inference is that $Q = Kf^n$ is not a valid relationship; in fact, damping in PC boards does not appear to be a simple function of frequency. Q is probably a complex function of mass, stiffness, and geometry, and may also be strongly affected by the boundary conditions on the PC board. Well-controlled testing would be needed to investigate the damping behavior in more depth.

Methods of increasing damping.- Because of the low inherent damping in PC boards, methods of increasing damping were investigated. A PC board's natural frequency and Q were measured, then the effects of bonding strips of resilient material to the board were evaluated using a swept sine vibration input. The strip arrangements, size, and type of material were varied between tests. Six different materials were investigated, including silicone rubber and various proprietary viscoelastic epoxy compounds. The effect of bonding a constraining layer of fiberglass on top of the damping strip was also measured. Reference 25 gives details of the test program and identifies materials used.

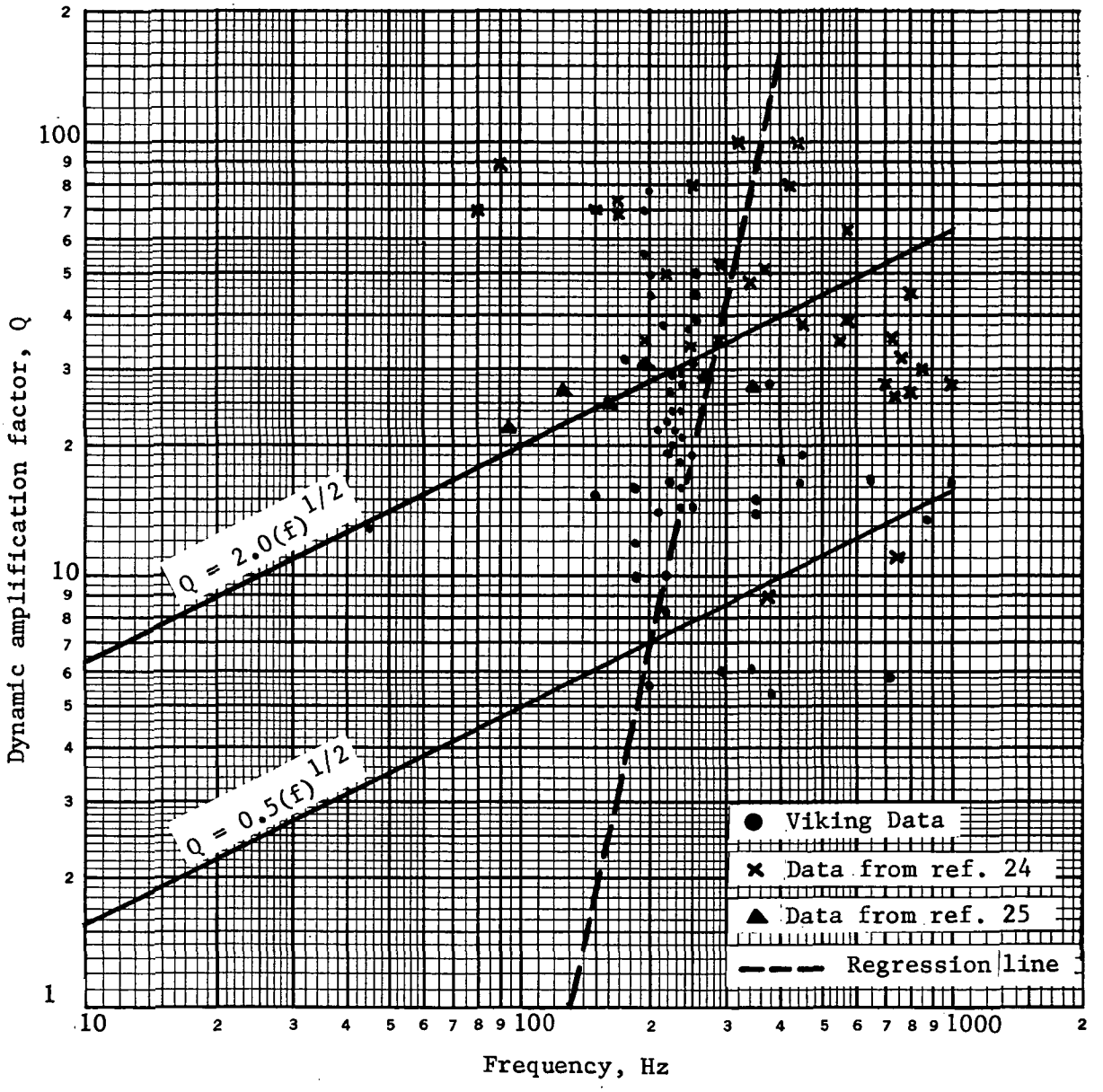

Figure 61.- Comparison of measured damping data with Steinberg's prediction boundaries.

Table 12 summarizes the results of the study and shows that one of the damping strips, capped with a fiberglass layer, reduced Q from 45 to 3.2 with only a small change in natural frequency.

TABLE 12.- SUMMARY OF ADDITIVE DAMPING TEST RESULTS

Damping material	Constraint layer thickness, cm	Natural frequency of board, Hz	Q
--	--	230	45.0
Silicone rubber	--	245	22.0
Material A	--	225	20.0
Material B	--	205	40.0
	0.0254 (0.01)	230	10.5
	0.1778 (0.07)	240	5.5
Material C	--	225	31.5
	0.0254 (0.01)	270	12.0
	0.1778 (0.07)	250	3.4
Material D	--	220	12.5
	0.0254 (0.01)	270	12.0
	0.1524 (0.06)	290	6.3
Material E	0.0254 (0.01)	260	16.5
Material F	0.0254 (0.01)	220	6.5
	0.1778 (0.07)	275	3.2

Figure 62 shows the most effective damping treatment found--installing strips in a XX arrangement, each strip capped by a fiberglass constraint layer. This treatment was used on a PC board with six-point attachment. Different attachment configurations may require different strip configurations for optimum damping. The overall conclusion was that the approach described can be a highly effective method of controlling vibration. If a severe vibration environment is anticipated, provisions for applying this technique are recommended in the early design stage for payload-components containing PC boards.

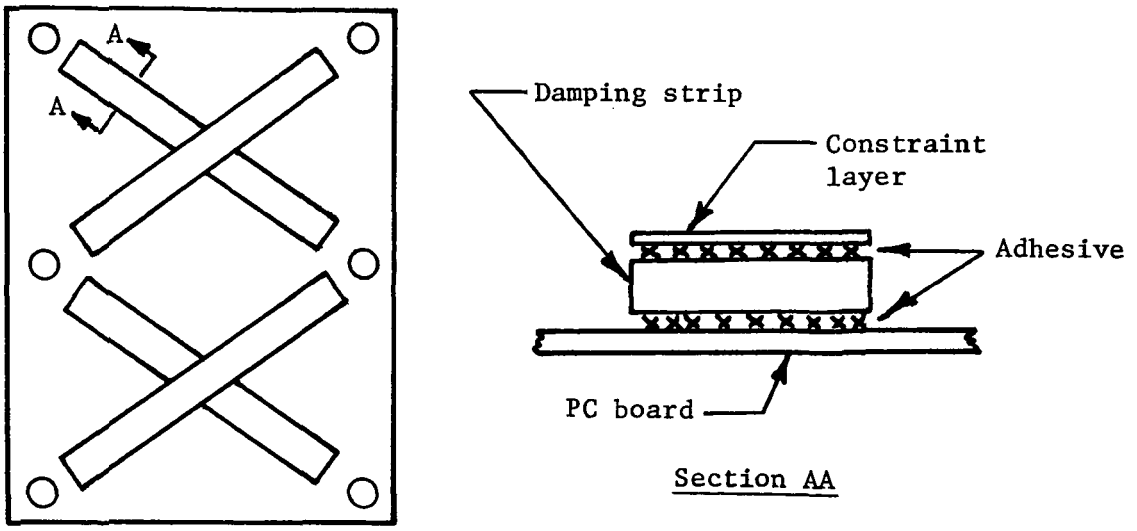

Figure 62.- PC board with damping treatment.

Another method of controlling vibration in PC-boards, piece parts, and connections inside an electronic assembly is to fill the housing with an encapsulant (potting compound) that surrounds the parts, preventing excessive vibration responses. On a few Viking components, rigid polyurethane foam was used successfully in this manner. It does have the inherent disadvantage that, after potting, it is difficult and costly to service the inside of the box. To gain access to the parts, it is necessary to dig out the foam, with a high probability of damage to the parts. Even so, for some components using relatively cheap off-the-shelf electronics, it may be cost effective to use rigid potting for vibration protection, then simply discard and replace a defective box rather than repair it.

A new potting technique has recently been developed (ref. 26) that appears to avoid the servicing problems associated with rigid foam encapsulants. In this method, low-density foamed silicone rubber particles are poured and packed into the voids in the electronics package. The particles can easily be removed for repair or rework of the package, then replaced.

Reference 26 describes testing of a PC board assembly to determine the effectiveness of the technique. Four different commercially available silicone foam rubbers were tested and found to behave equally effectively. Two particle shapes (flakes and pellets) were used, with no apparent difference in effectiveness. Figure 63 shows the results of the sine vibration test. After encapsulation, the PC board's resonant response was reduced by a factor of 10 or more. The technique appears to have significant advantages over other vibration reduction treatments, and it is recommended that its application to future payload components

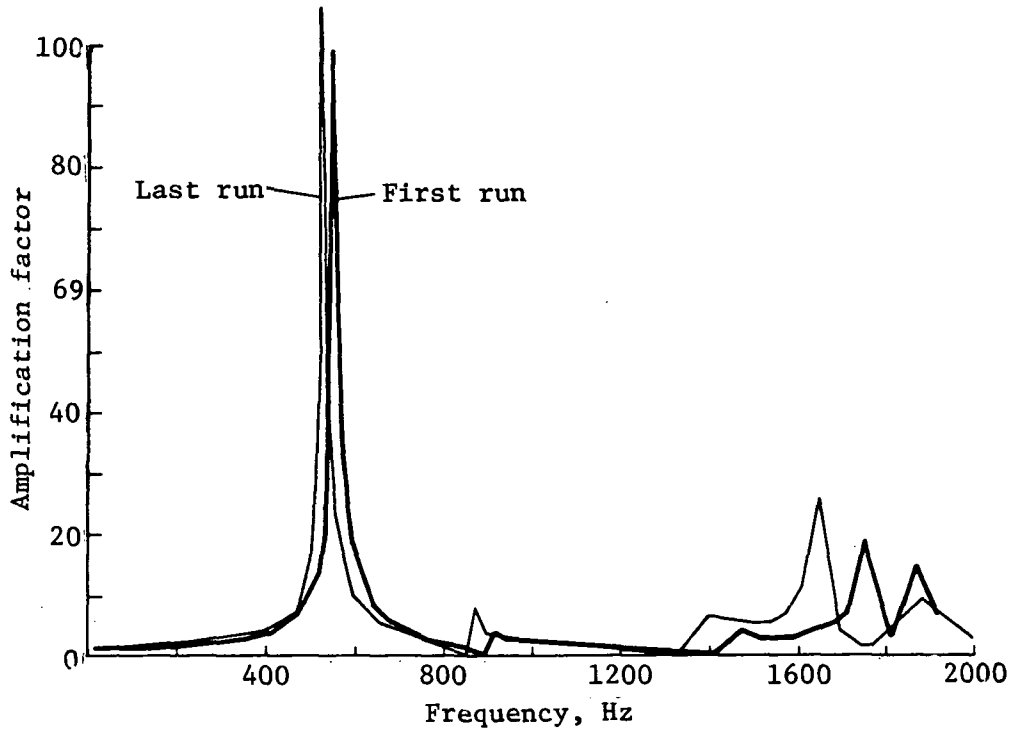

a. Without encapsulation

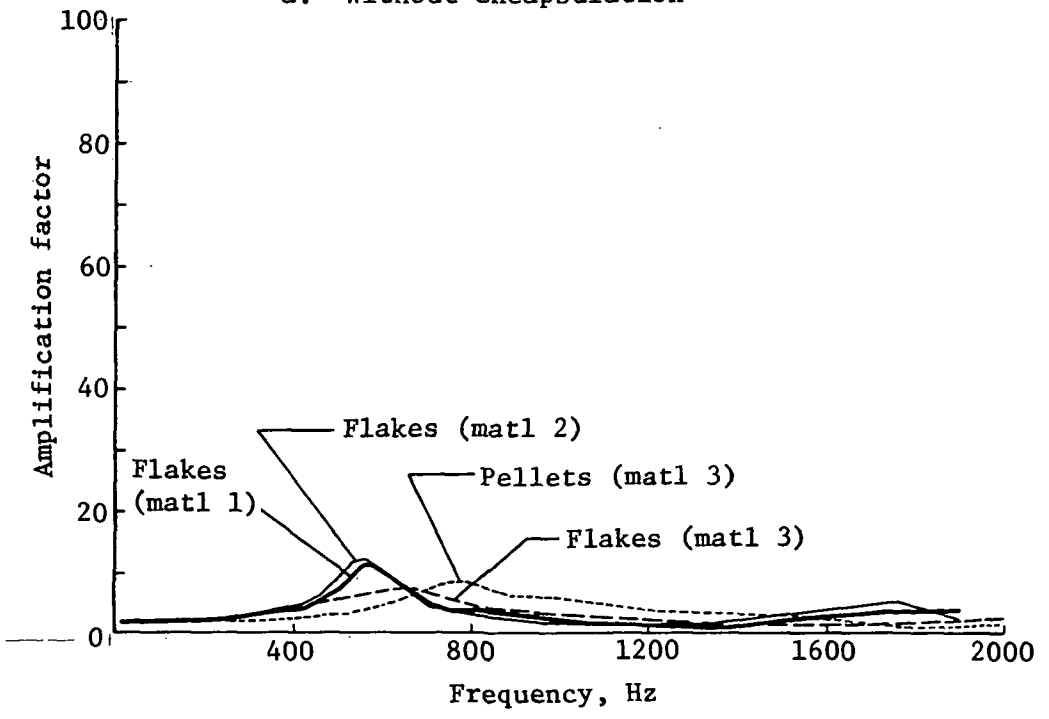

b. With encapsulation

Figure 63.- Effect of silicone foam rubber encapsulation on PC board response (from ref. 26).

be seriously considered. However, the possibility of heat build-up inside the component due to reduced ventilation should be considered.

Pyrotechnic Shock

Prediction technique.- The technique developed for estimating the shock environment generated by pyrotechnic devices on the Viking was described earlier. Using test data from the pyrotechnic shock test bed and proof test capsule (PTC), a check on the accuracy of the technique showed that the peak value of the shock spectrum at some distance from the source is predicted quite well, but acceleration levels in the middle frequency range (100 to 1000 Hz) tend to be overestimated. The PTC data (fig. 11) indicate that this error increases with the number of bolted joints in the shock transmission path, leading to the conclusion that bolted joints do actually attenuate the ramp of the spectrum, contrary to the assumption made on the Viking Project. Figure 64 shows an attempt to evaluate ramp attenuation. Data from the PTC base-cover separation test were used. These were measured at points involving one, two, and three joints and were plotted earlier as figures 23b, c, and d, respectively. In figure 64, the straight lines on each graph represent the ramp of the predicted spectrum, allowing for 0%, 10%, 20%, and 30% reduction for each joint. The figure shows that a reduction of 30% for each joint gives reasonable results. Thus, based on the Viking data, it is recommended that the following joint attenuation philosophy be adopted when predicting pyro shock environments for future payloads:

Assume a peak attenuation of 30% and a ramp attenuation of 30% for each bolted joint in the shock path, up to a maximum of three joints.

Pyro shock attenuation methods.- During the early part of the Viking Project a study was performed to identify and evaluate techniques for reducing the severity of the pyro shock environment. Details of the study were discussed in ref. 16, and significant results are summarized in this report.

Four basic approaches were considered:

1) Reduce the shock produced by the pyrotechnic source;

2) Isolate the shock source from its supporting structure;

3) Increase the attenuation occurring in mechanical joints in the shock path between the source and the components;

4) Shock mount the components.

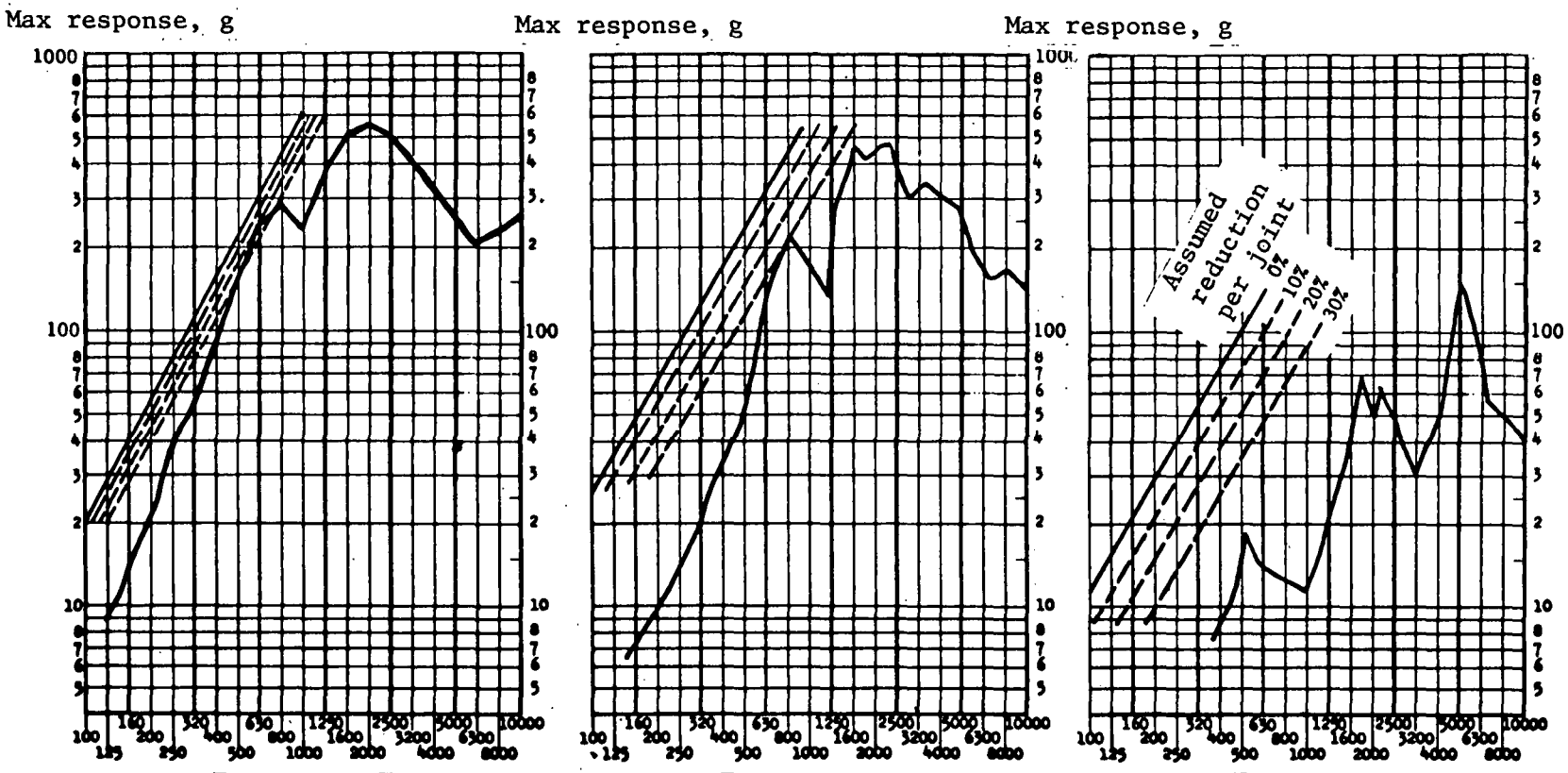

a. One joint b. Two joints c. Three joints

Figure 64.- Joint attenuation as applied to the ramp of a pyro shock spectrum.

Method 1 is obviously the most desirable. Some progress has recently been made in the industry to develop separation nuts with low shock output. Martin Marietta tests of a very preliminary version of a low-shock nut indicated that the source spectrum peak was reduced from approximately 15 000 to less than 6000 g. Later testing of a more refined version at JPL (ref. 27) showed that performance improved to a point where the source spectrum peak was only about 1000 g. It is recommended that use of these nuts be considered for future applications. As far as is known, no similar work is in progress to reduce the shock output of other pyrotechnic devices such as pin pullers, valves, or cable cutters.

Method 2 was investigated in some depth. This approach is very dependent on the particular application considered. For example, separation nuts usually connect major structural elements and are required to transmit large forces, so that soft isolation materials cannot be added to the system. However, a small reduction in source spectrum peak was obtained at the Viking Lander body/basecover truss interface by using metal spacers between the separation nut and mounting structure--the source level was reduced from a peak of 9000 to 7000 g. Because of this very minor improvement, the technique is not recommended unless the need is critical.

Method 3 received the most attention in the study. To investigate the feasibility of increasing the attenuation properties of a mechanical joint, a number of tests were run on a model incorporating a simple mechanical interface in which different materials could be inserted. A shock pulse was applied on one side of the joint, and the shock level was measured on both sides. Figure 65 shows the test setup, including accelerometer locations and joint details.

Three families of materials were investigated: metals, hard nonmetals, and soft nonmetals. To provide a basis for comparison with subsequent joint configurations, the joint was first tested with no insert. Figure 66 shows the results of this test. A total of 35 joint configurations were tested. In every case, the effectiveness of the configuration was judged, in terms of the resulting shock spectra on the side of the interface farthest from the input, by comparison with the result from the untreated joint. In summary, test results showed the following.

1) The untreated joint (no insert) showed a reduction of approximately 40 to 50% of the input spectrum across the full frequency range (fig. 66).

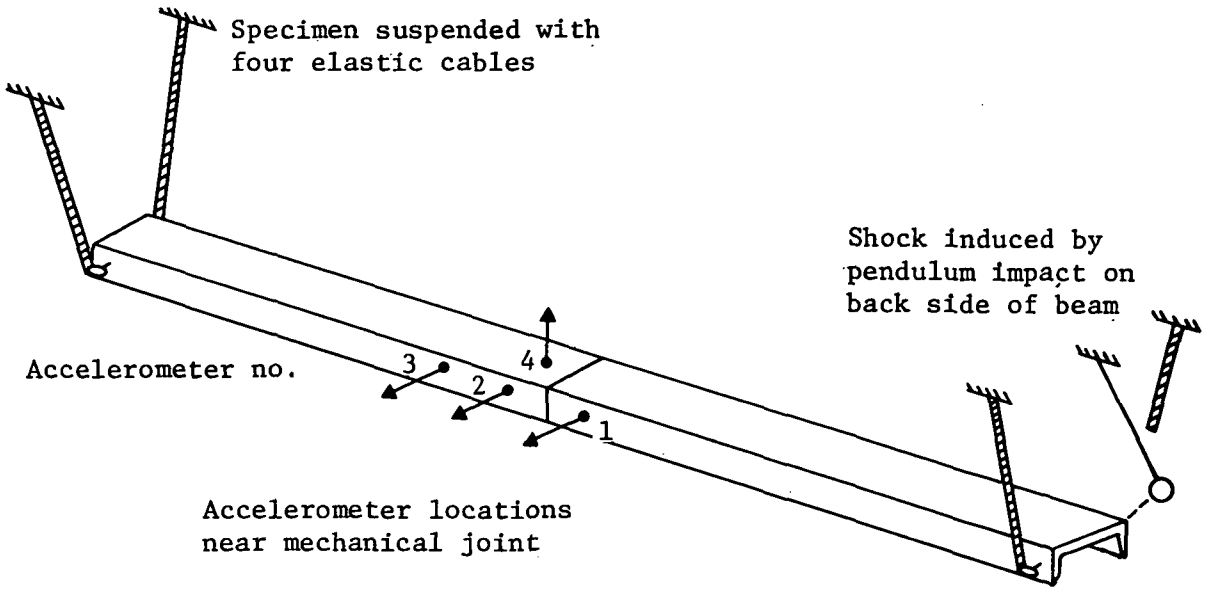

a. Beam specimen test setup

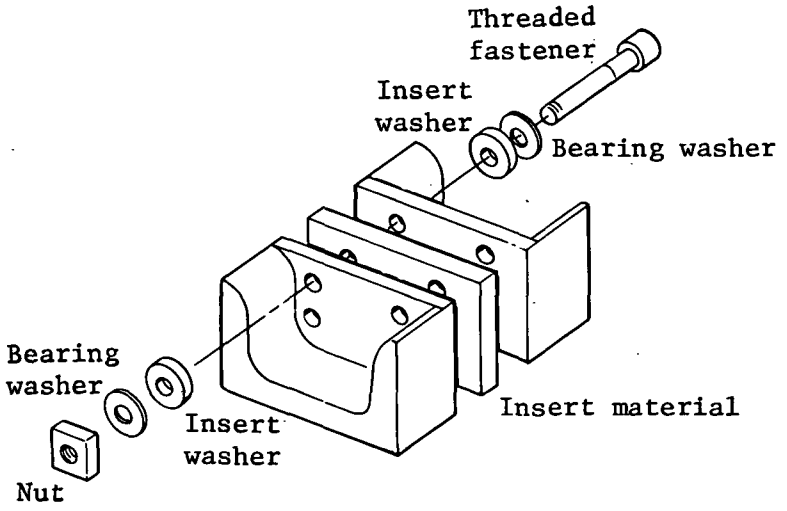

b. Joint details

Figure 65.- Test configuration for joint attenuation investigation.

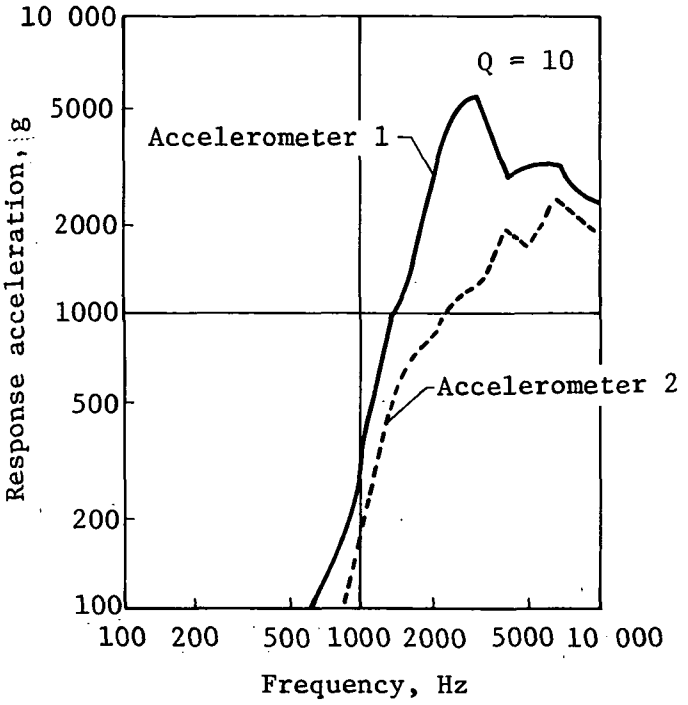

Figure 66.- Shock reduction across untreated joint.

2) Metal inserts in the joint provided an additional reduction, but only in the high-frequency range. The most effective arrangement used alternate layers of magnesium and steel (M-S-M-S). This provided an additional reduction of 30 to 40% compared to the untreated joint (fig. 67). Multiple inserts of steel were no more effective than a single steel insert, giving an additional reduction of 20 to 30%.

3) No significant attenuation was achieved using inserts of hard nonmetals.

4) Soft elastomeric materials were found to contribute significant reductions, on the order of 40% at high frequencies, decreasing to about 30% at lower frequencies (fig. 68). Although this technique would not be suitable for joints carrying heavy loads, it may be applicable to component bracketry where conventional shock isolators cannot be used for thermal or other reasons. The reduction in joint strength caused by the inserts was not measured.

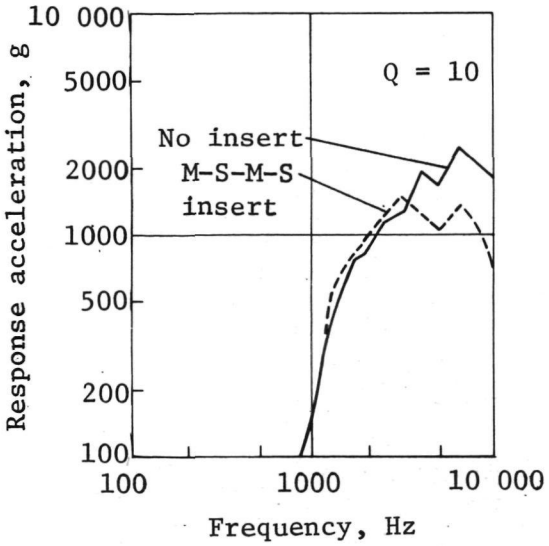

Figure 67.- Effect of using metal inserts.

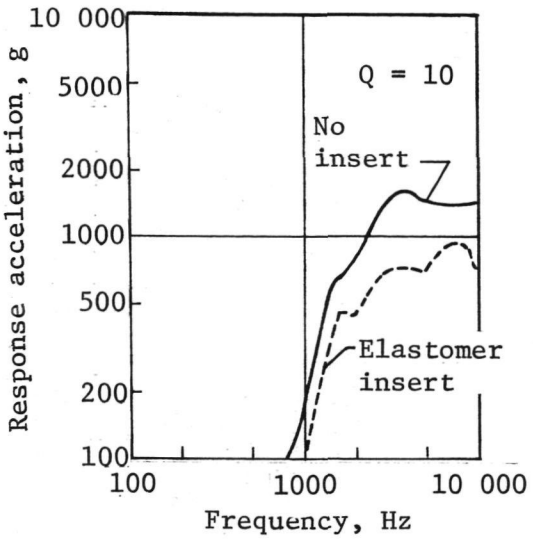

Figure 68.- Effect of using soft elastomer insert.

A test program was conducted to investigate various approaches to Method 4--shock isolation of affected components. Shock tests were performed on a light motor-driven switch and a relatively heavy relay assembly (fig. 69). A series of tests was performed on the switch using a number of different isolation materials made up into washers assembled with the component (fig. 70). For comparison, the first test was performed with the switch hard mounted on the fixture. Table 13 summarizes the materials used, resulting natural frequency of the box, and shock reduction achieved.

Figure 71 shows typical component shock spectra for several isolators. A noticeable feature is the response peak that occurs at the natural frequency of the component on its mountings.

A review of the data from this test series shows that very effective shock isolation (up to 94%) can be obtained on a light component using washers of soft elastomeric material at the component mounting. As the mounted natural frequency decreases, it depends on the amount of torque applied to the fastener because the preload in the washer affects the spring rate and, hence, the frequency. Miniature grommet-type mounts, which should exhibit behavior similar to the soft-washer concepts tested, are available from several isolation-mount manufacturers.

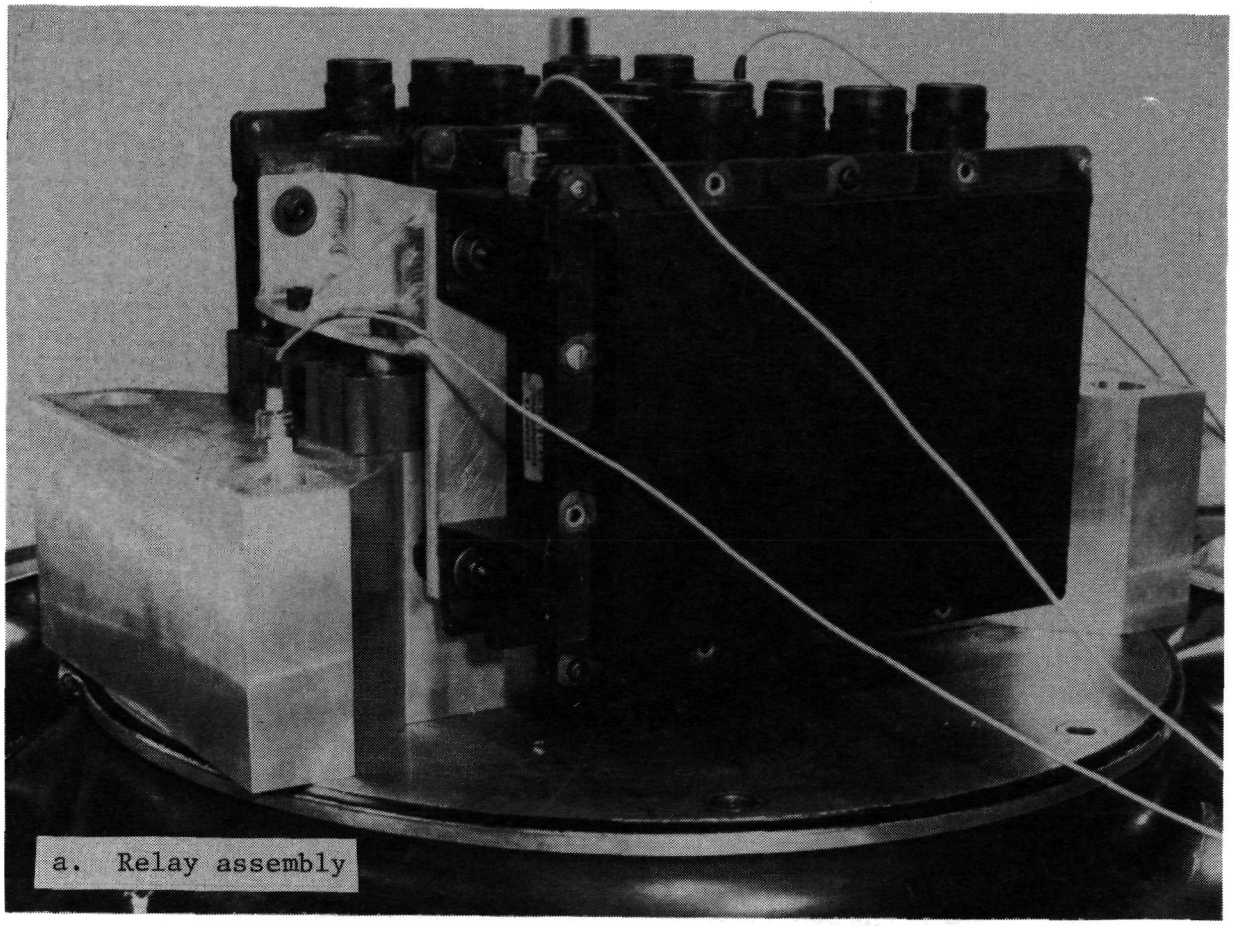

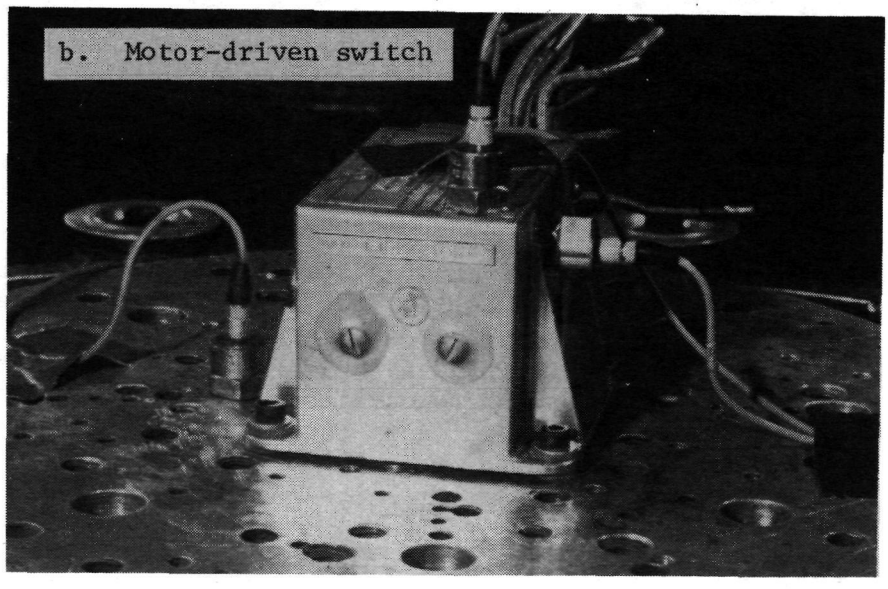

Figure 69.- Investigation of shock-isolator effectiveness.

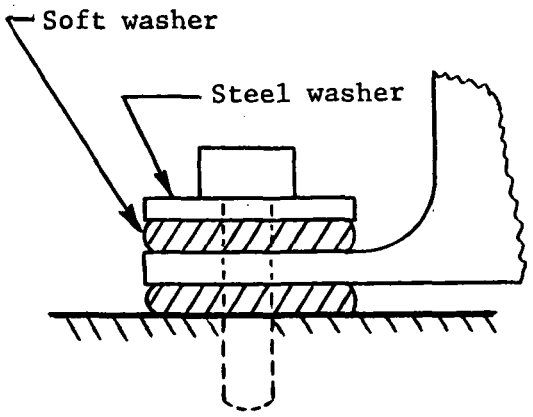

Figure 70.- Isolation-washer assembly detail.

TABLE 13.- SUMMARY OF MDS TEST RESULTS

Configuration number	Isolation washers			Approximate natural freq, Hz	Shock reduction rel to baseline configuration, %
	Material	Durometer	Thickness mm (in.)		
1 (hard mtd baseline)	--	--	--	--	--
4	Material X	75	2.4 (0.094)	600	33
5	Silicone rubber	50	1.6 (0.063)	375	88
6	Silicone rubber	50	1.6 (0.063)	450	84
7	Neoprene	50	3.2 (0.125)	450	71
9	Neoprene	50	1.6 (0.063)	550	50
11	Neoprene	50	6.4 (0.25)	225	84
13	Material Y	40	3.2 (0.125)	360	88
14	Material Z	10	6.4 (0.25)	100	94

Note: Natural frequency is affected by torque on fastener. For these tests, torque was approximately 0.011 N-m (1 lb-in.), above which material flow became evident.

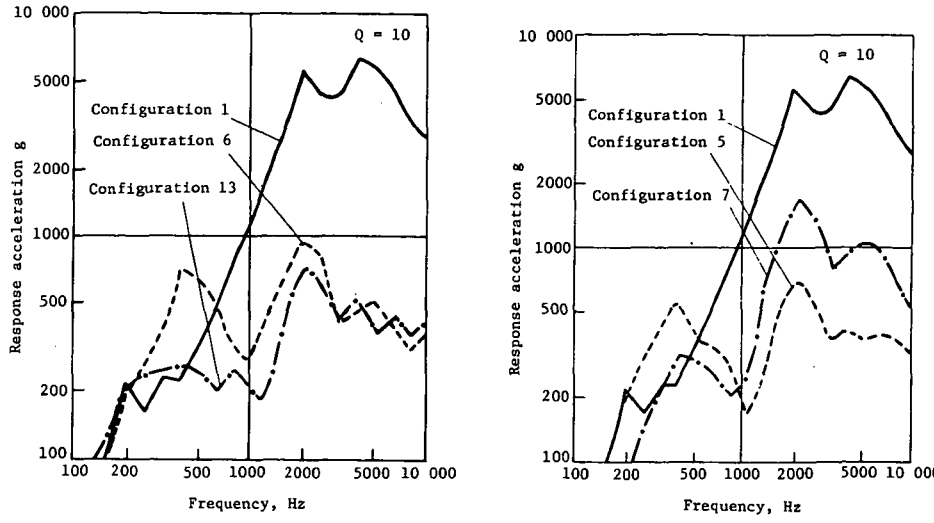

Figure 71.- Typical shock spectra measured on isolated motor-driven switch.

A single test was performed on the relay assembly, which was mounted on conventional low-frequency vibration isolators (fig. 69a). The purpose of the test was to measure the effectiveness of such mounts in providing isolation from a high-frequency transient input like a pyro shock. As shown in figure 72, the mounts were very effective, reducing the input spectrum from a peak of about 4000 to approximately 100 g across a wide frequency range of 200 to 10 000 Hz. The relay-assembly isolators were in a plane through the assembly cg, which avoided secondary rocking-mode responses. Where cg mounting is not practical, a less effective performance should be expected.

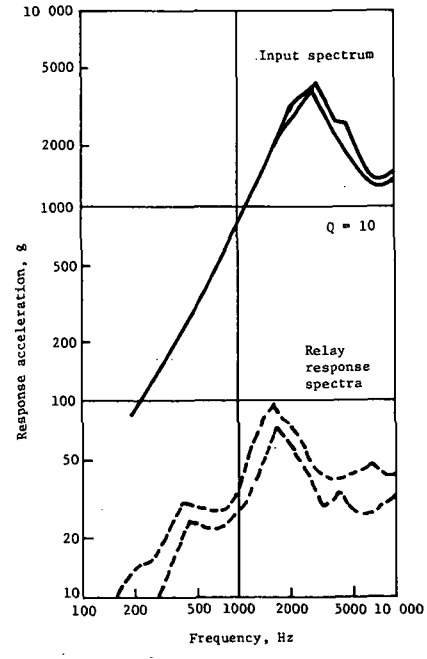

Figure 72.- Relay-assembly shock spectra.

Design and Qualification Test Factors

Several different values for the design and qualification test factor, defined as

$$TF = \frac{\text{Qualification level}}{\text{Flight acceptance level}},$$

were used on the Viking Project, depending on the dynamic environment involved. For the sine environment, a factor of 1.5 was applied. For overall random vibration level, TF = 1.66 (4.5 dB) was initially used. Later, this was decreased to TF = 1.41 (3 dB). Pyrotechnic and mortar shock environments used TF = 1.2; the landing shock condition used TF = 1.25. Finally, for acoustic testing, the factor was 2.0 (6 dB on sound pressure level). These variations in TF reflected the degree of confidence associated with the various environmental predictions and were therefore justifiable. This may be true for many future programs; however, for the particular case of Shuttle payloads, estimates of dynamic environments should be reasonably accurate after data are obtained on the first few flights, so that ignorance of the environment should contribute little to the test. Test factors should also be related to the type of payload being tested; a retrievable payload provides an opportunity to analyze failures and correct future designs, so that a higher risk (and therefore a smaller test factor) may be acceptable. On the other hand, a single-mission planetary exploration experiment would require a more conservative test factor to achieve the necessary high reliability.

In a recent Martin Marietta study (ref. 28) it was found that a range of values for random vibration test factor is in use in the aerospace industry. Table 14 lists some examples.

It would be desirable to have consistent industry-wide philosophy for test factors. This would not be easy to achieve because of the many different missions and types of payloads likely to be launched in the future. However, a properly selected approach would result in considerable cost savings. As a start, based on Viking experience, it is recommended that a nominal test factor of 3 dB be used for vibration, shock, and acoustics.

The test duration factor applied to vibration and acoustic test specifications is necessarily related to the particular payload mission. Based on Viking experience, a nominal factor of 3 times expected flight exposure is recommended; a factor of 5 was originally specified, but this was later considered to be too high.

Design factors can easily become over-conservative because of safety margins being applied at various stages of payload development. For example, the weights engineer is likely to estimate

TABLE 14.- COMPARISON OF BASES FOR TEST REQUIREMENTS

User	FA level	Qual level	TF
NASA/MSFC	Qual level - 6 dB	97.5% confidence level from flight data	2
MMC-NASA/LRC (Viking)	97.5% confidence level from flight data	FA + 4.5 dB (later FA + 3 dB)	1.66 (1.41)
NASA/GSFC	97.5% confidence level from flight data	FA x 1.25	1.25
McDonnell-Douglas	Mean flight level	FA + 6 dB	2
USAF (MIL-STD-1540A)	95% confidence level from flight data	FA + 6 dB	2
Rockwell International (Orbiter environment spec)	97.5% confidence level from flight data	FA x 1.3	1.3

the weight of components conservatively to allow for growth in the design; the dynamics engineer may introduce further conservatism during the usual enveloping of data to obtain an environmental estimate; finally, the stress engineer tends to use maximum allowable material properties and low-tolerance structural-member sizes. An example of the magnitude of the conservatism in margins that can build up in primary structure during the design process was made evident by the aeroshell dynamic compatibility test. Early in the Viking Project, the aeroshell was subjected to static qualification tests. As part of those tests, ultimate static loads equal to design limit load plus 25% were applied to the aeroshell tank trusses. At that time, the design limit load was 4.5 g in the longitudinal axis. During the dynamic compatibility test, measured levels were as high as 8.6 g for a 1.5 g input level, with no sign of failure. These numbers indicate that more margin was built into the truss design than was necessary; the actual margin may have been quite high. This is a common situation in structural design, and it is seldom likely to be cost effective to redesign the structure to achieve more optimum margins. The problem should be addressed in the early stages of the design process. It is recommended that this "stack-up" of margins be monitored and, if necessary, reduced by the project engineer who controls payload development.

Loads Analysis

A wide variety of payloads will be launched in the next decade, using both disposable and reusable boosters. In many cases, primarily associated with Space Shuttle, payloads will be launched, deployed, recovered, and returned to Earth, then relaunched for

further use in space. This capability will significantly affect the tradeoff between expenditures for in-depth loads analysis and the cost of correcting any malfunctions and repeating the mission. Many of these payloads will not be weight-critical, so that relatively large safety margins can be applied to attain a high level of confidence in the design and survivability of the payload. For weight-critical payloads that must be designed with smaller margins, Viking experience can be applied to good effect.

In most respects, the Viking approach was conservative. Table 15 compares measured loads in the VLC adapter members during the TC-4 flight with predicted peak loads and static-tested capabilities. Some measured loads in the table were close to analytical predictions; others differed considerably.

TABLE 15.- MEASURED VLCA LOADS VERSUS ANALYTICAL PREDICTIONS AND CAPABILITIES FOR TC-4 LIFTOFF

Flight measurement no.	JPL member no.	Expected peak loads, N (lb)	Tested capability, N (lb)	Flight measured loads, N (lb)
CY186S	750	+12 966 (+ 2 915)	+20 853 (+ 4 688)	+ 9 341 (+ 2 100)
		- 4 163 (- 936)	-14 447 (- 3 248)	- 3 558 (- 800)
CY187S	751	+12 019 (+ 2 702)	+22 312 (+ 5 015)	+ 7 117 (+ 1 600)
		- 7 966 (- 1 791)	-12 953 (- 2 912)	- 3 558 (- 800)
CY188S	752	+10 164 (+ 2 285)	+24 242 (+ 5 450)	+ 9 341 (+ 2 100)
		- 1 721 (- 387)	-13 771 (- 3 096)	- 444 (- 100)
CY189S	753	+12 837 (+ 2 886)	+24 242 (+ 5 450)	+11 120 (+ 2 500)
		- 4 154 (- 934)	-13 771 (- 3 096)	- 890 (- 200)
CY190S	754	+12 526 (+ 2 816)	+22 312 (+ 5 016)	+10 230 (+ 2 300)
		- 8 362 (- 1 880)	-12 953 (- 2 912)	- 2 669 (- 600)
CY191S	755	+12 508 (+ 2 812)	+20 853 (+ 4 688)	+ 9 786 (+ 2 200)
		- 3 665 (- 824)	-14 448 (- 3 248)	- 890 (- 200)

The statistical approach to loads data calculations was adequate from the standpoint that it did predict higher loads than were actually measured, and the mission was a success.

Discrepancies in predicted versus measured loads caused some VLC adapter members to be overdesigned. Future payloads may be less subject to these errors when new analytical concepts are applied, especially for multiple-mission payloads. The design process starts with preliminary predicted loads, and the more accurate these are, the fewer loads analysis cycles will be needed. In a multiple-mission situation, good data should be available after the initial flights. Thus, with suitable prediction techniques, accurate estimates of the new payload environments can be obtained.

Not all payloads will be as sensitive to low-frequency environments as Viking. However, for those that are, the designer is faced with first determining if there is a legitimate concern for structural loads. If necessary, a set of loads analyses could be performed. A coupled model of the payload and booster could be formed and response analyzed in the time domain. Uncertainties in the flight data and modeling must again be handled statistically by some approach similar to that used for Viking. This method is very costly. To gain more confidence in the design, additional loads cycles must be performed with fully coupled booster-payload models.

Two recently developed analytical methods should be considered for application to future payloads. Modal parameter perturbation studies (ref. 29) can yield valuable information about the effect on the overall coupled system of small changes in the structural properties, without having to repeat the complete loads analysis. The method of mode selection (ref. 30) could be used to determine significant nodes to be used in a loads analysis, rather than arbitrarily truncating the set of nodes. Use of these techniques could add considerably to the confidence level associated with models developed for design loads calculations.

There are a number of potential methods for reducing the cost of loads analyses. Reference 29 briefly reviews some of the possibilities. Most techniques account for or extract the payload feedback into the payload-booster interfaces and determine what the new responses will be for a new payload. For example, one technique now being investigated attempts to more or less "ratio" the interface accelerations from flight to flight. Referring to the sketch on the next page, the accelerations for a combined launch vehicle and any payload can be written as:

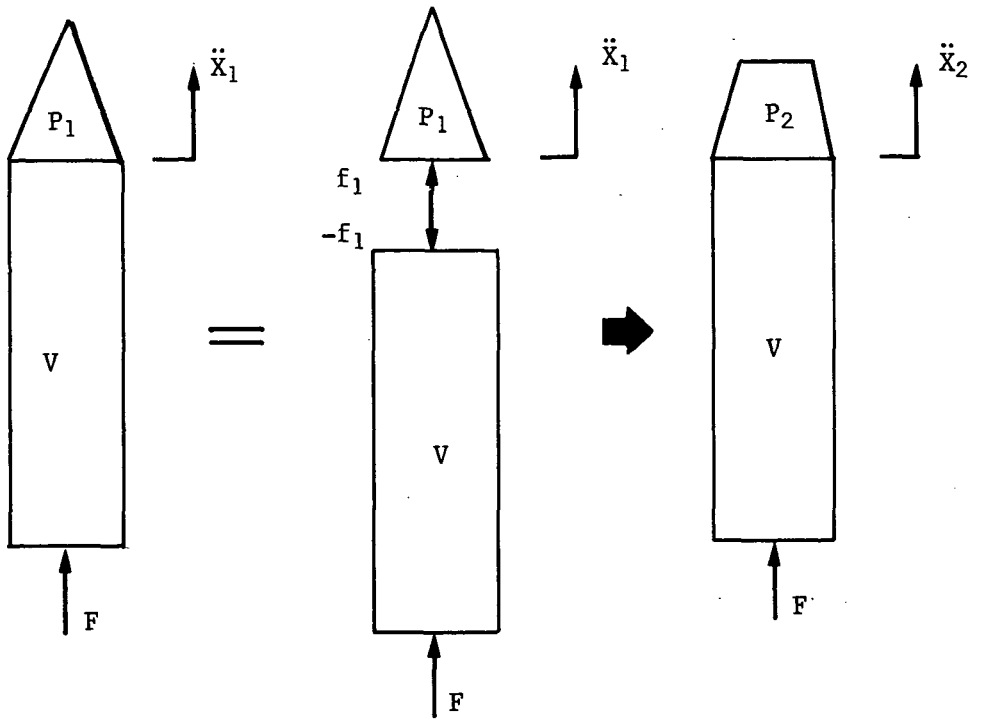

V = Boost vehicle;

P_1 = Payload 1;

P_2 = Payload 2.

$$\left[Z(\omega)\right]_{VP_1} \left\{\ddot{X}_1(\omega)\right\} = \left\{F(\omega)\right\} \tag{14}$$

where:

$\left[Z(\omega)\right]_{VP_1}$ = impedance from external loads to payload interface;

$\left\{\ddot{X}_1(\omega)\right\}$ = interface accelerations for P_1 as a function of frequency (ω);

$\left\{F(\omega)\right\}$ = external loads for structure as a function of frequency (ω).

From here on, all equations will apply in the frequency domain and the (ω) will be omitted. From the free-body diagram in the sketch, there is also this relationship:

$$\left[Z\right]_{P_1} \left\{\ddot{X}_1\right\} = \left\{f_1\right\} \tag{15}$$

where:

$\left[Z\right]_{P_1}$ = impedance of payload 1 to the interface loads;

$\left\{f_1\right\}$ = interface loads.

Considering the free-body diagram of the boost vehicle above, the interface acceleration can be written:

$$\left\{\ddot{X}_1\right\} = \left[M\right]_V \left\{F\right\} + \left[M\right]_{VI} \left\{f_1\right\} \tag{16}$$

where:

$\left[M\right]_V = \left[Z\right]_V^{-1}$ = mobility of vehicle alone due to $\left\{F\right\}$;

$\left[M\right]_{VI}$ = mobility of vehicle at payload interface due to interface loads.

From equation (15)

$$\left\{f_1\right\} = \left[Z\right]_{P_1} \left\{\ddot{X}_1\right\} \tag{17}$$

Substituting in equation (16) yields

$$\left\{\ddot{X}_1\right\} = \left[M\right]_V \left\{F\right\} - \left[M\right]_{VI} \left[Z\right]_{P_1} \left\{\ddot{X}_1\right\} \tag{18}$$

or

$$\left(\left[M\right]_{VI} \left[Z\right]_{P_1} + \left[I\right]\right) \left\{\ddot{X}_1\right\} = \left[M\right]_V \left\{F\right\} \tag{19}$$

where

$\left[I\right]$ = "unity" matrix.

An equation similar to equation (19) can be written for payload 2:

$$\left(\left[M\right]_{VI} \left[Z\right]_{P_2} + \left[I\right]\right) \left\{\ddot{X}_2\right\} = \left[M\right]_V \left\{F\right\} \tag{20}$$

Now, if two critical assumptions are made—first, that no changes are made in boost-vehicle dynamic characteristics from flight to flight, and second, that no changes occur in the forcing functions between flights the following relationship can be written:

$$\left\{\ddot{X}_2\right\} = \left(\left[M\right]_{VI} \left[Z\right]_{P_2} + \left[I\right]\right)^{-1} \left(\left[M\right]_{VI} \left[Z\right]_{P_1} + \left[I\right]\right) \left\{\ddot{X}_1\right\} \tag{21}$$

Equation (21) states that, if the interface accelerations are known from one flight and the dynamic impedance characteristics are known, the new interface accelerations can be calculated in the frequency domain.

As stated above, the feasibility of this technique is now being studied. Important considerations include the effect of the assumptions on the practicality of frequency-domain loads analysis. A typical application would be to gain confidence that predicted interface accelerations will not be exceeded because of changes in mission profiles and/or unexpected transients.

Compiled information from flight data can provide one other possible advantage. By knowing the impedance characteristics of a payload and referring to the interface acceleration data bank and launch-vehicle mobility characteristics, a payload designer can determine whether the payload has a low-frequency loads problem that requires more analysis. This approach is similar to the recommendation in the *Titan Users' Guide* that payloads be designed to have all structural modes above approximately 25 Hz to stay away from low-frequency phenomena like POGO. However, if there are modes below 25 Hz, with knowledge of the payload's dynamic characteristics, the criticality of the structural loads problem can be determined.

Test Program

Test Philosophy

To minimize costs, the many different payloads for Space Shuttle and other future programs require modification of current test philosophy. As described in ref. 31, single-mission planetary exploration experiments may require an extensive test program to achieve the high reliability required for this type of mission, whereas a minimum test program may be sufficient for multiple-mission experiments that can be returned, repaired, and reflown. A number of studies (ref. 29, 31, 32) discuss the problem of reducing costs of test programs. In varying degrees, the studies examine the effects of test factors, levels of assembly testing, commonality of components and experiments, and the prototype versus the protoflight concept.

The prototype concept (fig. 73) is designed to produce maximum confidence for high-reliability payloads, particularly for multiple-mission programs with nonreturnable payloads. Obviously, this concept is the most costly, requiring a complete set of dedicated test hardware and testing at each assembly level. However, it may still be cost effective for a particular program if a mission failure can be prevented.

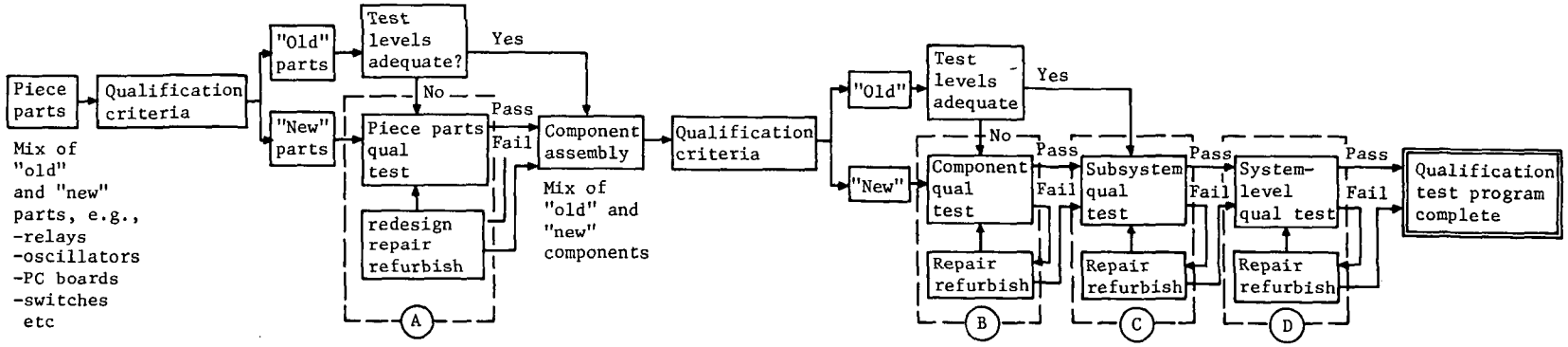

Qualification test program

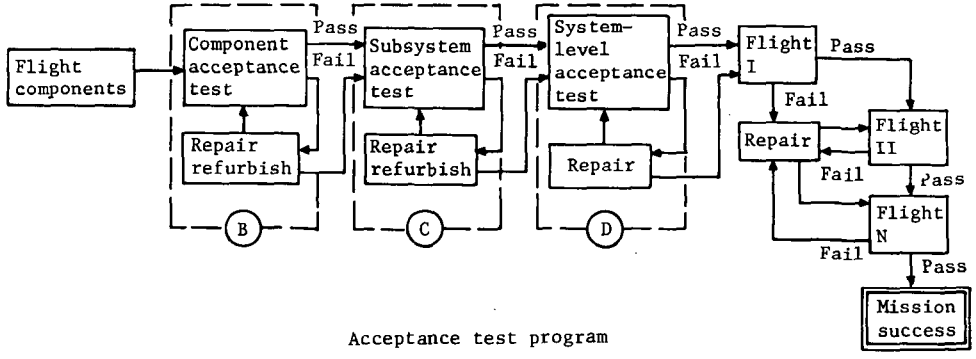

Acceptance test program

Figure 73.- Prototype test program.

Elimination of one or more levels of testing (A, B, C, or D in fig. 73) can reduce test program costs, with an associated increase in risk. A likely candidate for elimination is the "piece-parts" qualification program. Although useful to screen out poor designs, this level of assembly testing is often superfluous because the environment (level and spectrum shape) in the component assembly is often unrelated to previous qualification criteria.

An alternative approach is proposed. Establish a verification test for piece parts similar to that established by Simpkinson for Apollo components (ref. 10). Test environments should be established at the highest practical level, depending on the fragility of the parts, so that parts will be "qualified" for use in the majority of components for anticipated applications. The chassis designer-dynamicist will then know the degree of protection required if the predicted environment exceeds the demonstrated capability of the parts. Obviously, to establish fragility levels, this approach will require an initial economic investment in testing to failure.

In the protoflight concept (fig. 74), flight hardware is tested to qualification levels for acceptance durations. This test philosophy is particularly applicable to one-of-a-kind payloads that can be returned, repaired, and reflown. The major cost savings is in eliminating the expenses of test-dedicated hardware and a qualification test program. Of course, there is an associated increase in risk of flight failure.

Documentation

Regardless of the test philosophy selected, early planning, scheduling, and documentation of the test program are important facets of every payload program. On the Viking Project, this was accomplished with the *Viking Structural Verification Plan*--a detailed plan for verifying Viking Lander structure, including a description of the analyses and tests to be accomplished and their interrelationships. Hardware and general instrumentation requirements were defined, test objectives and prerequisites stated, and success criteria and recovery plans in case of failure were specified. Finally, the document included a flow chart of major tests, environments, and facility requirements.

The second phase of test documentation consists of detailed test and instrumentation plans for each major test, from which test procedures (step-by-step operations) can be prepared. Finally, the test report provides details of how the test was conducted, data acquired, and a description of any anomalies or deviations from the test plan. The data are then available for correlation with other tests and flight measurements and for evaluation of criteria.

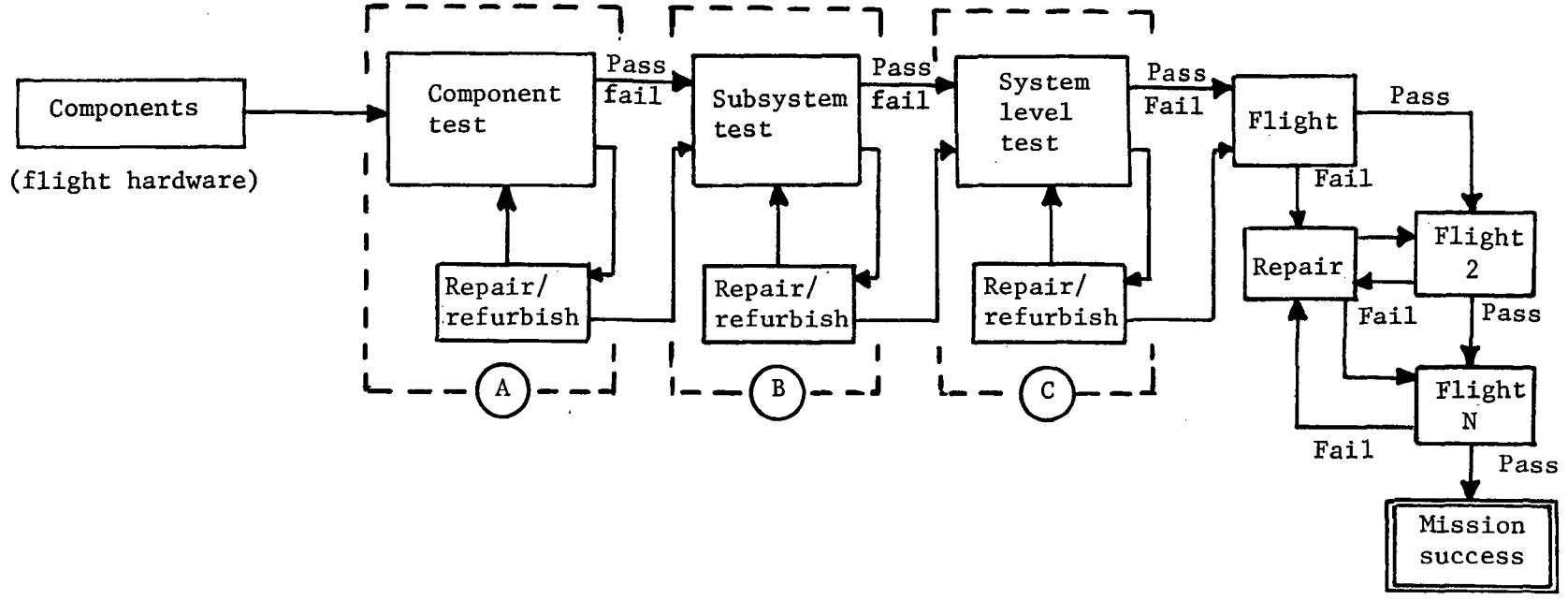

Figure 74.- Protoflight test program.

Documentation for a payload test program should begin by classifying the payload in terms of its mission and reliability requirements, perhaps in the form shown in figure 75. Test requirements and margins are then established for the payload. Knowing the classification for his particular hardware, the payload developer can then prepare the verification plan and document proposed analyses and tests required to establish the integrity of the payload for the intended mission. In many cases, this plan should include a willingness to accept a reasonable risk of flight failure--a concept that has previously been unacceptable in the industry.

The verification plan strongly depends on allowable weight. If the payload is not weight critical, the designer may rely heavily on analyses and "comfortable" margins in the structure so that minimum testing is required. For weight-critical payloads, the plan must include a more extensive test program. In either approach, the plan should include maximum use of components and experiments that can be considered previously qualified on other payloads and launch vehicles.

With this approach, a high percentage of payloads may reasonably do without two levels of assembly testing shown in figure 73, retaining the component assembly test and either the subsystem- or system-level test. The latter choice should include consideration of existing facility capabilities relative to payload configuration and test requirements.

The payload program schedule should provide for maximum use of test-program data and provide enough time, not only for conducting the tests, but also for contingencies and recovery. An example is the acoustic or pyrotechnic shock development test conducted to establish component criteria. This type of test can be extremely cost effective in establishing realistic qualification criteria for components early in the program and avoiding overly conservative tests or, conversely, requalification of components because of exceedances. Unfortunately, hardware design and procurement schedules often preclude performance of these types of tests before the component qualification program, and the cost effectiveness is severely diminished.

Test Performance

The advent of digital analysis and control systems in the laboratory has established a potential new era in dynamic testing. Advantages and limitations of digital systems are discussed in some detail in ref. 33. Briefly, the advantages of digital systems are:

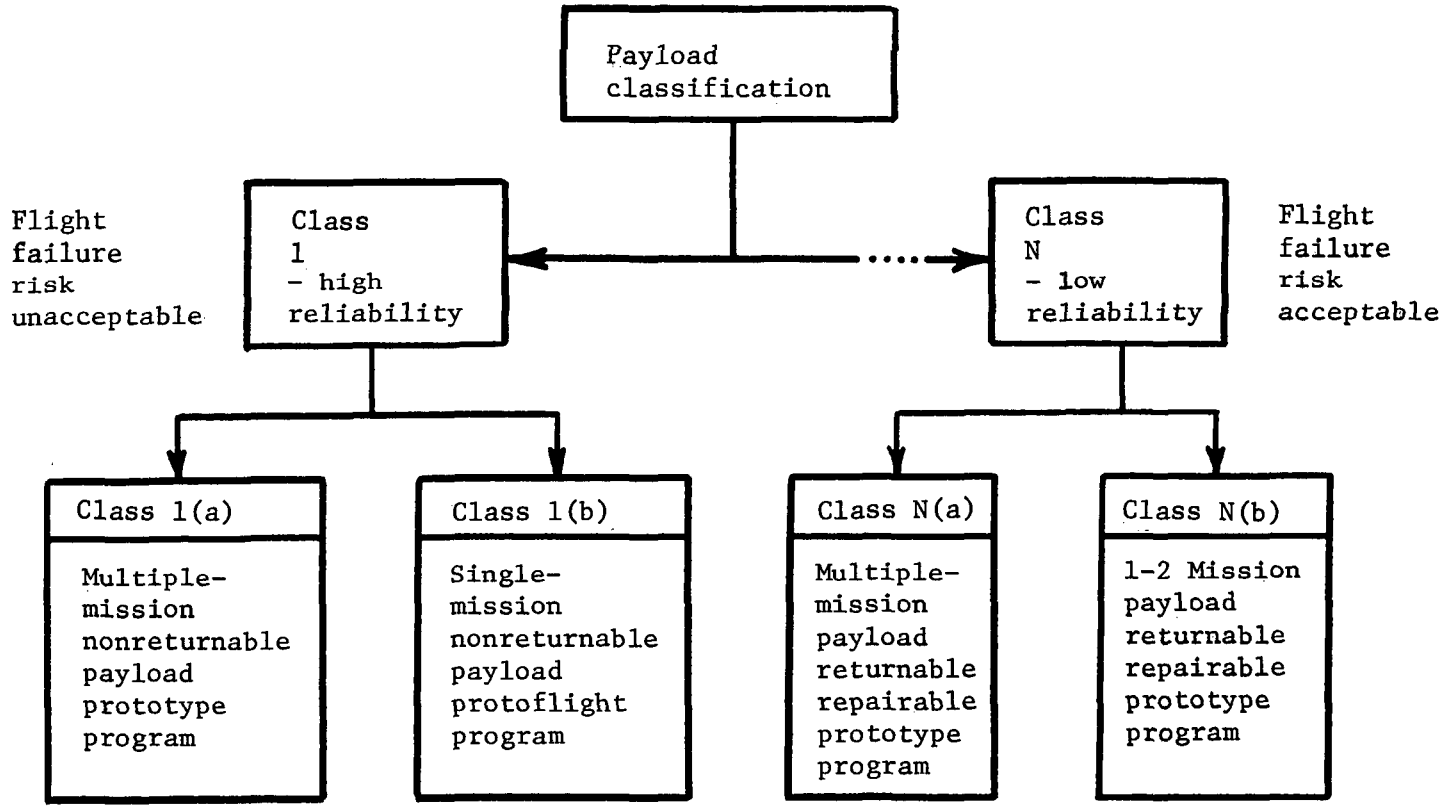

Figure 75.- Simplified payload classification plan.

1) Tighter test tolerances and improved simulation of dynamic environments;

2) Improved accuracy, speed, and versatility in data reduction;

3) Improved safety protection of test articles and equipment;

4) Reduction in test span time.

The last advantage is probably the greatest contributor to cost savings. Not only are the laboratory costs reduced, but the "standby" time of other disciplines awaiting the test hardware is also greatly decreased.

Recognizing that not all laboratories are equipped with digital systems and that the extensive capabilities of digital equipment are no substiture for sound engineering judgment in planning and conducting tests, the following discussion and recommendations for dynamic testing are presented.

Modal survey (GVS) tests.- Recent technological advances in modal survey techniques and equipment provide the potential for significantly reducing costs for this type of testing. These sophisticated methods have been demonstrated on small structures and models, but the capabilities have not been proved on large, complex structures. Recent improvements include techniques for extracting modes from random or transient excitation and displaying mode shapes on a CRT, which may eliminate the previous time-consuming slow sine sweeps and resonance dwells. Assuming that these improved methods and equipment will prove successful on large, complex structures, the potential cost benefits for future payloads are significant.

The primary objective of modal survey testing is to obtain data with which to verify and refine analytical models required for structural loads and control-system analyses. Documentation in the form of a data bank of these analyses and test results for the different payload classes should provide analysts with enough information to confidently model future payloads and eliminate or minimize model survey testing.

Sine-sweep qualification tests.- On the Viking Project as well as a number of programs described in the literature, it has been demonstrated that local overtesting during sine tests of large complex test articles (a frequent problem caused by excessive amplitude build-up at resonant frequencies) can be avoided using either analog or digital response control techniques. Unfortunately, implementation of response-control and load-limiting techniques can be very expensive and there are questions about the validity and usefulness of results of such testing in the first place. There-

fore, as a general philosophy for future payloads, it is proposed that sine sweep testing be eliminated and replaced with analysis.

There will no doubt be exceptions to the general philosophy in the form of large, heavy components and subsystems that may couple with POGO or other launch-vehicle transients. For these exceptions, transient and/or stepped sine tests are recommended to replace conventional sine sweep tests.

Pyrotechnic shock tests.- Shock synthesis techniques, particularly those using transfer-function calculations in digital control systems, have vastly improved shaker simulation of pyrotechnic shock, particularly with regard to tolerances on the input waveform or shock-spectrum amplitudes. However, there is strong evidence that shaker, drop, and "hammer-impact" tests produce relatively greater responses in the test item than an actual pyrotechnic event. This is probably due to the coherence of the input function at specimen mounting points for the simulative tests.

It is recommended that actual pyrotechnic devices be used for testing future payload components. We recognize that this type of testing is more expensive than simulation techniques, but test costs should be more than offset by reduction in test-induced failures. On the Viking Project, a pyrotechnic "test bed" simulating the Lander body was used very successfully.

Random vibration tests.- Establishment of more realistic criteria (e.g., fig. 76) and reduction of qualification test factors (if adopted) will impose more stringent requirements on the control and tolerances of laboratory shaker systems. Digital control systems provide the ability to meet these requirements. Upper and lower test limits can be superimposed on the control spectrum to ensure that an acceptance test environment will not exceed the qualification level in any frequency band. This should help reduce the required qualification factors because, in the past, this factor was based in part on test tolerances achievable with shaker systems. The result will be fewer failures in laboratory tests.

A major contribution to cost reduction is the time saved in conducting tests. Test parameters can be set up quickly, stored, and recalled as necessary. Another significant economic factor, often overlooked, is the versatility and speed of data measurement and analysis. In the past, many of analyses like cross power spectra, cross correlation, coherence, required off-line analog-to-digital conversion and processing by large, expensive digital computers. The dynamicist now has these analytical tools at his fingertips as built-in options in most digital control systems.

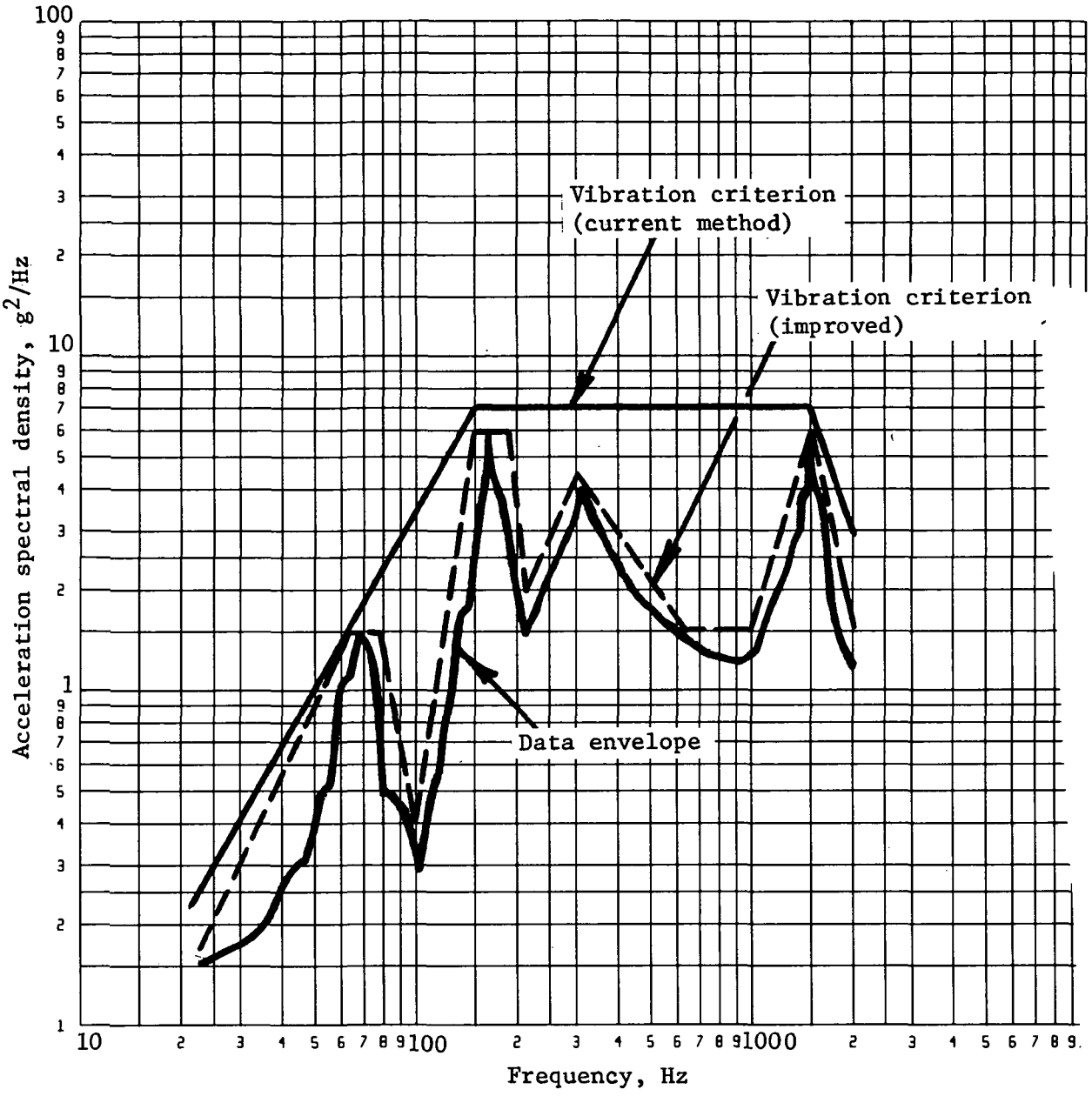

Figure 76.- Comparison of vibration spectra.

Separation and deployment tests.- As a general rule, these events are the most difficult to simulate in the laboratory. Therefore, rather than spend considerable time and money on an elaborate attempt at simulation, a more realistic approach is to analyze flight and test conditions and conduct only those tests necessary to verify the analytical techniques. These tests are useful for finding problems like manufacturing tolerance build-ups, stiction, clearance, and misalignment.

In summary, recommended practices to reduce costs for future payload test programs are listed below.

1) Classify payloads according to mission and reliability requirements. Establish test levels and margins as required for each payload class.

2) Thoroughly document the payload program. Begin with a plan for verification of the payload flight worthiness, detailing the analyses required, testing to be performed, and the interaction between analyses and test data. Include careful comparisons of the costs of required analyses versus testing. Delete as many levels of assembly testing as possible, but schedule hardware and tests to obtain maximum benefit from test results. Documentation should end with detailed test reports and data contributed to a data bank for application to future payloads of the same or similar classification.

3) To avoid requalification testing, use components common to other payloads or launch vehicles to the maximum possible extent.

4) Plan and schedule the test program to minimize hardware span time. Use common fixtures and minimize setups and instrumentation as much as possible. Digital control and analysis systems can significantly contribute to time and cost savings, both directly in test performance and indirectly in reducing data-reduction computer costs.

Flight Program

The flight measurements program conducted on Viking was described earlier. Data from Viking flights are included in ref. 34, which summarizes loads data obtained on the first four Titan/Centaur flights. Because of limitations on the number and frequency range of available channels, fewer transducers were installed than was desirable. The loads analysis was adequately supported by flight data, but relatively little information was obtained on high-frequency environments affecting components. The acoustic environment was measured and the data revealed that the predicted environment was inaccurate, both in level and

spectrum shape. However, the only high-frequency acceleration data obtained were at three structural hardpoints, so that it was not possible to calculate acoustic and vibration transfer functions under flight conditions.

Some future space programs may not be subject to the usual telemetry and payload weight and volume restrictions. An important example is the Space Shuttle program, on which it should be feasible to provide enough instrumentation channels to obtain good coverage of the entire Orbiter structure for verification of analysis, as well as spatially detailed definition of the payload-bay environment. Some of the more important data should be telemetered to ground stations to be used for diagnoses in case of launch-vehicle malfunction. However, to ensure that the data will have adequate frequency range and resolution, most of the measured data should be recorded on board for later playback and analysis. Special care must be taken to preserve accurate time synchronization among all data channels.

For convenience, the frequency range over which the data are acquired is broken down into low- and high-frequency regions. The low-frequency region includes frequencies up to 50 or 100 Hz, depending on the launch vehicle, and is the region in which maximum vehicle transient loads are experienced by the primary structure. In this range, analytical methods can be used with confidence to predict dynamic loads provided they are adequately verified with flight data. Instrumentation intended to provide low-frequency data should include strain gages, accelerometers, load cells, and engine pressure transducers. Because these data will be used to check and refine the loads analysis, transducer locations should be selected to support the analysis to the maximum possible extent. The Viking Project demonstrated the benefits of having close coordination between system-level ground tests, flight instrumentation, and loads analysis.

The high-frequency region (above $\sim$100 Hz) covers the range associated with the acoustic environment and resulting random vibration, and with short-duration transients such as pyrotechnic shock, so instrumentation for this range should consist of piezoelectric accelerometers and microphones.

Reference 35 provides detailed recommendations on improved techniques for acquiring and analyzing flight data on Shuttle payloads. As mentioned, signal conditioning equipment is now available that can provide multiple outputs for a common input. Each output section can have its own gain and filter characteristics, so that, for example, an accelerometer could operate in several frequency and dynamic ranges at different periods in the mission.

Data acquired on Shuttle flights will eventually provide a solid statistical basis for loads and environmental analyses, which should therefore have high confidence levels associated with the predicted values, providing the analysis-test-flight process is properly coordinated. For example, considerable improvement in accuracy and cost effectiveness could be realized if all flight test data were available in digital form. Using digital computers, significant advances in data analysis techniques have been made in the last few years. To take full advantage of these methods, digital data should be acquired directly, rather than obtained by analog-to-digital conversion. Almost all new large-scale test control systems are digitally based, and digital flight-type tape recorders and other instrumentation are now available, so that, from an overall system viewpoint, switching to an all-digital philosophy could probably be done without excessive cost.

To calculate flight loads experienced on the Viking Project, a system was set up for processing flight data from the first launch immediately upon receipt. These were compared with calculated allowable loads to verify that no changes had to be made before the second launch. There will be a need for a similar rapid checkout system on programs such as Space Shuttle in which flights will occur in quick succession. Potentially dangerous anomalies need to be recognized as soon as possible so that appropriate steps can be taken to avoid catastrosphic failures.

CONCLUSIONS AND RECOMMENDATIONS

The extensive structural dynamics information obtained from the development and flights of the Viking spacecraft has been assembled, reviewed, and summarized in this report. The information is the basis for recommended dynamic design criteria and a philosophy to reduce costs for future payloads, as summarized in this section.

CONCLUSIONS

Environments and Criteria

Late revisions of vibroacoustic environments required some retesting of components. Early definition of significant acoustics and improved vibration prediction techniques are needed to minimize this on future programs. Methods of predicting the propagation of pyrotechnic shock in a structure were developed and refined through an extensive development test program. Shock attenuation methods were investigated, and the effectiveness of commercial shock isolators in a pyrotechnic shock environment was evaluated.

The potential benefits of additive damping treatment on PC boards were investigated. It was concluded that the maximum response of the boards could be greatly decreased by proper application of constrained layers of viscoelastic material to the board surface.

Analytical Technology

Analytical models can be used to accurately predict overall vehicle and large-component dynamics. For high-reliability weight-critical payloads like Viking, test verification of the analytical model is essential. The use of strain-gaged spacecraft truss members as calibrated load cells during the VDS flight significantly aided in determining predicted flight loads for design of the primary load-carrying structure. The Viking aeroshell POGO test and subsequent mission successes demonstrated that structure can be designed and built to minimum margins, even to the point of elastic buckling, without failure. However, the Viking approach would amount to "overkill" for payloads that are not weight critical.

Flight Programs

The Viking proof flight provided the unique opportunity of launching a dynamic simulation of the spacecraft to verify modeling techniques. The Space Shuttle is one future program that will provide the same opportunity for all multimission payloads. The dynamic flight instrumentation on the Viking A and B flights was insufficient for future applications. Early Shuttle flights should be adequately instrumented to provide environmental and loads data for correlation with analyses.

Recommendations

Environments and Criteria

1) Establish payload classifications based on size, configuration, mounting conditions, weight criticality, and mission reliability requirements.

2) Establish an industry-wide common basis for defining different design and test margins for the payload classes. Be willing to accept some risk of flight failure for returnable payloads.

3) Create a bank of flight and test data for each payload class that can be used to establish and update environmental criteria with statistical confidence. The goal is to minimize design and test factors through reduction of uncertainty factors and "stack-up" of safety margins.

Documentation

The payload contractor should prepare a structures verification plan defining the analyses and test-program requirements for ensuring the payload's structural integrity. The prototype or protoflight approach should be selected based on the number of payloads required and the reliability requirement for the particular payload classification. With a verification plan established, schedule the program to allow for contingencies and to provide for maximum use of the test results.

Loads Analyses

Minimize the loads cycle analyses and tests required based on weight criticality and design margins available. For many payloads,

one or two loads analysis cycles will be enough to verify that payload modes are not within the critical load range of launch-vehicle frequencies, and that there is enough design margin for steady-state and other load conditions. To minimize the cost of loads cycle analyses, application of new simplified loads analysis techniques should be investigated. However, to minimize the risk of a mission failure, for high-reliability weight-critical payloads, extensive analysis verified by test should be performed.

Test Program

1) Establish minimum qualification (or verification) criteria for piece parts and eliminate the formal piece-parts qualification program on an individual payload basis. The integrity of the part in the component assembly then becomes the responsibility of the designer and the dynamics analyst. Although the cost of such a test is relatively small (compared to component, assembly, or system-level tests), the cost savings will be significant because of the large numbers involved.

2) Eliminate sine-sweep qualification testing as a general requirement at all levels of assembly testing. There will be exceptions, of course, and for these cases, some form of decaying sine testing should be considered. In cases where system level sine tests are required, employ response control and load-limiting techniques to prevent test-peculiar failures of primary structure.

3) To the greatest extent possible, use actual pyrotechnic devices and test beds to test components to this environment. Although test costs are expected to be higher, overall cost savings should result through minimization of test failures, repair, and retest resulting from excessively severe coherent inputs typically resulting from tests using shakers and shock machines.

4) To minimize test setup and span time, provide for maximum common use of fixtures and test and analysis equipment available.

5) To minimize test tolerances and allow the use of multiple breakpoint random spectra, improve techniques and equipment for control of shakers. Further development is needed to establish impedance control techniques for more realistic simulation in vibration testing.

Flight Program

Establish a comprehensive, coordinated, integrated flight measurements program including standardized techniques and formats for data acquisition and reduction. Generate a data bank that includes sufficient structural details and measurement locations to permit improved, more-realistic definition of criteria for future payloads. For multiple-mission programs like Space Shuttle, the recommended approach is to acquire as much information as possible on both launch vehicle and payloads during early flights, reducing instrumentation on later flights to that required for diagnostic purposes and checks on data-bank statistics. For initial Shuttle flights, on-board recording with time correlation of Orbiter events is essential for retention of necessary phase information.

Increased coordination and communication between government agencies and the payload community is needed to acquire, analyze, disseminate, and use test and flight data for maximum technical and economic benefit.

Langley Research Center
National Aeronautics and Space Administration
Hampton, Virginia 23665
August 30, 1977

REFERENCES

1. Saunders, H. and Nestler, D. E.: "Prediction of the Boundary Layer Acoustic Pressure Levels of a Blunt Nose Re-Entry Vehicle at High Mach Numbers." *Shock and Vibration Bulletin No. 35.* Part 7, April 1966.

2. Hellweg, R. D.: *Prediction of Entry Acoustical Environments,* Martin Marietta Report R72-48614-001, vol. II, June 1972.

3. Chobotov, T. and Powell, A.: *On the Prediction of Acoustic Environments from Rockets.* Ramo Wooldridge Corporation Report GM-TR-190, 3 June 1957.

4. Eldred, K., et al: *Vibration in Space Vehicles.* WADD Report TR-61-62, December 1961.

5. Beranek, L. L.: *Noise Reduction.* McGraw-Hill, 1960.

6. Barrett, R. E.: *Techniques for Predicting Localized Vibration Environments of Rocket Vehicles.* NASA TN D-1836, October 1963.

7. Franken, P. A.: "Sound Induced Vibrations of Cylindrical Vehicles." *J. Acoustical Soc. America,* vol. 34, no. 4, April 1962.

8. Winter, E. F. and Van der Laan, W. F.: *Recommended Procedures for Predicting Random Vibration Environments in MSFC Aerospace Vehicles.* Measurement Analysis Corporation Report MAC 504-19, September 1967.

9. Barnoski, R. L., et al: *Summary of Random Vibration Prediction Procedures.* NASA CR-1302, April 1969.

10. Simpkinson, S. H.: "Testing to Ensure Mission Success." *Aeronautics and Astronautics,* March 1970.

11. Meltzer, E. C.: *Compilation of Shock and Vibration Flight Data from Eight Thor-Related Vehicles.* NASA CR-196, March 1965.

12. Mansour, M. N.: *Mariners 6 and 7 Dynamic Environment.* JPL Document 605-232, June 1970.

13. Parker, G. L.: *Launch Dynamic Environment of the Surveyor Spacecraft.* JPL Technical Report 32-1289, September 1968.

14. Clevenson, S. A.: *Lunar Orbiter Flight Vibration Data and Comparisons with Environmental Specifications.* NASA TN D-6006, September 1970.

15. Kacena, W. J., McGrath, M. B. and Rader, W. P.: *Aerospace Systems Pyrotechnic Shock Data, Volume I.* Martin Marietta Report MCR-69-611, (Contract NAS5-15208, NASA/GSFC), March 1970.

16. Barrett, S. and Kacena, W. J.: "Methods of Attenuating Pyrotechnic Shock." *Shock and Vibration Bulletin 42,* part 4, January 1972.

17. Benfield, W. A. and Hruda, R. F.: "Vibration Analysis of Structures by Component Mode Substitution." AIAA/ASME 11th Structures, Structural Dynamics and Materials Conference, Denver, Colorado, April 1970.

18. Wada, B. K.: "Viking Orbiter - Dynamics Overview." *Shock and Vibration Bulletin 44,* part 2, August 1974.

19. Wada, B. K., Garba, J. A. and Chen, J. A.: "Development and Correlation: Viking Orbiter Analytical Dynamic Model with Modal Test." *Shock and Vibration Bulletin 44,* part 2, August 1974.

20. Day, F. D. and Wada, B. K.: "Unique Flight Instrumentation/ Data Reduction Techniques Employed on the Viking Dynamic Simulator." *Shock and Vibration Bulletin 45,* part 2, February 1975.

21. Newbrough, D. E., Colonna, R. A. and West, J. R.: "Development and Verification of the Vibration Test Requirements for the Apollo Command and Service Module." *Shock and Vibration Bulletin 37,* part 5, January 1968.

22. Steinberg, D. S.: *Vibration Analysis for Electronic Equipment.* John Wiley and Sons, New York, 1973.

23. Arnold, J. T. and Strother, F. P.: "A Practical Approach to the Prediction of the Natural Frequency of Printed Circuit Boards." *Shock and Vibration Bulletin No. 35,* part 7, February 1966.

24. Isado, N. M. and Shear, J. C.: "Vibration Response of Printed Circuit Boards." *Shock and Vibration Bulletin No. 42,* part 3, December 1969.

25. McCandliss, W. H. and Stahle, C. V.: "Controlling Vibration of Viking Lander Electronic Packages." presented at 44th Shock and Vibration Symposium, October 1973.

26. Palmisano, R. R. and Neily, D. W.: "Particulate Silicone Rubber: An Effective, Removable Encapsulant for Electronic Packaging." *Shock and Vibration Bulletin 46,* part 4, August 1976.

27. Prescott, S. N.: "Pyrotechnic Shock Reduction." *Shock and Vibration Bulletin No. 44*, part 3, August 1974.

28. Rader, W. P., et al: *Analytical Trade Study of the STS Payload Environment.* NASA CR-144233, Martin Marietta Report MCR-76-166, March 1976.

29. White, C. W., Maytum, B. D.: "Eigensolution Sensitivity to Parametric Model Perturbations." *Shock and Vibration Bulletin No. 46*, part 5, August 1976.

30. Abbott, P. W. and Morosow, G.: "Mode Selection." *Proceedings of the ASME Winter Meeting, 1971.*

31. Stahle, C. V. and Gongloff, H. R.: *Vibroacoustic Test Plan Evaluation.* vol I, II and III, GE Document 73SDS4223, (Contract NAS5-20906), June 1976.

32. Stahle, C. V. and Gongloff, H. R.: *Astronomy Sortie Vibration, Acoustics and Shock Program Planning, Phase I.* GE Document 74SD4246, September 27, 1974.

33. *Seminar on Understanding Digital Control and Analysis in Vibration Test Systems.* The Shock and Vibration Information Center, Naval Research Laboratory, Washington, DC, May 1975.

34. Kachadourian, G.: *A Summary of Spacecraft Loads Data from Four Titan Centaur Launch Vehicle Flights.* NASA CR-2645, March 1977.

35. Rader, W. P., et al: *A Study to Define an In-Flight Dynamics Measurement and Data Applications Program for Space Shuttle Payloads.* (Contract NAS1-13377) Martin Marietta, NASA CR-144892, November 1975.

Page intentionally left blank

BIBLIOGRAPHY OF VIKING TEST REPORTS

Barrett, S.: *Summary Report, LDTM Launch and Entry Acoustics Test.* Report VER-285, Martin Marietta Corporation, Denver, Colorado, May 1974.

Fortenberry, James W., and Rader, Paul: "Fail Safe Forced Vibration Testing of the Viking 1975 Developmental Spacecraft." *Shock and Vibration Bulletin No. 45,* Part 3. The Shock and Vibration Information Center, Washington, D.C., June 1975.

Kacena, W. J.: *LDTM Aeroshell Separation Test and Correlation Report.* Report TR-3720383, Martin Marietta Corporation, Denver, Colorado, October 1974.

Kacena, W. J.: *LDTM Base Cover Separation Test and Correlation Report.* Report TR-3720382, Martin Marietta Corporation, Denver, Colorado, October 1974.

Kacena, W. J.: *LDTM Base Cover Separation Pyro Calibration Verification Test.* Report TR-3720371, Martin Marietta Corporation, Denver, Colorado, 24 May 1973.

Kacena, W. J.: *LDTM Mortar Fire Test Report.* Report TR-3720373, Martin Marietta Corporation, Denver Colorado, May 1973 (unpublished).

Kacena, W. J.: *LDTM Leg Deployment/PEVT Test.* Report TR-3720364, Martin Marietta Corporation, Denver, Colorado, 11 May 1973.

Kacena, W. J., and Sheppard, D.: *LDTM Orbiter/Lander Separation Test and Correlation Report.* Report TR-3720479, Martin Marietta Corporation, Denver, Colorado, October 1974.

Pohlen, Joe C., et al: "The Evolution of the Viking Landing Gear." *Tenth Aerospace Mechanisms Symposium,* Jet Propulsion Laboratory, Pasadena, California, April 22-23, 1976.

Schwantes, S. N.: *LDTM Terminal Descent GVS.* Report TR-3720363, Martin Marietta Corporation, Denver, Colorado.

Vigil, R. A.: *LDTM Launch Configuration GVS and Aeroshell GVS.* Report LDTM-TR-017, Martin Marietta Corporation, Denver, Colorado, 24 July 1973.

Vigil, R. A.: *LDTM Mid-Frequency Vibration Test.* Report TR-3720462, Martin Marietta Corporation, Denver, Colorado, 31 May 1974.

Vigil, R. A.: *Aeroshell Dynamic Capability Test (POGO).* Report TR-3720517, Martin Marietta Corporation, Denver, Colorado, 1 April 1975.

1. Report No.	2. Government Accession No.	3. Recipient's Catalog No.
NASA CR-3014		

4. Title and Subtitle	5. Report Date
Viking Dynamics Experience with Application to Future Payload Design	July 1978
	6. Performing Organization Code

7. Author(s)	8. Performing Organization Report No.
Stanley Barrett, W. Paul Rader and Kenneth R. Payne	MCR-77-144

9. Performing Organization Name and Address	10. Work Unit No.
Martin Marietta Corporation P.O. Box 179 Denver, Colorado 80201	11. Contract or Grant No. NAS1-14370
	13. Type of Report and Period Covered Contractor Report
12. Sponsoring Agency Name and Address National Aeronautics and Space Administration Washington, D.C. 20546	14. Sponsoring Agency Code

15. Supplementary Notes

Langley Technical Monitor: Brantley R. Hanks

Topical Report

16. Abstract

The extensive structural dynamics information gained during development and flight of the Viking spacecraft was assembled and used as a framework for the study. Analytical and test techniques are discussed. Areas in which hindsight indicated erroneous, redundant, or unnecessarily severe design and test specifications are identified. Recommendations are made for improvements in the dynamic design and criteria philosophy, aimed at reducing costs for future payloads.

17. Key Words

Viking Spacecraft
Dynamic Loads and Environments
Acoustics, Vibration, Shock
Dynamic Testing

18. Distribution Statement

Unclassified - Unlimited

Subject Category 18

19. Security Classif. (of this report)	20. Security Classif. (of this page)	21. No. of Pages	22. Price
UNCLASSIFIED	UNCLASSIFIED	164	$8.00

NASA-Langley, 1978

National Aeronautics and Space Administration

Washington, D.C.
20546

Official Business
Penalty for Private Use, $300

SPECIAL FOURTH CLASS MAIL
BOOK

Postage and Fees Paid
National Aeronautics and
Space Administration
NASA-451

NASA

POSTMASTER: If Undeliverable (Section 158 Postal Manual) Do Not Return